The Human Induced Pluripotent Stem Cell Test as an Alternative Method for Embryotoxicity Testing

Inaugural dissertation

for the attainment of the title of doctor
in the Faculty of Mathematics and Natural Sciences
at the Heinrich Heine University Düsseldorf

presented by

Saskia Galanjuk

from Bonn-Bad Godesberg

Düsseldorf, December 2022

from the IUF – Leibniz Research Institute for Environmental Medicine

at the Heinrich Heine University Düsseldorf

Published by permission of the

Faculty of Mathematics and Natural Sciences at

Heinrich Heine University Düsseldorf

Supervisor: Prof. Dr. Ellen Fritsche

Co-supervisor: Prof. Dr. Vlada Urlacher

Date of the oral examination:

Der Humane Induzierte Pluripotente Stammzelltest als Alternative Methode zur Embryotoxizitätstestung

Inaugural-Dissertation

zur Erlangung des Doktorgrades
der Mathematisch-Naturwissenschaftlichen Fakultät
der Heinrich-Heine-Universität Düsseldorf

vorgelegt von

Saskia Galanjuk

aus Bonn-Bad Godesberg

Düsseldorf, Dezember 2022

Angefertigt am IUF – Leibniz-Institut für umweltmedizinische Forschung GmbH

an der Heinrich-Heine-Universität Düsseldorf

Gedruckt mit der Genehmigung der

Mathematisch-Naturwissenschaftlichen Fakultät der

Heinrich-Heine-Universität Düsseldorf

Berichterstatter:

1. Prof. Dr. Ellen Fritsche

2. Prof. Dr. Vlada Urlacher

Tag der mündlichen Prüfung:

Table of contents

1 Introduction

1.1 Reproductive toxicity

According to the World Health Organization (WHO), an estimated 6 % of newborns worldwide are born with a developmental defect in the form of a structural or functional anomaly. The actual percentage is estimated to be even higher, as abortions and stillbirths are not included. The most common severe developmental anomalies include heart defects, neural tube defects, and Down syndrome (WHO, 2022). Most of the causes are unknown but it is assumed that around 3 % of manifested developmental disorders can be attributed to exposure to chemical substances. In general, environmental exposure e.g. to chemicals or drugs during pregnancy has been gaining recognition as contributing factor to adverse prenatal developmental outcomes (Weinhold, 2009; Nicoll, 2018). There is ubiquitous exposure of pregnant women to various chemicals including pesticides and drugs that are known to cause developmental defects (Bradman et al., 2003; Woodruff et al., 2011). Since there is a massive lack of data regarding the risk assessment of existing chemicals, it is assumed that the percentage is even higher (National Research Council, 2000). In the early 1960s, the drug thalidomide caused numerous children to be born with developmental defects mainly affecting the limbs. Thalidomide was prescribed against nausea and as a sleep-inducing drug. Only since that incident did pharmaceuticals and environmental chemicals undergo a risk assessment, especially focusing on their potential to induce reproductive toxicity (Peters et al., 2015; Spielmann, 2017).

Reproductive toxicity can be induced by substances that exhibit an adverse effect on the reproductive system in males and females disturbing the integrity of the reproductive system. Such substances can directly affect the reproductive organs with an impact on pregnancy outcomes or the endocrine system. Manifestations can appear in e.g. gamete production and transport, fertility, or gestation (US EPA, 1996). Developmental toxicity as a subcategory of reproductive toxicity is seen as the adverse effects of substances on the developing organism. This includes the exposure before conception of either parent until the time of sexual maturation of the offspring. Developmental toxicity can include the death of the developing organism, structural abnormalities, altered growth, or functional deficiencies (US EPA, 1991). As developmental toxicity is not only limited to effects that occur prenatally, a further division into the term embryotoxicity is made. Embryotoxicity includes adverse effects of substances that crossed the placenta barrier affecting the development of the embryo and leading to structural or functional abnormalities and postnatal manifestations of such effects. Teratogenicity is a special case of embryotoxicity. It implies that teratogens induce or increase the frequency of structural disorders in the offspring. Teratology originally comprises birth defects of structural nature, however, nowadays teratology also includes functional effects. For example,

thalidomide mentioned above is a teratogen by definition. The capability of a substance to induce embryotoxicity is dependent on six established principles (Wilson, 1977).

Principle 1: The susceptibility of species toward substances is dependent on the genotype. This means the inter- and intraspecies variability leads to the manifestation of embryotoxicity in several different ways caused by differences in e.g. pharmacokinetics or receptor sensitivity. While the same substance can exert no effect on one species, another species can experience tremendous embryotoxic effects (Wilson, 1977; Peters et al., 2015). Principle 2: The susceptibility of the progeny toward substances is dependent on the developmental stage. During the first two weeks *post conceptionem* (p.c.) the risk of malformation is considered low because the pluripotent state of the cells allows for repair or the progeny dies which is known as the all-or-none law. The highest susceptibility is during organogenesis (days 15–56 p.c.), most malformations occur during this time frame. After that period, the susceptibility toward toxicants decreases during the fetal period until birth. Principle 3: Toxicants act through relatively few specific mechanisms on developing cells and tissues to initiate abnormal embryogenesis. For example, neural tube defects are caused by several toxicants but most act on the folic acid balance. Principle 4: The manifestations of embryotoxicity are various and include normal development after complete recovery, death, malformations, growth restriction, functional disorder, and carcinogenesis. Principle 5: The nature of toxicants determines whether they will reach the embryo or not. This is primarily dependent on the ability of the toxicant to cross the placenta barrier which is more likely the more lipophilic the substance is. Principle 6: Manifestations of toxicants are dose-response related. All toxicants possess a no-effect level at which no toxicity is observed. Passing this threshold, the teratogenic range is reached followed by the embryo-lethal and maternal toxic range (Wilson, 1977; Paulus, 2016).

To prevent developmental disorders a substance has to be identified as reprotoxic which results in either withdrawal from the market, non-approval for the market, or restricted approval with specific pregnancy labeling (Peters et al., 2015). For this, a risk assessment has to be performed on a wide range of substances that already exist and substances that will be developed for the market (ECHA, 2022).

1.2 Hazard and risk assessment in the field of reproductive toxicology

Risk assessment needs to be performed on e.g. chemicals, pharmaceuticals, and pesticides. Different agencies worldwide, e.g. the European Chemical Agency (ECHA), the United States Environmental Protection Agency (US EPA), and the Food and Drug Agency (FDA), were established to take care of this task. To assess the risk that a substance poses to human and environmental health, the responsible agencies published test guidelines (TG) that help in risk assessment. The process of risk assessment is divided into four different steps that are implemented in the mentioned guidelines. First, hazard

identification is performed. In this step, the profile of toxicity for a respective substance is described along with the occurrence in the environment. Second, the dose-response assessment is conducted. This step includes the extrapolation of assessed data to achieve a certain concentration at which toxicity occurs. The third step is the exposure assessment. It assesses the time, magnitude, and ways a population could be exposed to the substance. The fourth and last step is the risk assessment which includes all the previous steps and evaluates the likelihood that the hazard of a substance manifests in exposed populations (National Research Council (US), 2007). The provided guidelines help in performing the data assessment, as well as the evaluation of the data and how to interpret them. In the 20th century, guidelines from the US EPA as well as the Organisation of Economic Co-operation and Development (OECD) were provided for the assessment of reproductive toxicology. To minimize the tests that are necessary to perform when registering a substance, guidelines of the US EPA and OECD were harmonized (Iyer, 2017). In the European Union (EU), the Registration, Evaluation, Authorisation, and Restriction of Chemicals (REACH) legislation went into force in 2007, stipulating that every substance with a manufacturing or import tonnage of ten or more has to be evaluated for its potential to induce reproductive toxicity. This regulation lead to an increase in experiments performed under OECD guidelines for reproductive toxicity assessment, namely TG 414, 415, 416, 421, 422, 426, and 443 (OECD, 1983, 2001, 2007, 2016a; b, 2018b; a) which are all performed *in vivo*. However, since 2019 TG 415 (OECD, 1983) was deleted. An estimation from 2009 predicted the use of 49 Million vertebrates and a total cost of 6.7 billion € only for the assessment of reproductive toxicity (Rovida and Hartung, 2009). Fulfilling the regulation REACH using OECD guidelines is logistically and financially not feasible and is not in compliance with the 3Rs; refinement, reduction, and replacement of animal testing (Russell and Burch, 1959). The ECHA, therefore, supports the development and use of alternative methods which is reflected in the publication of the report “The use of alternatives to testing on animals for the REACH Regulation” every three years since 2011 (ECHA, 2011, 2014, 2017, 2020). Within the OECD guidelines some endpoints e.g. skin corrosion and irritation, skin sensitization, serious eye damage and irritation, and mutagenicity and genotoxicity are covered by *in vitro* tests. However, the vast majority of animals used for conducting experiments under OECD guidelines fall under the category of reproductive toxicity testing of which no *in vitro* guideline exists up to date (Rovida and Hartung, 2009; Pistollato et al., 2021). Therefore, there is an urgent need for *in vitro* tests as alternative methods for animal testing to accomplish the REACH regulation in compliance with the 3Rs.

1.2.1 Validated alternative methods for reproductive toxicity testing

The rising demand for the validation of alternative methods lead to the foundation of the European Union Reference Laboratory for Alternatives to Animal Testing (EURL ECVAM) in 2011 hosted by the Joint Research Centre, Institute for Health and Consumer Protection (IHCP). EURL ECVAM validated the above-mentioned *in vitro* testing guidelines for regulatory purposes. Three *in vitro* assays for the

category of reproductive toxicity were also evaluated by ECVAM namely the Rat Limb Bud Micromass Test using cells of rat limb buds, the Rat Post-Implantation Whole Embryo Culture (WEC) employing whole rat embryos, and the Embryonic Stem Cell Test (EST) which makes use of two permanent mouse cell lines (Genschow et al., 2002). Out of these tests, the EST is the only test that is devoid of permanent use of animals. However, none of the tests were validated for regulatory purposes. Limitations of the tests were reported by Spielmann et al. (2006) and need to be addressed for further validation for regulatory purposes. Up to date none of the tests were re-validated by EURL ECVAM. The EST is described in more detail as its basic concept is adapted in the herein-developed human induced pluripotent stem cell test (hiPS Test). The EST is based on the mouse embryonic stem cell (mESC) line D3 and the mouse fibroblast cell line 3T3 assessing the endpoints beating of differentiated embryonic bodies (EBs) and cell viability. For the latter endpoint, D3 and 3T3 cells are plated in six replicates per condition plus negative and positive control on one 96-well plate. After ten days, an MTT assay is performed. From a concentration-response curve, the half maximal inhibitory concentration (IC_{50}) at which growth is inhibited by 50 % of the control level is determined and expressed as IC_{50}3T3 and IC_{50}D3 for the respective cell lines. For the endpoint beating of differentiated EBs, D3 cells are cultured as hanging drops on the lid of a petri dish for three days forming EBs, already exposed to the substance of interest in a certain concentration. Then, EBs are cultured as a cell suspension in a petri dish for additional two days. On day five, one 24-well plate is used for one condition plating one EB per well in a medium devoid of leukemia inhibitory factor (LIF). Under these conditions, EBs adhere to the matrix and start to grow out differentiating into contracting cardiomyocytes. On day ten, the presence of beating EBs per condition is scored, and the number of contracting EBs in the solvent control is set as 100% resulting in a percentage of beating EBs per condition normalized to the control (Genschow et al., 2004).

1.3 Embryonic heart development

The EST reflects an early process of embryonic development with specific regard to cardiomyocyte differentiation. However, the development of a mouse and human heart differs in terms of e.g. developmental time and gene expression (Uosaki and Taguchi, 2016). To direct *in vitro* differentiation of human stem cells into cardiomyocytes by modulating the differentiation process, it is of utmost importance to understand the anatomical and cell biological specification processes during human embryonic heart development.

1.3.1 Anatomical embryonic cardiogenesis

During embryonic development, the cardiovascular system is the first functional apparatus arising on day 18/19 p.c. (Betts et al., 2013; Schünke et al., 2018). The early development of the cardiovascular

system is necessary as the embryo is not able to absorb enough nutrients solely via diffusion when a layer thickness above 0.1 mm is reached.

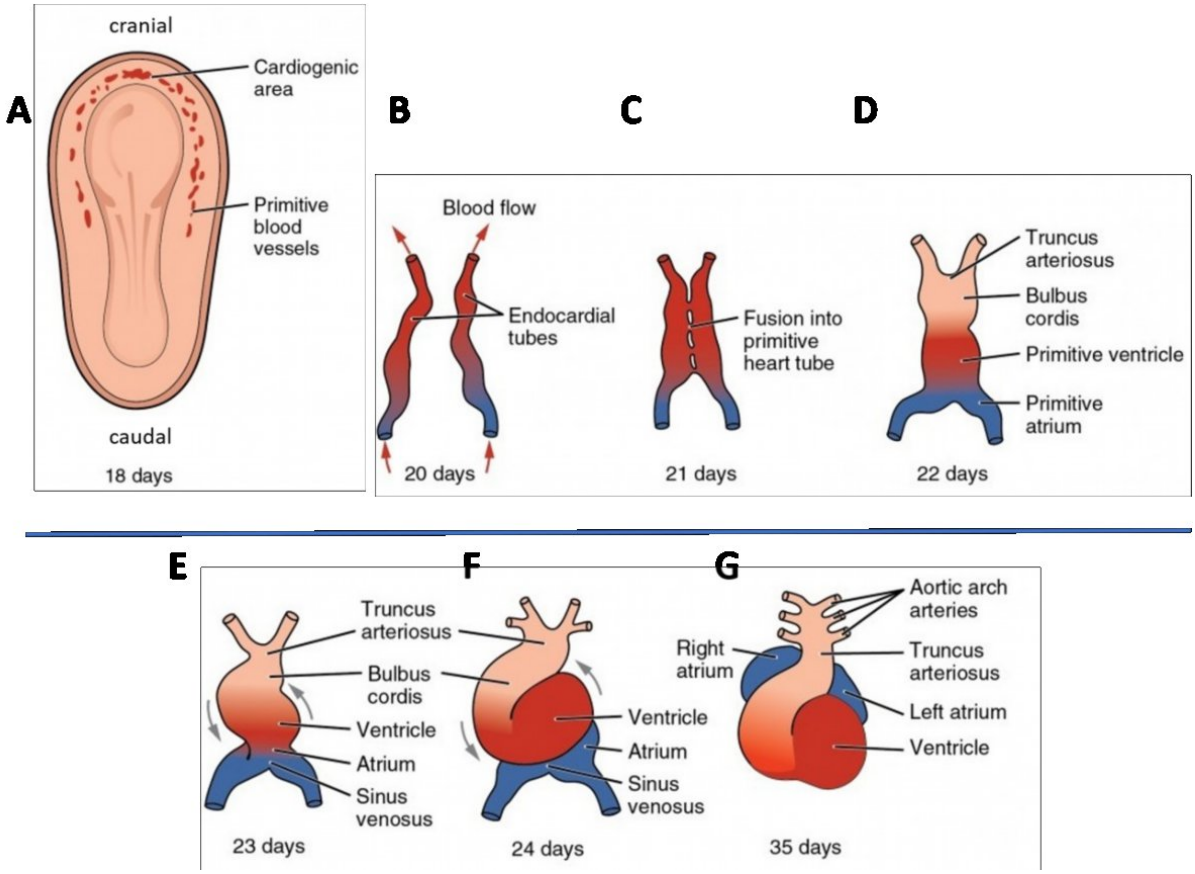

Figure 1: Depiction of the human heart development.

A:

Cardiovascular development commences on day 18 with the formation of the cardiogenic area. **B, C:** On day 20, two endocardial tubes formed which fuse on day 21. **D:** The primitive heart tube with four different regions is present on day 22. **E, F:** Looping of the heart tube starts on day 23. **G:** On day 35, the looping led to the basis of the four-chambered heart. Adapted from Betts et al., (2013).

Cardiogenesis takes place starting with the formation of the horseshoe-shaped cardiogenic area on day 18 (Figure 1 A) where pairs of endocardial tubes form (Figure 1 B). The fusion of the two endocardial tubes (Figure 1 C) forms a singular primitive heart tube on day 21 (Figure 1 D). Cells of the myocardial plate migrate and border the outer heart tube while the endocardium lines the inside. A colloidal extracellular matrix, the cardiac jelly, lies between these layers containing numerous proteins e.g. glycoproteins, collagen, and glycosaminoglycans. In this state, a distinguishable orientation is already present i.e. the cranial atrial and the caudal ventricular pole. Extra- and intraembryonic veins enter the heart tube caudal. The linear heart tube already exhibits first contractions on day 21 pumping the blood from caudal to cranial into the pairs of dorsal aortas that are connected to the placenta via the umbilical arteries. The heart tube undergoes an elongation before it forms the S-shaped heart tube (cardiac looping) on day 23 (Figure 1 E). During the formation of the S-shape, the cardiac jelly

slowly vanishes resulting in a close distance between the endocardium and myocardium. After the initial asymmetrical looping to the ventrocaudal and right side (D-loop), five regions of the heart tube are definable from the outflow to the inflow side i.e. *truncus arteriosus*, *bulbus cordis*, *ventriculus primitivus*, *atrium primitivus*, and the *sinus venosus* (Figure 1 E, F). These parts give rise to distinct areas of the adult heart; the *bulbus cordis* will become the right ventricle, and the *ventriculus primitivus* forms the left ventricle. Besides the two auricles, the *atrium primitivus* forms the anterior part of both atria while the posterior portion is formed from the *sinus venosus*. The *sinus venosus* also forms the sinoatrial node and the coronary sinus. The basis of the heart is thus fully formed (Figure 1 G). From the fourth week of development onwards, complex septation processes lead to the formation of the inner chambers of the heart and thus to the formation of the four-chambered heart, at the same time the cardiac septa and valves are formed (Hinrichsen, 1990; Betts et al., 2013; Gutberlet, 2017; Ulfig and Brand-Saberi, 2017).

1.3.2 The myocardium

The three-layered heart wall is composed of the inner endocardium, the cardiac muscle (myocardium), and the outer epicardium (Betts et al., 2013). Intercalated discs appear at the connection points of adjacent cardiomyocytes on the Z-line (Figure 2) and contain desmosomes, adherens junctions, and gap junctions. Desmosomes function as anchor points holding the cells together to withstand mechanical stress during contractions. Adherens junctions also build mechanical intercellular bridges between adjacent cells. They function as an anchor point for actin filaments and keep the cardiomyocytes close together enabling transmission of contractile force from one cell to another. The function of gap junctions is the electric coupling of the cardiomyocytes connecting their cytoplasm (Betts et al., 2013). An excitation originates from the sinus node and spreads evenly across the atria and is then transmitted to the myocardium of the ventricles via the AV node and the His bundle. Excitation signals are generated autonomously from the nervous system via pacemaker cells. These cells are self-excitable and able to fire action potentials on their own, which is called autorhythmicity (Betts et al., 2013).

In the heart, the thickness of the myocardium varies between the right ventricle of ~4 mm and the left ventricle of ~15 mm which is due to the generation of a great amount of pressure of the left ventricle to overcome the higher resistance of pumping blood into the long system circuit than the right ventricle that pumps blood into the shorter pulmonary circuit (Zilles and Tillmann, 2010; Betts et al., 2013). Cardiomyocytes contain myofibrils and densely packed mitochondria to maintain the ability to contract. They show a distinct organization of myofibrils that consist of myofilaments which in turn are composed of thin actin filaments and thick myosin filaments (Figure 2). These units constitute the contractile part of cardiomyocytes and are arranged parallel to each other along the longitudinal axis

of the cell and are subdivided into shorter units called sarcomeres by transverse Z-disks. Thin actin filaments are anchored to the Z-discs while the myosin filaments project into the actin filaments from the middle of a sarcomere to both sides. The I-band surrounding the Z-line is the region of thin filaments that is not superimposed by myosin filaments. The A-band is defined as the whole length of the myosin filaments. The H-zone is the region of myosin filaments not overlapping with actin filaments and the M-line represents the middle of a sarcomere (Figure 2) (Betts et al., 2013).

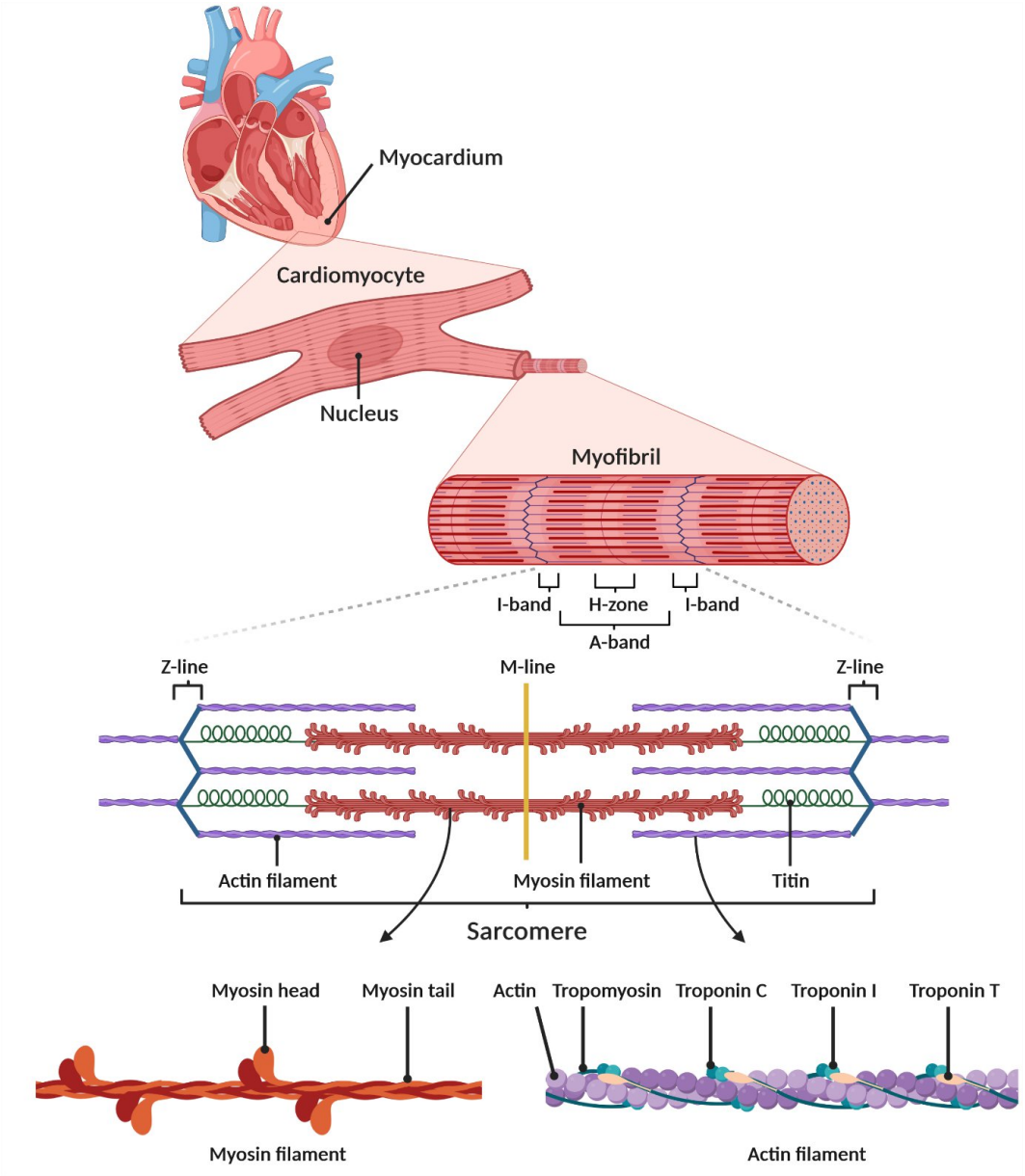

Figure 2: Myofibril structure of the heart.

The myocardium consists of cardiomyocytes that contain myofibrils. Myofibrils show a typical organization of sarcomeres arranged in repeating units which are composed of thin actin and thick myosin filaments and titin. The myosin filament is rod-shaped and has so-called myosin heads. The actin filament is composed of actin polymerized into a filament surrounded by tropomyosin. The troponin complex consisting of Troponin I, C, and T is bound to tropomyosin at a regular distance. The sarcomere is divided into multiple sections i.e. the I-band, A-band, H-zone, Z-line, and M-line. Adapted from Golob et al. (2014). Created with biorender.com.

Contractions lead to a shortening of the muscle, with the thin and thick filaments sliding past each other. Although there is an overall shortening of each sarcomere, the individual filaments retain their original length. When the muscle relaxes, this process is reversed. In addition to actin and myosin, other proteins within the sarcomere are involved in the processes described. Troponin and tropomyosin are regulatory proteins bound to the actin filament (Betts et al., 2013; Golob et al., 2014). The filamentous protein titin reaches from the Z-line to the M-line (Figure 2). Titin behaves like a spring during the contraction and relaxation of the sarcomere and prevents hyperextension (Golob et al., 2014).

1.3.3 Cell biological embryonic cardiogenesis

As the focus of this study is cardiomyocyte differentiation from human induced pluripotent stem cells (hiPSCs), the cell biological development of these cells is described herein. However, the adult functional human heart is composed of multiple cell types including atrial and ventricular cardiomyocytes, cardiac fibroblasts, endocardiac cells, cells of the valves, connective tissue cells, cells of the conduction system, as well as smooth muscle cells and endothelial cells of the coronary arteries and veins (Betts et al., 2013).

Cell biological embryonic cardiogenesis is about the specification of progenitor cells, their migration to a distinct area, and ultimately the differentiation into the necessary cell types. The formation of the cardiogenic area (Figure 1 A) arises from the mesoderm. Together with the ecto- and endoderm the mesoderm is formed during gastrulation as one of the three germ layers. It is further divided into three main regions, namely the paraxial mesoderm, the intermediate mesoderm, and the lateral mesoderm. Cardiac mesoderm cells are a precursor cell population that migrate out of the primitive streak to the positions of the two heart fields (Saga, 2000). An early marker for the cardiac mesoderm progenitor cell population is mesoderm posterior 1 (*Mesp1*). As soon as *Mesp1*-positive cells leave the primitive streak, *Mesp1* is downregulated. Tracing experiments marking the cells permanently as soon as they once expressed *Mesp1* showed that *Mesp1*-expressing cells were present in all heart-related lineages including the myocardium, the endocardium, conduction cells, and the epicardium. In addition, *Mesp1* induces and promotes the expression of key cardiac genes including GATA binding protein 4 (*Gata4*), heart and neural crest derivatives expressed 2 (*Hand2*), and NK2 homeobox 5 (*Nkx2.5*) directly binding to parts of these genes (Bondue and Blanpain, 2010). Additionally, *Mesp1* suppresses the expression of early mesodermal and endodermal genes promoting cardiovascular specification while inhibiting other cell fates. As mentioned before, *Mesp1*-positive cells mark both heart fields migrating to different positions. One cell population is a subpopulation of the lateral mesoderm which splits morphologically into two layers namely the somatic mesoderm that abuts the ectoderm and the splanchnic mesoderm that abuts the endoderm (Hinrichsen, 1990). Cardiac mesoderm cells of the

splanchnic mesoderm are referred to as the first heart field (FHF) building the cardiac crescent. Studies in chicken and mice have proven that the second heart field (SHF) is a subpopulation located in the pharyngeal mesoderm which is a subdomain of the paraxial mesoderm (Kelly et al., 2001; Mjaatvedt et al., 2001; Waldo et al., 2001; Zaffran et al., 2004). Splanchnic mesoderm and pharyngeal mesoderm are contiguous (Kelly et al., 2001).

It is generally agreed on that the FHF gives rise to the primitive heart tube showing a left-ventricular fate but ultimately giving rise to the left ventricle, atrioventricular canal, sinus venosus, and parts of the atria (Meilhac et al., 2004). Cells of the FHF express cardiac markers before the formation of the primitive heart tube already in the cardiac crescent while cells of the SHF are kept in a proliferating state (Meilhac et al., 2004). After formation of the primitive heart tube arising from the FHF, the SHF lies dorsally and medially adjacent to the poles of the heart tube. Timely shifted, cells of the SHF migrate and contribute to the poles of the heart tube leading to its elongation. Ultimately the SHF gives rise to the right ventricle, the outflow tract, and parts of the atria (Stalsberg and DeHaan, 1969; Virágh and Challice, 1973; de la Cruz et al., 1977; Meilhac et al., 2004). However, not much is known about the cell biological processes that lead to the formation of the heart tube. Nevertheless, mutations were identified that led to a perturbation of this process. The absence of *Gata4* or forkhead box protein P4 (*Foxp4*) leads to cardiac bifida which is characterized by the development of two hearts due to the lack of fusion of the two halves of the cardiac crescent at the midline (Kuo et al., 1997; Molkentin et al., 1997; Li et al., 2004). In general, a specific marker for the FHF remains elusive. The marker T-box transcription factor 5 (*Tbx5*) was thought to be exclusively for the FHF but was also detected to be present in subdomains in the SHF (Bruneau et al., 2001; Xie et al., 2012). Initially, Insulin gene enhancer protein 1 (*Isl1*) was thought to mark cells of the SHF (Cai et al., 2003). However, follow-up studies revealed the expression of *Isl1* in the FHF and the SHF (Prall et al., 2007) suggesting that *Isl1* plays a pivotal role in the control of proliferation in general not being specifically expressed in a progenitor cell population or the heart fields (Van Den Berg et al., 2009). However, other SHF-exclusive markers were identified, namely fibroblast growth factor 10 (*Fgf10*) and forkhead box H1 (*Foxh1*) (Kelly et al., 2001; von Both et al., 2004). Mutations of the SHF mostly lead to arterial and venous pole defects (Ward et al., 2005), reviewed in Zaffran and Kelly (2012). A more recent study showed that cells expressing *Mesp1* are already distinguishable into cells of the FHF and SHF (Lescroart et al., 2014), which will enable the possibility of detecting more specific markers for the FHF and SHF in the future.

1.3.4 Main signaling pathways involved in cardiogenesis

The spatial-temporal orchestration of multiple signaling pathways during embryonic development is of utmost importance for initiating and reaching the correct cell process e.g. proliferation, differentiation, migration, and specification. For cardiomyocyte differentiation, three signaling

pathways are the main drivers namely the WNT, bone morphogenetic protein (BMP), and fibroblast growth factor (FGF) signaling pathways. For the differentiation of hiPSCs into cardiomyocytes *in vitro*, it is important to understand and modulate these pathways in a distinct time frame.

1.3.4.1 WNT signaling pathway

The name WNT originates from a combination of the gene names *wingless* and *wingless-type MMTV integration site family, member 1* (*int1)* that are conserved throughout the species *Drosophila melanogaster* and mammals (Rijsewijk et al., 1987). WNT proteins are cysteine-rich secreted glycoproteins and play an important role in regulating elementary cellular processes such as differentiation, proliferation, and cell polarity and act through different signaling pathways (Tian et al., 2010). The canonical WNT pathway is the best-understood one and will be explained further as it plays a major role in cardiomyocyte differentiation.

In the activated form of the pathway, WNT proteins act on target cells by binding to a receptor complex consisting of the G protein-coupled receptor frizzled and low-density lipoprotein receptor-related protein 5/6 (LRP5/6) (Figure 3, left). Subsequently, the signal is transduced to dishevelled. The protein dishevelled is then recruited to the receptor complex binding the destruction complex consisting of glycogen synthase kinase 3 β (GSK3B), casein kinase 1 α 1 (CK1A), and the scaffold proteins adenomatous polyposis coli (APC) and axin. As a consequence, β-catenin accumulates in the cytoplasm and translocates to the nucleus. There it interacts with DNA-binding transcription factors from the transcription factor/lymphoid enhancer-binding factor (TCF/LEF) family, activating the expression of specific target genes. In the inactivated form of the pathway, cytoplasmic β-catenin levels are kept low by continuous phosphorylation mediated through the destruction complex (Figure 3, right). After its phosphorylation by the destruction complex, β-catenin is degraded via the ubiquitin-proteasome system. Thus, the accumulation of β-catenin and its translocation to the nucleus is prevented (Logan and Nusse, 2004).

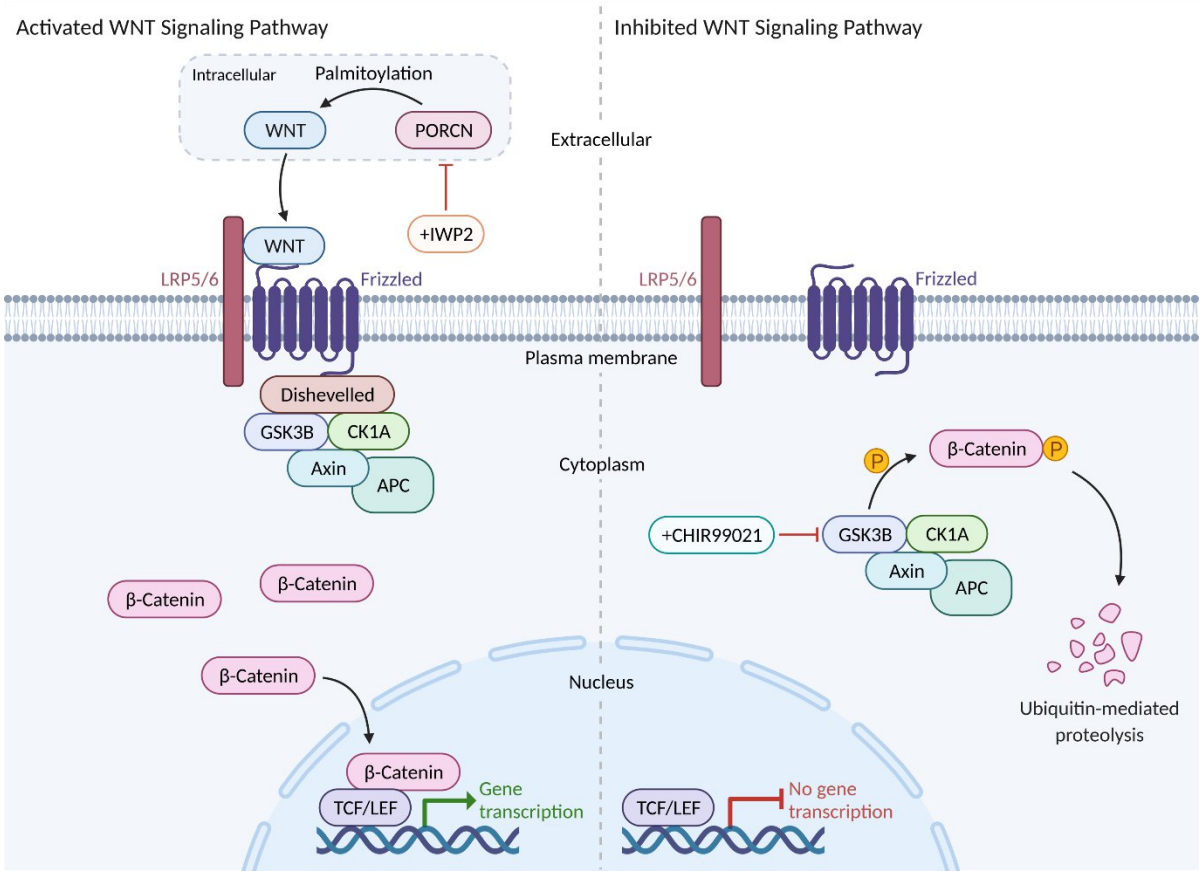

Figure 3: Canonical WNT signaling pathway.

On the left side, the ligand WNT is present binding to the receptor complex of frizzled and LRP5/6. Dishevelled is then recruited to the receptor complex binding the destruction complex composed of GSK3B, CK1A, APC, and axin. Subsequently, β-catenin accumulates in the cytoplasm and enters the nucleus. A complex of β-catenin and TCF/LEF activates target genes. A modulated inhibition is achieved by adding IWP2. This small molecule inhibits the function of PORCN which palmitoylates the WNT protein before its secretion. On the right side, the ligand WNT is not present. The destruction complex continuously phosphorylates β-catenin which is then degraded by ubiquitin-mediated proteolysis. Thus, preventing gene transcription. A modulated activation of the pathway is achieved by adding CHIR99021. This small molecule blocks GSK3B which is part of the destruction complex leading to its inactivation. Then, β-catenin accumulates and enters the nucleus activating gene transcription by binding to TCF/LEF. LRP5/6 = low-density lipoprotein receptor-related protein 5/6, TCF/LEF = transcription factor/lymphoid enhancer-binding factor, IWP2 = Inhibitor of WNT production 2, PORCN = Porcupine, GSK3B = glycogen synthase kinase 3 β, CK1A = Casein kinase 1 α 1, APC = adenomatous polyposis coli. Adapted from "Wnt Signaling Pathway Activation and Inhibition", by BioRender.com (2022). Retrieved from https://app.biorender.com/biorender-templates.

Modulation of the WNT pathway *in vitro* is achieved using small molecules. The addition of inhibitor of WNT production 2 (IWP2) leads to the inhibition of the WNT pathway (Figure 3, left). This is mediated through the inhibition of porcupine (PORCN), an enzyme involved in the palmitoylation of WNT proteins. Without this step, WNT proteins are not secreted and can not reach their respective receptor (Chen et al., 2009; You et al., 2016). On the other hand, the activation of the pathway is mediated through the small molecule CHIR99021 (CHIR), which directly inhibits GSK3B which is part of the destruction complex (Naujok et al., 2014), leading to the accumulation of β-catenin (Figure 3, right). The activation and inhibition of the WNT signaling pathway play an important role during heart

development as it has a biphasic role (Naito et al., 2006). While early in development the activation of the WNT pathway promotes the development of the lateral mesoderm, the inhibition at a later stage is necessary to define the heart fields (Ueno et al., 2007).

1.3.4.2 BMP signaling pathway

BMPs belong to the transforming growth factor beta (TGFβ) superfamily of proteins. The name BMP stems from the original discovery to induce bone and cartilage formation, however, they are now known to play crucial roles in embryogenesis and development (reviewed in Wang et al., 2014). BMPs are heterodimeric proteins that bind to the two heterodimeric transmembrane serine/threonine kinase receptors type I and type II. The TGFβ superfamily comprises seven type I and four type II receptors but not all of them are capable of binding BMPs. Within type I receptors, three are able to bind BMPs, namely, Activin-like kinase (ALK) 2, 3, and 6 (Ten Dijke et al., 1994; Ebisawa et al., 1999). Of the type II receptors, three can bind BMPs, namely, BMPR-II, ActR-IIA, and ActR-IIB (Rosenzweig et al., 1995; Macías-Silva et al., 1998).

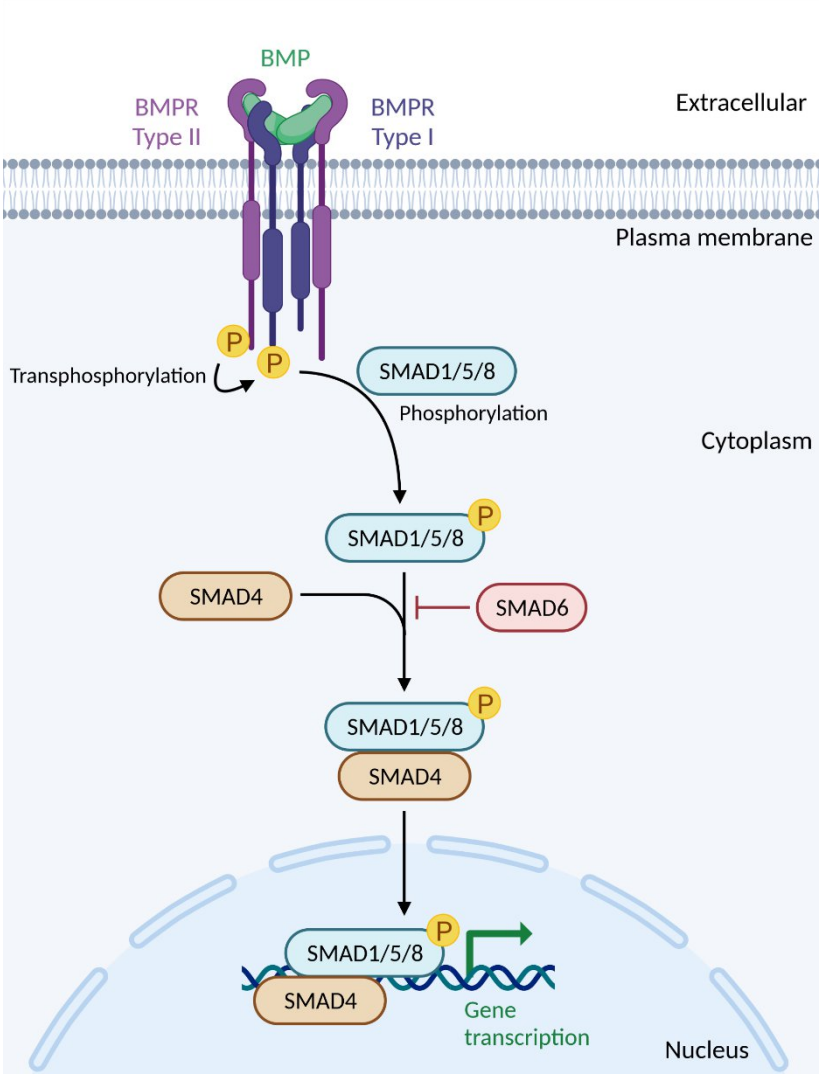

Figure 4: BMP canonical SMAD-dependent signaling pathway.

The signal transduction cascade is initiated by the binding of BMPs to two dimers of type I and type II serine/threonine kinase receptors. The activated type II receptor then transphosphorylates the type I receptor which in turn phosphorylates SMAD1, 5, or 8. SMAD4 then binds to the phosphorylated SMAD1, 5, or 8 building a complex that translocates into the nucleus where it regulates gene expression. SMAD6 acts as an inhibitor regulated by a negative feedback loop. BMP = bone morphogenetic protein, SMAD = small mothers against decapentaplegic homolog. Adapted from "BMP Signaling Pathway", by BioRender.com (2022). Retrieved from https://app.biorender.com/biorender-templates.

Once BMP has bound to the receptor complex, the type II receptor transphosphorylates the type I receptor activating it (Figure 4). Subsequently, the type I receptor phosphorylates one of the receptor-regulated small mothers against decapentaplegic homologs (SMAD) named R-SMADs. R-SMADs involved in BMP signaling are SMAD1, 5, and 8. The phosphorylated R-SMAD forms a complex with SMAD4 translocating into the nucleus and ultimately regulating gene transcription functioning as a transcription factor (Figure 4). SMAD6 is an inhibitory SMAD whose transcription is activated via BMP signaling resulting in a negative feedback loop inhibiting receptor activity (Afrakhte et al., 1998; Goto et al., 2007).

BMP4 in particular is involved in the mesoderm formation early on during gastrulation. As a result, *Bmp4*-null mice are embryonically lethal, lacking the mesoderm (Winnier et al., 1995). The addition of BMP4 is an important approach to modulating the pathway for mesoderm formation *in vitro*. Later on during development, BMP4 is required for outflow tract septation, cushion remodeling, and valve maturation (McCulley et al., 2008).

1.3.4.3 FGF signaling pathway

FGFs are a large family of 22 proteins of which four are intracellular and 18 are secreted proteins that interact with four alternatively spliced variants of the FGF receptor (*$FGFR_{1-4}$)* genes resulting in seven forms of signaling tyrosine kinase FGF receptors, regulating diverse biological processes including cell proliferation, differentiation, survival, and migration (Ornitz and Itoh, 2015). FGF binding leads to the dimerization and activation of the FGFRs. Heparan Sulfate ProteoGlycan (HSPG) acts as an essential cofactor for the binding of FGFs (Kan et al., 1993). Activated FGFRs mediate intracellular signaling including the STAT (Dudka et al., 2010), PLCG (Peters et al., 1992), RAS-MAPK (Kouhara et al., 1997), and PI3K-AKT (Lamothe et al., 2004) pathways. In this work, the role of FGF2 is important which is also referred to as basic FGF. It promotes the development of mesoderm (Burdsal et al., 1998) and in mouse stem cells promotes cardiomyogenic differentiation (Kawai et al., 2004).

1.4 Human induced pluripotent stem cells

Human iPSCs represent an unlimited human cell source and possess the same characteristics as human embryonic stem cells (hESCs), e.g. self-renewal, pluripotency, and capability to differentiate into cells of all three germ layers. Furthermore, no embryos are required for the generation of hiPSCs, eliminating ethical concerns that are associated with embryonic stem cell (ESC) research. Induced PSCs were first generated by Prof. Dr. Shinya Yamanaka and colleagues from murine and human fibroblasts introducing a battery of transcription factors into the cells via a gammaretrovirus. The so-called Yamanaka cocktail consists of key transcription factors responsible for pluripotency namely octamer-binding protein 4 (*OCT4*), SRY (sex determining region Y)-box transcription factor 2 (*SOX2*), Kruppel-like factor 4 (*KLF4*), and MYC proto-oncogene, bHLH transcription factor (*c-MYC*) (Takahashi and Yamanaka, 2006; Takahashi et al., 2007). Since the discovery of hiPSCs, research with hiPSCs has become one of the fastest-growing research areas and numerous methods have been developed to facilitate the generation of these cells. It was discovered that hiPSCs can be obtained not only from fibroblasts (Takahashi et al., 2007) but also from e.g. extraembryonic tissue from the placenta, umbilical cord (Cai et al., 2010), blood mononuclear cells (Loh et al., 2009), or cells from urine (Zhou et al., 2012). In principle, every somatic cell is suitable to be reprogrammed into iPSCs (reviewed in Raab et al., 2014). Furthermore, the techniques of expressing the key transcription factors in the cell were improved. The original work used retroviral vectors and similar to lentiviral vectors, these bear

the disadvantage of integrating into the genome and potentially interfering with transcriptional active parts of the genome which may influence translation studies. Today, non-integrating systems e.g. episomal vectors, and methods based on small molecules or proteins as well as viral vectors such as Adenovirus and Sendaivirus are used (reviewed in Al Abbar et al., 2020).

Suitable *in vitro* models reflecting the human heart are of great interest and gained recognition in recent years in the life sciences. These models can reflect basic physiological and pathological processes as well as being of great importance for substance screening and the investigation of the toxicity of drugs and chemicals. One of the earliest approaches to generating beating cardiomyocytes based on human cells was the formation of EBs using hESCs cultured in a serum-containing medium (Kehat et al., 2001). After the development of hiPSCs, this approach was adapted and it was proven that hiPSCs are also capable to differentiate into cardiomyocytes exhibiting expression of cardiomyocyte-specific proteins such as myosin, cardiac troponin, and α-actinin (Zhang et al., 2009). However, the purity of hiPSC-derived cardiomyocytes was often low, which compromises reproducibility and limits the use of the cells for downstream applications (Mummery et al., 2012; Smith et al., 2017). Advances have been made in increasing the efficiency of generating high-purity hiPSCs-derived cardiomyocytes resulting in the development of multiple protocols based on the temporary modulation of the WNT signaling pathway using shRNAs or small molecules (Lian et al., 2012, 2013; Burridge et al., 2014; Zhang et al., 2015). Besides the modulation of the WNT signaling pathway, these studies showed that the modulation of the BMP, Activin/Nodal, and FGF pathways can also be advantageous for cardiomyocyte differentiation. Human iPSC-derived cardiomyocytes generated with those methods represent embryonic to fetal-like features depending on the period of culture *in vitro*. Assays that investigate embryotoxicity by differentiating human stem cells with specific regard to the development into cardiomyocytes have been developed over the past years (Adler et al., 2008; Aikawa, 2020; Lauschke et al., 2020; Walker et al., 2021).

1.5 Aim of this thesis

The paradigm shift in toxicology is driving the development of human-based *in vitro* test methods, also in the field of reproductive toxicology. New approach methodologies (NAMs) are developed for risk assessment fit for regulatory purposes while reducing animal testing (Gibb, 2008; Pistollato et al., 2021; Stucki et al., 2022). Therefore, this study aimed to establish and characterize a hiPSC-based *in vitro* embryotoxicity test as an alternative method for animal testing with specific regard to the differentiation into beating cardiomyocytes. Substances with known positive and negative effects on embryonic development were tested for NAM predictivity.

Therefore, the following tasks were addressed:

1) Set-up of the hiPSC-based test system for the generation of beating cardiomyocytes.

2) Molecular and cellular characterization of the differentiating hiPSCs.

3) Set-up of a test method for embryotoxicity testing with a training set of compounds.

2 Materials

2.1 Laboratory equipment

Table 1: Laboratory equipment.

Product	Labeling	Manufacturer
Analytical scale	A200S	Sartorius
Benchtop centrifuge	MIKRO 220/220R (Type 2205) and MIKRO 22R (Type 1110)	Hettich
Centrifuge	Rotanta/RPC D-7200	Hettich
CO_2-Incubator	CB 170	Binder
Digital microscope system	DMS1000 B (Light Base MDG33)	Leica Microsystems
Electronic repetitive pipette	Multipette E3x	Eppendorf
Flake ice maker	AF200	Scotsman
Flow cytometer	FACSCanto II Cell Analyzer	Becton, Dickinson and Company
Freezer container	Mr. Frosty	Thermo Scientific
Fridge-freezer combination	Liebherr Comfort CUP 3021	Liebherr
High-content screening imaging platform	CellInsight CX7 LZR Platform	Thermo Scientific
Mechanic repetitive pipette	Multipette M4	Eppendorf
Microcentrifuge	SBS-MZ-4000/6-1.5	Steinberg Systems
Microscope	Olympus CKX53SF	Olympus
Microscope camera	SC50	Olympus
Multimode-microplate-reader	Infinite 200 PRO	Tecan Trading AG
PCR-cycler	Rotor-Gene Q	Qiagen
Pipet aid	Pipetus	Hirschmann
Single-channel pipettes (0.5-10/10-100/100-1000µL)	Research plus	Eppendorf
Sterile workbench	Mars Class 2 Safety Cabinet	Scanlaf
Thermocontrol System	MATS Type-TL	Leica Microsystems
Thermocycler	T3 Thermocycler	Biometra
Ultra low-temperature freezer	HERAFreeze HDE50086FV	Thermo Fisher Scientific
Vacuum pump	N86 LABOPORT	KNF Neuberger
Vortex shaker	REAX 2000 RS-VA10	Heidolph Phoenix Instrument

2.2 Consumable supplies

Table 2: Consumable supplies.

Product	Product number	Manufacturer
Cell culture plate, 24-well	83.3922	Sarstedt
Cell culture plate, 48-well	677180	Greiner Bio-One
Cell culture plate, 6-well	83.3920	Sarstedt
Cell culture plate, 96-well	655161	Greiner Bio-One
Combitips advanced, 0.1 mL	0030089618	Eppendorf
Combitips advanced, 0.5 mL	0030089634	Eppendorf
Combitips advanced, 10 mL	0030089677	Eppendorf
Combitips advanced, 5 mL	0030089871	Eppendorf
Counting chamber, C-Chip Neubauer improved	DHC-N01	NanoEnTek
Cryovials, 2 mL	710522	Biozym Scientific
Filter tips, 10 µL	07-602-8300	nerbe plus
Filter tips, 100 µL	692066	Biozym Scientific
Filter tips, 1000 µL	692078	Biozym Scientific
Parafilm	4AJ-9170002	Lab Unlimited
PCR 0.1 ml 4-Tube and 4-Cap Strips	711200X	Biozym Scientific
Reaction vessel, 0.5 mL	6.266.733	Faust Lab Science
Reaction vessel, 1.5 mL	616201	Greiner Bio-One
Reaction vessel, 2.0 mL	0030 120.094	Eppendorf
Reaction vessel, 5.0 mL	72.701.400	Sarstedt
Sample tubes for flow cytometry	55.1579	Sarstedt
Screw cap tube, 15 ml	62554502	Sarstedt
Screw cap tube, 50 ml	62559001	Sarstedt
Serological pipette, 10 mL	607180	Greiner Bio-One
Serological pipette, 25 mL	760180	Greiner Bio-One
Serological pipette, 5 mL	606180	Greiner Bio-One

2.3 Materials for cell biological work

2.3.1 Cell culture media components and additives

Table 3: Cell culture media components and additives.

Product	Product number	Manufacturer
2-Phospho-L-Ascorbic Acid 10g	013-12061	FUJIFILM Wako Pure Chemical Corporation
Accutase	A11105-01	Life technologies
Animal-Free Recombinant Human FGF-basic (154 a.a.)	AF-100-18B	PeproTech
Chemically Defined Lipid Concentrate	11905031	Thermo Fisher Scientific
CHIR99021	4423	Tocris
Dimethyl sulfoxide (DMSO) 99,5 %	A994	Carl Roth GmbH + Co. KG
DMEM/F12, without L-glutamine	21331020	Thermo Fisher Scientific, Gibco
Dorsomorphin	sc-200689 3093	Santa Cruz Biotechnology Tocris
DPBS, calcium, magnesium	14040174	Thermo Fisher Scientific, Gibco
Dulbecco's Phosphate Buffered Saline w/o Ca^{2+}, Mg^{2+}	D8537	Merck
Human Activin A recombinant protein	78001	Stemcell Technologies
Human serum albumin	05-720-1B	Biological Industries
Human TGF beta 1 Carrier-Free Recombinant Protein	15538796	Thermo Fisher Scientific, eBioscience
Human Transferrin	T8158	Merck
ITS Premix Universal Culture Supplement	354350	Corning
IWP2	3533	Tocris
KnockOut DMEM	10829018	Thermo Fisher Scientific, Gibco
L-Glutamine (200 mM)	25030081	Thermo Fisher Scientific, Gibco
Penicillin-Streptomycin	P06-07050	PAN-Biotech
Recombinant Human BMP4 Protein	314-BP	R&D Systems
Y-27632	HB2297	HelloBio
Sodium selenite ≥ 98 %	S5261	Merck

2.3.2 Coating solutions

Table 4: Coating solutions.

Product	Product number	Manufacturer
Human recombinant Laminin 521	LN521	BioLamina AB
Matrigel matrix high concentration, growth factor reduced, LDEV-free	354263	Corning

2.3.3 Materials for gene expression analysis

Table 5: Materials for gene expression analysis.

Product	Product number	Manufacturer
DEPC H_2O	T143	Carl Roth
DNase I Digest Kit, peqGOLD	12-1091-01/02	VWR Peqlab
dNTP Mix	NU-1006L	Jena Bioscience GmbH
Ethanol ≥ 70 %, denatured	T913.2	Carl Roth
Ethanol ≥ 99,5 %, extra pure	5054.4	Carl Roth
M-MLV reverse transcriptase + RT Reaction Buffer (5x)	M170A	Promega
Oligo (dT)15	PM-303L	Jena Bioscience GmbH
peqGOLD Total RNA Kit	13-6834	VWR
QIAquick PCR Purification Kit	28104	Qiagen
QuantiFast SYBR Green PCR	204056	Qiagen

2.3.4 Materials for flow cytometry analysis

Table 6: Materials for flow cytometry analysis.

Product	Product number	Manufacturer
BD Cytofix Fixation Buffer	554655	BD Biosciences
BD Horizon Fixable Viability Stain 510	564406	BD Biosciences
BD Perm/Wash Perm/Wash Buffer	554723	BD Biosciences
BD Pharmingen Stain Buffer (FBS)	554656	BD Biosciences
For human induced pluripotent stem cell analysis		
BD Pharmingen FITC Mouse anti-SSEA-4	560126	BD Biosciences
BD Pharmingen FITC Mouse IgG3, κ Isotype Control	555578	BD Biosciences
BD Stemflow Human Pluripotent Stem Cell Transcription Factor Analysis Kit	560589	BD Biosciences
For cardiomyocyte analysis		
BD Pharmingen Alexa Fluor 647 Mouse Anti-GATA4	560400	BD Biosciences
BD Pharmingen Alexa Fluor 647 Mouse IgG1 κ Isotype Control	557732	BD Biosciences
BD Pharmingen PE Mouse Anti-Cardiac Troponin T	564767	BD Biosciences
BD Pharmingen PE Mouse IgG1, κ Isotype Control	550617	BD Biosciences
REAfinity REA Control Antibody (I), human IgG1, FITC	130-118-354	Miltenyi Biotec
REAfinity α-Actinin (Sarcomeric) Antibody, anti-human/mouse/rat, FITC	130-119-806	Miltenyi Biotec

BD = Becton, Dickinson and Company

2.3.5 Materials for immunocytochemistry

Table 7: Materials for immunocytochemistry.

Product	Product number	Manufacturer
Bisbenzimid H 33258 (Hoechst 33258)	B1155	Merck
DPBS (10x) w/o Ca^{2+} and Mg^{2+}	P04-53500	PAN-Biotech

Goat anti-Mouse IgG (H+L) Cross-Adsorbed Secondary Antibody, Alexa Fluor 488	A-11001	Thermo Fisher Scientific
Goat serum	G9023	Merck
Mouse Anti-Cardiac Troponin T antibody [1C11]	ab8295	Abcam
Paraformaldehyde (PFA)	P6148	Merck
Triton X-100	T8787	Merck

2.3.6 Substances for cell exposure

Table 8: Substances for cell exposure.

Substance	CAS-Nr.	Product number	Manufacturer
5-Fluorouracil	51-21-8	F6627	Merck
Nocodazole	31430-18-9	M1404	Merck
Penicillin G sodium salt	69-57-8	PENNA	Merck
Triclabendazole	68786-66-3	32802	Merck
Triclabendazole sulfoxide	100648-13-3	35391	Merck

2.4 Software

Table 9: Software.

Software	Version number	Application
BD FACSDiva	6.1.3	Flow cytometry analysis
cellSens Entry	1.18	Microscope
FlowJo	10.7.1	Flow cytometry analysis
GraphPad Prism	8.4.3.686	Statistical analysis
HCS Studio Navigator	6.6.2	Fluorescence microscope
i-control	3.22	Multimode-microplate-reader
ImageJ	1.53a	Image editing
Microsoft Excel	1808	Statistical analysis
Microsoft Word	1808	Text processing
Rotor-Gene Q Series	2.3.4	qRT-PCR analysis

BD = Becton, Dickinson and Company

3 Methods

With regards to the cell culture, all described methods hereinafter were performed under sterile conditions using aseptic techniques. Media and reagents used for cell culture were heated to 37 °C in a water bath before application if not stated otherwise.

3.1 Coating of culture plates

Regardless of the coating, plates were equilibrated at room temperature (RT) for at least 15 min before use. The coating solution was always entirely removed with a vacuum pump before cells were seeded in the respective medium.

3.1.1 Biolaminin 521

Human iPSCs were routinely cultured on 6-well plates (Sarstedt, #83.3920) coated with LN521 (BioLamina, #LN521). The stock solution (100 µg/mL) was aliquoted into smaller single-use aliquots of 150 or 250 µL and stored at -20 °C until further use. Working solutions were prepared by diluting LN521 to 5 µg/mL with PBS with $Ca^{2+}/Mg^{2+\,(+/+)}$ (Thermo Fisher Scientific, #14040174). One 6-well was coated with 1 mL of the working solution consisting of 50 µL LN521 and 950 µL of PBS $^{+/+}$. To ensure an equal growth of the cells, coverage of the entire well with the working solution was a necessity. For storage, plates were covered with Parafilm to reduce evaporation and were placed at 4 °C for 24 h before usage. Following these storage conditions, coated plates can be used for up to four weeks.

3.1.2 Matrigel

Every procedure including the handling of Matrigel was performed on ice, all materials used were prechilled to 4 °C. The Matrigel stock solution was stored at -20 °C. Working solutions were prepared by diluting the Matrigel stock solution 1:3 with KnockOut DMEM (KODMEM) (Thermo Fisher Scientific, #10829018). The working solution was refrozen at 1 mL aliquots in 15 mL conical tubes at -20 °C. For coating, one 1 mL Matrigel aliquot was placed on ice. A volume of 24 mL 4 °C cold KODMEM was pipetted into a 50 mL conical tube also placed on ice. A volume of 6 mL KODMEM was taken out of the 24 mL to dissolve the Matrigel working solution by pipetting up and down with a 10 mL serological pipette. The Matrigel solution was then transferred to the remaining volume of KODMEM, resulting in a total volume of 25 mL and a dilution of 1:75. The solution was further diluted at 1:4 with KODMEM. For this, two 50 mL conical tubes were prefilled with 36 mL of 4 °C cold KODMEM on ice. In each 50 mL tube, 12 mL of the already pre-diluted Matrigel solution was added resulting in a 1:300 solution. For coating a 24-well plate (Sarstedt, #83.3922), 300 µL of the Matrigel solution was added to each well ensuring an equal distribution on the surface, 150 µL was used for 48-well plates (Greiner Bio-One, #677180). For 96-well plates, 50 µL per well was used. The plates were sealed with Parafilm to

reduce evaporation and placed on a flat surface at RT over night. Afterward, the plates were kept at 4 °C for a maximum of four weeks. The coated plates were stored at 4 °C for at least 24 h before usage for cell culture.

3.2 Cell culture media

The compositions of cell culture media for hiPSC and cardiomyocyte culture are shown in Table 10–12. All components were dissolved and stored according to the manufacturer's advice. To prevent repeated heating of media for cell culture usage, only required volumes of media were taken and heated to 37 °C.

Table 10: Composition of the FTDA medium for hiPSC culture adapted from Frank et al. (2012).

Component	Manufacturer, product number	Stock concentration	Final concentration
DMEM/F12 without L-glutamine	Thermo Fisher, 21331020	Not applicable	Not applicable
Chemically Defined Lipid Concentrate	Thermo Fisher, 11905031	100 %	1 %
Human serum albumin	Biological industries, 05-720-1B	10 %	0,1 %
L-Glutamine	Thermo Fisher, 25030081	200 mM	2 mM
Penicillin Streptomycin	PAN-Biotech GmbH, P06-07050	10,000 U/mL 10 mg/mL	100 U/mL 0,1 mg/mL
Animal-Free Recombinant Human FGF-basic (154 a.a.)	PeproTech, AF-100-18B	25 µg/mL	50 ng/mL
ITS Premix Universal Culture Supplement	Corning, 354351	Insulin 5 µg/mL Transferrin 5 µg/mL Selenious Acid 5 ng/mL	Insulin 5 ng/mL Transferrin 5 ng/mL Selenious Acid 5 pg/mL
Human Activin A recombinant protein	Stemcell technologies, 78001	10 µg/mL	4 ng/mL
Human TGF beta 1 Carrier-Free Recombinant Protein	Thermo Fisher, 34834882	1 µg/mL	0,2 ng/mL
Dorsomorphin	Tocris, 3093	500 µM	50 nM

For the subcultivation of hiPSCs, the FTDA medium (Table 10) was supplemented with 10 µM of the small molecule Y-27632 (HelloBio, #HB2297). Cells were incubated in this medium within the first 24 h before switching to FTDA without Y-27632.

The composition of the ITS medium which was used on day zero of the differentiation protocol is shown in Table 11. Concentrations of CHIR (Tocris, #4423) and BMP4 (R&D Systems, #314-BP) given in Table 11 were determined experimentally for the cell line iPS11 used in this work. To determine the optimal concentrations for differentiation of hiPSCs to cardiomyocytes, different concentration ranges for CHIR (0.5–1.75 µM) and BMP4 (0.75–2 ng/mL) were tested in combination in advance (Zhang et al., 2015).

Table 11: Composition of the ITS medium for induction of cardiomyocyte differentiation based on hiPSCs, adapted from Zhang et al. (2015).

Component	Manufacturer, product number	Stock	Final concentration
KnockOut DMEM	Gibco, 10829018	Not applicable	Not applicable
L-Glutamine	Thermo Fisher, 25030081	200 mM	2 mM
Penicillin Streptomycin	PAN-Biotech GmbH, P06-07050	10,000 U/ml 10 mg/ml	100 U/mL 0,1 mg/mL
ITS Premix Universal Culture Supplement	Corning, 354351	Insulin 5 µg/mL Transferrin 5 µg/mL Selenious Acid 5 ng/mL	Insulin 5 ng/mL Transferrin 5 ng/mL Selenious Acid 5 pg/mL
Y-27632	HelloBio, HB2297	10 mM	10 µM
Animal-Free Recombinant Human FGF-basic (154 a.a.)	PeproTech, AF-100-18B	25 µg/mL	25 ng/mL
Recombinant Human BMP4 Protein	R&D Systems, 314-BP	10 µg/mL	0,75 ng/mL
CHIR99021	Tocris, 4423	10 mM	1,75 µM

For further cultivation of cardiomyocytes, TS medium (Table 12) was used.

Table 12: Composition of the TS medium for hiPSC-derived cardiomyocyte culture adapted from Zhang et al. (2015).

Component		Company and order number	Stock	Final concentration
KnockOut DMEM		Gibco, #10829018	Not applicable	Not applicable
L-Glutamine		Thermo Fisher, #25030024	2 mM	0,02 mM
Penicillin Streptomycin		PAN-Biotech GmbH, #P06-07050	10,000 U/mL 10 mg/mL	100 U/mL 0,1 mg/mL
TS (×100)	hTransferrin	Merck, #T8158	0,55 mg/mL	5,5 µg/mL
	Sodium selenite	Merck, #S5261	0,67 µg/mL	6.7 ng/mL
2-Phospho-L-Ascorbic Acid		Wako, #01312061	250 mM	250 µM

The component TS is a transferrin/sodium selenite working solution. For preparation, 100 mg transferrin was dissolved in 181.82 mL PBS $^{-/-}$ and supplemented with 18.18 µL sodium selenite solution (stock concentration: 6.7 mg/mL). The final concentrations of transferrin and sodium selenite in the TS working solution were 0.55 mg/mL and 0.67 µg/mL, respectively. According to the cardiomyocyte differentiation protocol, TS medium was supplemented with 2 µM IWP2 (Tocris, #3533) on days two and three.

3.3 Human induced pluripotent stem cell culture

The hiPSC-line iPS11 was purchased from Alstem (#iPS11). Cells were retrieved from human foreskin fibroblasts and transfected footprint-free by ectopic expression of OCT4, KLF4, and L-MYC using Alstem episomal plasmids. To ensure a high-standard cell line to work with, a two-tiered-banking process producing a fully characterized Master Cell Bank (MCB) and a partially characterized respective Working Cell Bank (WCB) was generated according to Tigges et al. (2021). Characterization included the study of morphology, mycoplasma contamination, cell line identity, karyotype stability, cell antigen expression and viability, gene expression, pluripotency, and post-thaw recovery.

3.3.1 Thawing of hiPSCs

One cryovial of the WCB contained 1.5×10^6 cells. For thawing, one cryovial was taken out of the nitrogen tank and shortly deaerated under sterile conditions. Afterward, the cryovial was warmed in a water bath set to 37 °C until a pea-sized clump of frozen cells was left. The thawed solution was carefully transferred to a 15 mL conical tube. A volume of 1 mL FTDA (4 °C) was added dropwise to the

thawed cell suspension and the conical tube was shaken after each drop to ensure equilibration of the cells to the new external milieu. Afterward, 1 mL of cold FTDA was added to the cryovial to retrieve the remaining cells. This suspension was also transferred dropwise to the conical tube, which was again shaken after each drop. An additional 2 mL of cold FTDA was added to the conical tube slowly. Cells were centrifuged at 200 g for 5 min at RT. The supernatant was removed with a vacuum pump and cells were resuspended in 4 mL FTDA (37 °C) supplemented with 10 µM Y-27632. Before seeding, the coating solution was removed and 2 mL per LN521-coated 6-well was seeded. Cells were incubated at 37 °C and 5 % CO_2. After 24 h, the cell culture was treated as described in section 3.3.2. Cells were passaged three times before experiments were conducted to ensure a full recovery after thawing.

3.3.2 Cell passaging

Human iPSCs were routinely cultured as single cells on LN521-coated 6-well plates in FTDA medium at 37 °C and 5 % CO_2. Cells were monitored per working day examining their morphology and proliferation using a phase-contrast microscope. Cells were split twice a week when 90–100% confluence was reached. For cell passaging, hiPSCs were first washed once with 1 mL PBS $^{-/-}$ (Merck, #D8537) per 6-well using an aspiration system and serological pipettes to proceed fast preventing the cells to dry out. Then, cells were split enzymatically using 1 mL Accutase (Gibco, #A11105-01) supplemented with 10 µM Y-27632 per 6-well. Cells were incubated for 12 min at 37 °C and 5 % CO_2. After incubation time, the detachment of the cells was checked by shaking the plate carefully and observing floating cells. If cells did not detach, the plate was gently tapped several times on each side of the plate to facilitate the detachment. Afterward, Accutase was diluted by adding 2 mL per 6-well of DMEM/F12 without L-glutamine using a 10 mL serological pipet. To singularize and further detach cells, the cell suspension in every well was pipetted up and down six times before cells were collected in a 50 mL conical tube. Cells in the conical tube were resuspended additional ten times and counted in a Neubauer-improved chamber using an aliquot of 10 µL. Next, the conical tube was tilted before taking out the needed amount to ensure an equal distribution of the cells. Depending on the time until 90–100% confluence was supposed to be reached, 3×10^5 or 4×10^5 cells per 6-well for four or three days, respectively, were centrifuged at 200 g for 2 min at RT. The supernatant was aspirated using a vacuum pump and cells were resuspended in 2 mL FTDA supplemented with 10 µM Y-27632 per 6-well and plated on an LN521-coated 6-well plate. The coating solution was removed beforehand. Note that exposure to 10 µM Y-27632 should not exceed 24 h. The next day onwards, cells were further cultivated in FTDA without Y-27632. Human iPSCs were supplied with an additional 0.5 mL FDTA for every day in culture (2.5 mL per 6-well on the first day after splitting, 3 mL per 6-well on the second day after splitting, etc.). When hiPSCs were in culture for four days, cells were split as described above. However, after at least 2 h cells were fed with an additional 2 mL without Y-27632 to guarantee the survival of the prolonged period (one day) without medium replacement. An induction into cardiomyocytes was only performed

when cells were in culture for three days, otherwise, the efficiency of the induction was reduced. A confluence of 90–100% was critical for the induction as well. Cells were cultured for a maximum of 12 passages for cardiomyocyte differentiation.

3.4 Differentiation of human induced pluripotent stem cells to cardiomyocytes

Cardiomyocyte differentiation was performed as described in Zhang et al. (2015) for 2D cell cultures with minor changes described hereafter. As mentioned above, induction was performed when hiPSCs were cultured for three days and reached a confluence of 90–100%. First, the medium of desired wells was refreshed with 2 mL FTDA per 6-well. After at least 2 h, cells were treated for cell passaging as described in section 3.3.2. After counting, 2.75×10^5 cells per Matrigel-coated 48-well were centrifuged at 200 g for 2 min at RT. The supernatant was aspirated with a vacuum pump and cells were resuspended and seeded in 800 µL per 48-well in ITS medium (Table 11). The plate was tapped carefully in a crosswise motion on an even surface thrice, to ensure a homogeneous distribution of the cells. Afterward, the plate was incubated vibration-free for 20 min at RT to let the cells settle down and attach to the matrix, then the plate was transferred to the incubator (37 °C, 5 % CO_2). After 24 h, ITS medium was completely aspirated with a vacuum pump and replaced with TS medium (Table 12). On day two and three, the medium was removed and changed to TS medium supplemented with 2 µM IWP2. On day four, the medium was replaced with TS medium and changed every other day until day ten. Media changes after 24 or 48 h were performed with an allowance of ± 1 h per day. Of note, from day six onwards medium was changed carefully by manual pipetting with a micropipette as the cells started detaching from the matrix and got sucked in easily when using an aspiration system.

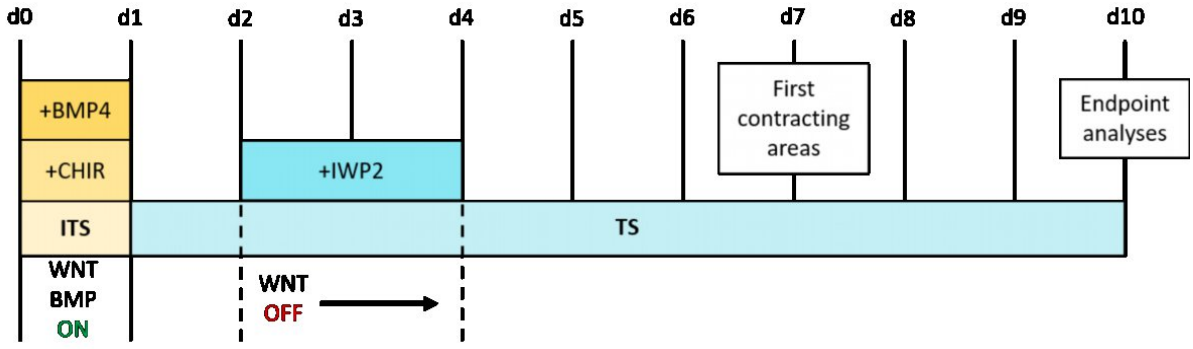

Figure 5: Schematic depiction of the cardiomyocyte differentiation protocol.

The protocol begins with the activation of the WNT and BMP signaling pathways provoked by CHIR and BMP4, respectively, which are components of the ITS medium used on day zero. After 24 h, the ITS medium is changed to TS medium. On days two and three the WNT pathway is inhibited by supplementing TS medium with IWP2. From day four to ten the medium is replaced every other day with TS medium devoid of pathway modulators. The first beating cardiomyocytes are observable on day seven. Endpoint analyses are performed on day ten. For media compositions see section 3.2. d = day. Adapted from Zhang et al. (2015) and Galanjuk et al. (2022).

3.5 Morphological assessment of the cell cultures

3.5.1 Morphological assessment of human induced pluripotent stem cells

The main focus of the characterization of the iPS11 cell line was the evaluation of the cells regarding their pluripotency. The almost unrestricted differentiation ability of the cells was a basic prerequisite for the subsequent cardiomyocyte induction. Evaluation criteria were the characteristic morphology of the hiPSCs and the expression of specific pluripotency markers at the protein level. The evaluation was also used to determine the latest cell passage to which induction of hiPSCs to cardiomyocytes was reasonable.

The morphology, as well as the proliferation behavior of the iPS11 cells, were assessed every working day using a phase-contrast microscope and were recorded by photo documentation (magnification: 40x and 100x). The following criteria were used for the optical assessment of the iPS11 culture (Wakui, 2017).

a) Presence of a homogeneous cell monolayer consisting of small round cells with defined margins and very dense cell growth.
b) High ratio of nucleus to the cytoplasm and multiple large nucleoli.
c) No or only very few zones with visibly differentiated cells.

The usual time to reach 90–100% confluence for the iPS11 cell line was three or four days depending on the initial cell density of 4×10^5 or 3×10^5 cells per well, respectively which has to be considered regarding the proliferation behavior. The presence of large areas of differentiated cells or changes in proliferation (longer time to reach confluence or poor adherence) will cause poor results in the downstream application of cardiomyocyte differentiation.

3.5.2 Morphological assessment of cardiomyocytes

From day one of the protocol onwards, cells were monitored on each working day using a phase-contrast microscope. Photo documentation was performed for each well (magnification: 40x) with the integrated camera system. Morphological criteria were set as part of the establishment of the hiPS Test and are described in the results part (see 4.3.1).

3.6 Flow cytometry analysis of the cell cultures

Flow cytometry is used to record the physical properties of cells such as size and granularity as well as the presence of specific markers labeled with fluorochromes. In a laminar flow, cells in a single-cell suspension individually pass one or multiple lasers. A laser emits monochromatic light of a specific wavelength hitting the cell. If the cell has been labeled with a fluorochrome that can be excited with that specific monochromatic light, the fluorochrome’s electrons will be shifted to a higher energy

state. Upon leaving the higher energy level back to the ground state, light of a higher wavelength is emitted with which the fluorochrome was excited. The emitted light passes through several dichroic mirrors. These mirrors filter out certain wavelengths of the light spectrum and allow only a portion of the light to pass. Photomultipliers detect the incoming wavelength and convert the light signal into an electrical signal. Further converters convert the electrical signal so that it can be read out and displayed by a computer, this is usually done in dot or contour plot diagrams, or histograms (Brown and Wittwer, 2000). The setup used for flow cytometry is shown in Table 13.

Table 13: Integrated laser lines and emission filters of the BD FACSCanto II system used for flow cytometry analyses to detect listed fluorochromes.

Laser line	Wavelength in nm	Emission filter	Fluorochrome
Violet	405	510/50	Fixable viability stain 510
Blue	488	530/30	FITC
Blue	488	585/42	PE
Blue	488	670 LP	PerCP-Cy 5.5
Red	633	660/20	Alexa Fluor 647, APC

FITC = Fluorescein isothiocyanate, PE = Phycoerythrin, PerCP = Peridinin-chlorophyll-protein, Cy = Cyanine, APC = Allophycocyanine

A sample of unstained cells was included in the set-up to detect possible autofluorescence of the cells and to set the gating for analysis (Table 14 and Table 15, Nr. 1). The discrimination between live and dead cells was performed by labeling the cells with the Fixable viability stain (FVS) 510 (Table 14 and Table 15, Nr. 2). Corresponding isotype controls were examined for each antibody used with the addition of FVS 510 (Table 14 and Table 15, Nr. 3). With the use of the isotype controls, an influence of non-specific binding of the used antibodies on the results could be excluded. Results were obtained from the sample that included all antibodies together and FVS 510 (Table 14 and Table 15, Nr. 4). Single stained samples with only one antibody were used to perform the compensation (Table 14, Nr. 5–8 and Table 15, Nr. 5–7). This approach is necessary as certain fluorochromes show a spectral overlap (e.g. FITC and PE) as the emitted light is not only measured in a single detector but in multiple, this phenomenon is called spillover. The problem of detection of one fluorochrome in multiple detectors is solved by the application of the mathematical method called compensation. Flow cytometry software can calculate spillover values by applying them to the data obtained. Only after compensation, the true level of staining is revealed. For the analysis of hiPSCs, a so-called Fluorescence Minus One (FMO) control was included (Table 14, Nr. 9) to detect any non-specific binding events between the additional antibody or its fluorochrome and the remaining antibodies of the kit used (BD Biosciences, 2022). All flow cytometry analyses were performed using a BD FACSCanto II system (for set up see Table 13) operated with the BD FACS Diva Software Version 6.1.3. For all experiments at

least 10,000 events per condition were recorded in the scatter gate. Further analysis was performed using FlowJo v10.7.1. For the preparation of cells, all steps were performed at RT unless stated otherwise. Washing steps were performed with a centrifugation step for 5 min at 200 g before the fixation step and 500 g after the fixation step. The supernatant was always decanted. Resuspension of cells was always performed through gentle vortexing. All incubation steps were performed under the exclusion of light.

3.6.1 Flow cytometry analysis of human induced pluripotent stem cells

Human iPSCs of the cell line iPS11 were analyzed for the presence of characteristic pluripotency markers. Three intracellular transcription factors i.e. homeobox protein NANOG (NANOG), OCT4, SOX2, and the membrane-bound glycosphingolipid stage-specific embryonic antigen-4 (SSEA4) were examined. For this purpose, the BD Stemflow Human Pluripotent Stem Cell Transcription Factor Analysis Kit (BD, #560589) covering the first three markers mentioned, was extended with the antibody BD Pharmingen FITC Mouse anti-SSEA-4 (BD, #560126) and the associated isotype control BD Pharmingen FITC Mouse IgG3, κ Isotype Control (BD, #555578). Additional fluorescence staining with BD Horizon FVS 510 (BD, #564406) was performed to discriminate between live and dead cells.

Table 14: Overview of sample types for flow cytometry analysis of iPS11 cell line including the pluripotency markers NANOG, OCT4, SOX2, SSEA4, and Fixable Viability Stain 510.

Nr.	Name	Components
1	Unstained	x
2	Viable cells	Fixable Viability Stain 510 (FVS 510)
3	Isotype controls	PE Mouse IgG1, κ Isotype Control PerCP-Cy 5.5 Mouse IgG1, κ Isotype Control Alexa Fluor 647 Mouse IgG2a, κ Isotype Control FITC Mouse IgG3, κ Isotype Control FVS 510
4	All antibodies	FITC Mouse anti-SSEA-4 PE Mouse anti-human Nanog PerCP-Cy 5.5 Mouse anti-Oct3/4 Alexa Fluor 647 Mouse anti-Sox2 FVS 510
5	SSEA4	FITC Mouse anti-SSEA-4 FVS 510
6	NANOG	PE Mouse anti-human Nanog FVS 510
7	OCT3/4	PerCP-Cy 5.5 Mouse anti-Oct3/4 FVS 510
8	SOX2	Alexa Fluor 647 Mouse anti-Sox2 FVS 510
9	FMO SSEA4	PE Mouse anti-human Nanog PerCP-Cy 5.5 Mouse anti-Oct3/4 Alexa Fluor 647 Mouse anti-Sox2 FITC Mouse IgG3, κ Isotype Control FVS 510

PE = Phycoerythrin, IgG = Immunoglobulin G, PerCP = Peridinin-chlorophyll-protein, Cy = Cyanine, FITC = Fluorescein isothiocyanate, SSEA4 = Stage-specific embryonic antigen-4, NANOG = Homeobox protein NANOG, OCT3/4 = Octamer-binding protein 3/4, SOX2 = SRY (sex determining region Y)-box 2, FMO = Fluorescence minus one

Cells were analyzed every second passage (p) from p4 to p20 at 90–100 % confluence. Human iPSCs of five 6-wells were dissociated as described in section 3.3.2 and counted in a Neubauer-improved chamber. For each staining condition (see Table 14), 1.2×10^6 cells were transferred into a 1.5 mL reaction tube labeled with the staining condition numbers 1–9 (Table 14) and centrifuged for 5 min at 300 g. The supernatant was decanted and cells were washed with 500 µL PBS $^{-/-}$ once. Samples 2–9 were resuspended in 500 µL FVS 510 diluted in PBS $^{-/-}$ (1:1000) for 15 min. Sample 1 was resuspended in 500 µL stain buffer (BD, #554656) instead. Then, all samples were washed twice with 1 mL stain buffer. Samples 3–5, and 9 were resuspended in 100 µL and samples 1, 2, and 6–8 in 120 µL stain buffer. 20 µL of the SSEA4 antibody was added to samples 4 and 5 and 20 µL of the respective isotype

control was added to samples 3 and 9. Samples were incubated for 25 min. Afterward, all samples were washed twice with 1 mL PBS $^{-/-}$ and fixated with 300 µL BD Cytofix Fixation Buffer (BD, #554655) for

20 min. Cells were washed twice with 1 mL PBS $^{-/-}$ and stored in 500 µL PBS $^{-/-}$ at 4 °C overnight. Centrifugation steps were performed at 500 g for 5 min after the fixation step. After centrifugation, all samples were resuspended in 300 µL BD Perm/Wash Buffer (BD, #554723) for 15 min. Cells were centrifuged for 5 min at 500 g and the supernatant was decanted. All antibodies and isotype controls were diluted 1:6 in Perm/Wash buffer. For this, samples 3, 4, and 9 were resuspended in 100 µL and samples 6–8 in 140 µL. An amount of 20 µL of antibodies and isotype controls each was added to the respective sample tubes (Table 14). Samples 1, 2, and 5 were resuspended in 160 µL Perm/Wash buffer. After 30 min incubation time, all samples were washed twice with 1 mL Perm/Wash Buffer and then resuspended in 300 µL stain buffer for analysis. For measurement, the samples were pipetted into flow cytometry tubes. The gating strategy used for the analysis is described in the results in section 4.1.3.

3.6.2 Flow cytometry analysis of cardiomyocytes

Flow cytometry analyses of cardiomyocytes were performed on days eight, nine, and ten of the differentiation protocol described in section 3.4. Fluorochrome-conjugated antibodies against GATA4, cTnT, and α-Actinin2 were used. For every day of analysis, 16 wells of a 48-well plate were pooled. For this, the medium was removed and 300 µL Accutase per 48-well was added, the plate was incubated for 7 min at 37 °C and 5 % CO_2. Cells were resuspended afterward using a 1000 µL pipette to ensure singularization. The plate was placed at 37 °C and 5 % CO_2 for an additional 3 min. The cells of all 16 wells were pooled into a 50 mL conical tube and wells were washed once with 300 µL PBS $^{-/-}$ which was also added to the conical tube. To further dilute the Accutase, 4.8 mL (300 µL/well) DMEM/F12 without L-glutamine was added to the cell suspension. Cells were resuspended with a 10 mL serological pipet 15 times to ensure a single-cell suspension. The suspension was distributed evenly to seven 2 mL reaction tubes. An overview of the required samples is shown in Table 15.

Table 15: Overview of sample types for flow cytometry analysis of hiPSC-derived cardiomyocytes including the markers cTnT, α-Actinin2, GATA4, and FVS 510.

Nr.	Sample	Components
1	Unstained	x
2	Viable cells	FVS 510
3	Isotype controls	PE Mouse IgG1, κ Isotype Control FITC REA Control Antibody (I), human IgG1 Alexa Fluor 647 Mouse IgG1 κ Isotype Control FVS 510
4	All antibodies	PE Mouse Anti-Cardiac Troponin T FITC α-Actinin (Sarcomeric) Antibody, anti-human/mouse/rat Alexa Fluor 647 Mouse Anti-GATA4 FVS 510
5	cTnT	PE Mouse Anti-Cardiac Troponin T FVS 510
6	α-Actinin2	FITC α-Actinin (Sarcomeric) Antibody, anti-human/mouse/rat FVS 510
7	GATA4	Alexa Fluor® 647 Mouse Anti-GATA4 FVS 510

hiPSC = Human induced pluripotent stem cell, FVS 510 = Fixable viability stain 510, PE = Phycoerythrin, IgG = Immunoglobulin G, FITC = Fluorescein isothiocyanate, GATA4 = GATA binding protein 4

Cells were centrifuged at 300 g for 5 min at 4 °C and washed once with 500 µL PBS $^{-/-}$. Afterward, samples 2–7 were resuspended in 500 µL FVS 510 diluted in PBS $^{-/-}$ (1:1000) and incubated for 30 min at 4 °C. Sample 1 was resuspended in 500 µL PBS $^{-/-}$ instead. All samples were washed twice with 500 µL stain buffer and fixated for 20 min in 500 µL of Cytofix Fixation Buffer. Cells were washed twice with 500 µL PBS $^{-/-}$ and stored in PBS $^{-/-}$ at 4 °C overnight. The next day, cells were centrifuged at 500 g for 5 min and resuspended in 500 µL Perm/Wash buffer. After 5 min of incubation, this step was repeated. For staining, samples were resuspended in Perm/Wash buffer with the amounts shown in Table 16. Then, the respective antibodies and isotype controls were added as indicated in Table 16.

Table 16: Pipetting scheme for the staining of intracellular markers cTnT, α-Actinin2, and GATA4 for flow cytometry analysis of hiPSC-derived cardiomyocytes on differentiation days eight, nine, and ten.

Nr.	Sample	Perm/ Wash buffer	PE-cTnT	FITC-α-Actinin2	Alexa Fluor 647-GATA4	PE-isotype control	FITC-isotype control	Alexa Fluor 647-isotype control
1	Unstained	100 µL	x	x	x	x	x	x
2	Viable cells	100 µL	x	x	x	x	x	x
3	Isotype controls	88 µL	x	x	x	5 µL	2 µL	5 µL
4	All antibodies	73 µL	5 µL	2 µL	20 µL	x	x	x
5	cTnT	95 µL	5 µL	x	x	x	x	x
6	α-Actinin2	98 µL	x	2 µL	x	x	x	x
7	GATA4	80 µL	x	x	20 µL	x	x	x

cTnT = Cardiac mucle Troponin T, hiPSC = human induced pluripotent stem cell, PE = Phycoerythrin, FITC = Fluorescein isothiocyanate, GATA4 = GATA binding protein 4

Of note, the PE isotype control (stock solution of 0.2 mg/mL) was prediluted 1:16.7 in Perm/Wash buffer to achieve a final concentration of 0.012 mg/mL. This step was necessary to adjust the isotype control concentration to the antibody concentration used in the staining. Samples were gently vortexed and incubated for 30 min. Then, cells were washed twice with 500 µL of Perm/Wash Buffer. Afterward, cells were resuspended in 300 µL stain buffer for analysis. For measurement, the samples were pipetted into flow cytometry tubes. The gating strategy used for the analysis is described in the results section 4.3.4.

3.7 Quantitative reverse-transcription polymerase chain reaction

Quantitative reverse transcription-polymerase chain reaction (qRT-PCR) is a sensitive method for the investigation and quantification of mRNA levels in cells or tissues and is considered a routine tool in molecular biology. The mRNA is the intermediate product of gene expression and will ultimately be the template for translation into polypeptides. Cellular processes are based on specific gene expression patterns during e.g. proliferation, differentiation, or survival. These changes can be detected by identifying the mRNA transcription levels (Farrell, 2017).

Quantitative RT-PCR first involves the reverse transcription of the RNA into the corresponding complementary DNA (cDNA). The cDNA serves as a template in the subsequent polymerase chain reaction (PCR), whose exponential amplification can be monitored in real-time using fluorescence-based detection methods (Bustin, 2000). The steps reverse transcription and PCR can be performed in one or two steps. In this work, the study of gene expression was performed in a two-step format. This

allows for generating a cDNA pool that can be analyzed for multiple genes. Marker genes over the time course of differentiation from hiPSCs to cardiomyocytes were examined i.e. *OCT4, MESP1, ISL1, GATA4, TNNT2, and ACTN2*. The determined expression levels of these genes were normalized to the expression level of the reference gene calnexin (*CANX*). The ubiquitous presence of ribonuclease (RNase) demands high caution when working with RNA samples. Therefore, to prevent any potential degradation of the RNA template, appropriate consumables, as well as reagents and buffer solutions with the necessary degree of purity declared as RNase-free, were used in the methods described below. All steps after RNA extraction were performed on ice.

3.7.1 Sample collection

Cells were differentiated as described in section 3.4. A time series of the differentiation protocol was generated to analyze the markers mentioned above. Lysates of three wells for each day of the protocol were collected and pooled using the TRK lysis buffer from the peqGOLD Total RNA Kit (VWR, #13-6834). For this, the medium of the respective wells was removed completely and 200 µL TRK Lysis Buffer was added to each well. Cells were lysed and homogenized by pipetting up and down several times and pooled into a reaction tube.

For analyzing markers after substance exposure, cells of the respective quadruplicates were lysed and pooled the same way but only on day ten of the differentiation protocol. All samples of lysed cells were stored at -80 °C until RNA extraction was performed.

3.7.2 RNA extraction

The peqGOLD Total RNA Kit was further used to purify the RNA. A volume of 300 µL was taken from each of the collected lysates, placed on an RNA Homogenizer Column, and centrifuged at 12,000 g for 2 min. A volume of 300 µL 70 % ethanol in dH_2O was then added to the flow-through and homogenized by pipetting up and down. For RNA binding, the sample was completely transferred to a peqGOLD RNA Mini Column and centrifuged at 10,000 g for 1 min. The resulting flow-through was discarded. For the subsequent washing step, 250 µL of RNA Wash Buffer I was added to the column. After centrifugation at 10,000 g for 1 min, the resulting flow-through was discarded. A DNase digestion step was performed using the DNase I Digest Kit (VWR, # 12-1091-01/02). For one sample, 75 µL was needed consisting of 1.5 µL DNase I and 73.5 µL DNase I Digestion Buffer I. The single components were multiplied by the number of samples present plus two to account for loss during pipetting, preparing a working solution. Then, 75 µL of the DNase-I solution was added to the membrane of each column and incubated for 15 min at RT. After the incubation time, 250 µL of RNA Wash Buffer I was added to the columns and centrifuged at 10,000 g for 1 min. The flow-through was discarded, followed by two additional washing steps, each with 500 µL 80 % ethanol in dH_2O and centrifugation at 10,000 g for 1 min. Then, to remove residual ethanol, the column was placed in a new collection tube and centrifuged at maximum speed

(31,514 g) for 2 min. For elution, the column was transferred to a 1.5 mL reaction tube and 30 µL of RNase-free water was added directly to the membrane. After an incubation time of 2 min, columns were centrifuged at maximum speed for 2 min.

3.7.3 RNA quantification

Quantification of the extracted RNA was performed by measuring the absorbance at a wavelength of 260 nm (A260) using a NanoDrop Microvolume Spectrophotometer. Blank values were measured in duplicates using the RNase-free water that was also used for elution during the RNA extraction step before measuring the samples. Furthermore, the recording of the blank value was repeated after the measurement of ten samples. For each measurement, 2 µL of the RNase-free water or 2 µL of the sample was used. The ratio of the absorbance values at 260 nm and 280 nm (A260/A280) was measured, which provides information about the purity of the RNA preparation. Values between 1.8 and 2.0 are considered to be high-purity RNA (VWR, 2022).

Some of the RNA preparations examined in this work were below this value. The A260/A280 ratio depends on the pH and ionic strength of the solvent used. In general, the use of a buffer system with a slightly alkaline pH and low salt content is recommended for the determination of RNA concentration and purity. Due to the slightly acidic pH of the RNase-free water used to elute the RNA, a strong reduction of the determined A260/A280 ratio may occur during absorbance measurement (Wilfinger et al., 1997; VWR, 2022). If A260/A280 ratios below 1.8 are measured in RNA samples, contamination could be present in the form of proteins, which are usually remnants of RNA isolation (Wilfinger et al., 1997). It should be noted that the amount of isolated RNA in the samples decreased continuously from day one to day ten of the time series of the differentiation protocol. Consequently, the detected A260/A280 ratios below 1.8 were determined in samples from differentiation days seven to ten, in which a lower RNA concentration was present. In these samples, the contaminating protein content was presumably more significant than in samples with higher RNA concentrations. RNA concentration, as well as the associated A260/A280 ratio, were calculated by the software based on the generally accepted extinction coefficients for nucleic acids (dsDNA 50 ng/µL, ssDNA 33 ng/µL, RNA 40 ng/µL) with the output shown in ng/µL (Matlock, 2015). Afterward, the RNA was stored at -80 °C until further use.

3.7.4 Synthesis of cDNA by reverse transcriptase

Depending on the RNA concentration of the samples, dilution with RNase-free water was performed to achieve an equal RNA concentration as starting point throughout the biological replicates of an experiment. It was necessary to adjust the concentrations to the sample with the lowest total amount of RNA within the three biological replicates in a volume of 7.8 µL.

According to the manufacturer's instructions, 0.56 µg of oligo (dt) 15 primer in a reaction volume ≤ 15 µL was used to generate the cDNA. For the first step, the following reaction mixture was pipetted; 1.25 µL oligo (dT) 15 primer (Jena Bioscience GmbH, #PM-303L) and 1 µL 10 mM dNTP mix (Jena Bioscience GmbH, #NU-1006L). This mixture is for only one sample and individual components were multiplied by the number of samples used plus three to account for loss during pipetting. To each sample, 2.25 µL of the mixture was added resulting in 10.05 µL in total. Primer annealing and subsequent reverse transcription reaction were performed using a Biometra thermal cycler T3. Annealing of the primers was performed at 64 °C for 5 min. Afterward, the samples were cooled to 4 °C. The following reaction mixture was prepared for the synthesis of cDNA; 5 µL RNase-free water, 4 µL RT Reaction Buffer (5×), and 1 µL M-MLV reverse transcriptase (Promega, #M170A). This mixture is for only one sample and individual components were multiplied by the number of samples plus three to account for loss during pipetting. To each sample, 10 µL of the mixture was added resulting in 20.05 µL in total. Synthesis of the cDNA was then performed in the thermal cycler at 37 °C for 52 min. To inactivate the enzyme reaction, the samples were kept at a temperature of 70 °C for 15 min after completion of the synthesis reaction. For further processing, the samples were cooled to 4 °C. After the reverse transcription reaction was completed, 30 µL of RNase-free water was added to each sample. Samples were stored at -20 °C until the performance of qRT-PCR.

3.7.5 Quantitative real-time PCR

Quantification of the expression levels of marker genes was performed using the QuantiFast SYBR Green PCR Kit (Qiagen, #204056). Primers were purchased from Eurofins, which provides two tubes, one forward and one reverse primer, or IDT which provides one tube containing both, forward and reverse primer. Primers from Eurofins were dissolved to 100 µM each in RNase-free water. Working solutions of 4 µM were prepared accordingly. Primers from IDT were dissolved in 1333 µL RNase-free water resulting in 3.75 µM for each primer in the mixture. Primers were stored at -20 °C. To achieve the same concentration of each primer in the mixture for the qPCR reaction, the following components were pipetted depending on the primers used (Eurofins or IDT).

	Eurofins primer	**IDT primer**
SYBR Green PCR Master Mix	7,5 µL	7,5 µL
3’ Primer	2,5 µL (4 µM)	2,68 µL (3.75 µM each)
5’ Primer	2,5 µL (4 µM)	
H_2O (RNase-frei)	x	2,32 µL
∑	12,5 µL	12,5 µL

The indicated volumes refer to the amounts needed to amplify a single sample. All components were multiplied by the number of samples used plus three to account for loss during pipetting. To one PCR reaction tube, 12.5 µL of the mixture was pipetted and 2.5 µL of the respective cDNA template was added afterward. The Rotor-Gene Q PCR cycler from Qiagen used in this work has a capacity of 72 samples per run. One experiment was analyzed with multiple primers if possible. A primer was not split into two runs even though the cycler was not fully loaded to avoid variability between samples with the same primer due to two different runs. The primers used in this work with the respective sequences (5'-3') for forward and reverse primers, as well as the product lengths, are shown in Table 17.

Table 17: Forward (FW) and reverse (RV) primer from 5' to 3' with the respective base pair (bp) lengths used in this thesis.

Gene	Sequence (5' to 3')	Product length	Company
ACTN2	FW: CTCAGACGCTCGTTAGCAT RV: CAACATCAGAATCAGCTCAAGC	150 bp	IDT
CANX	FW: GCTGGTTAGATGATGAGCCTGAG RV: ACACCACATCCAGGAGCTGACT	139 bp	Eurofins
CAPN	FW: TCCACCTGAAGGACCAGTGTCT RV: GTCCGAGACAATGAAGGCATGG	98 bp	Eurofins
GATA4	FW: TCCAAACCAGAAAACGGAAG RV: AAGACCAGGCTGTTCCAAGA	352 bp	Eurofins
ISL1	FW: CACAAGCGTCTCGGGATT RV: AGTGGCAAGTCTTCCGACA	202 bp	Eurofins
MESP1	FW: CTGCCTGAGGAGCCCAAGT RV: GCAGTCTGCCAAGGAACCA	102 bp	Eurofins
OCT4	FW: GTTGGAGGGAAGGTGAAGTTC RV: TGTGTCTATCTACTGTGTCCCA	103 bp	IDT
TNNT2	FW: TTCACCAAAGATCTGCTCCTCGCT RV: TTATTACTGGTGTGGAGTGGGTGTGG	166 bp	Eurofins

In addition to the samples from experiments, necessary controls were included in the setup of a run. A no-template control (NTC), containing all components of the reaction except the cDNA template, was included to detect primer dimer formation or cross-contamination. In addition, a negative control was included during the cDNA synthesis. For this purpose, a reaction mixture with all necessary components, except for the reverse transcriptase (No-RT control), was prepared. Without the addition of the reverse transcriptase, the RNA template can not be transcribed into cDNA. Subsequent amplification by a DNA-dependent DNA polymerase is therefore not possible. In the case of genomic DNA (gDNA) contamination, a clear signal is detectable in the No-RT control. Amplification of gDNA was further reduced in the PCR reaction by using intron-spanning primers (Nolan et al., 2006). The

quantification was performed with the following temperature program. First, a heat activation at 95 °C for 7 min was performed. Afterward, a two-step cycle was performed 45 times including a denaturation step at 95 °C for 10 s which was followed by the annealing/elongation at 60 °C for 35 s. After completion of the amplification reaction program, a melt curve analysis was performed in 1 °C steps from 75 to 99 °C to verify the specificity of the PCR reaction and the identity of the PCR products.

3.7.6 Quantification of cDNA

Quantification of the amplified cDNA of the genes *CANX*, capain10 (*CAPN10*), *OCT4*, *MESP1*, *ISL1*, and *TNNT2* was done by gel electrophoresis at the same time excluding contaminations. An agarose gel was prepared, consisting of 1 % agarose dissolved in 100 mL TRIS-Acetate-EDTA (TAE) buffer in a conical flask. To dissolve the agarose, the mixture was heated in a microwave until boiling, in between the heating was stopped and the mixture was swirled. After boiling and the complete dissolving of the agarose, the mixture was cooled to lukewarm under running water. Under the fume hood, 1 µL of Midori Green was added and mixed by swirling. The solution was then poured into the gel chamber and the comb was inserted. Removal of air bubbles was performed. The solution was left for 20 min to polymerize. Afterward, the gel chamber was transferred into the gel electrophoresis apparatus. A volume of 3 µL cDNA sample from the qPCR-RT was mixed with 12 µL TAE buffer and 3 µL loading dye (BioLabs, #N3236S). A DNA ladder (BioLabs, #N3236S) with a size range from 50 to 1350 bp was included as a size reference adding 12 µL TAE buffer and 3 µL loading dye to it. A volume of 12 µL per sample was pipetted into the wells after removing the comb. The run was performed at 130 V for 45 min. Using a Gel iX imager, the bands were visualized on the agarose gel with UV light and an image was generated using the INTAS GDS software.

3.7.7 Generation of PCR standards

For each primer used, standard curves were generated from the PCR products obtained in an initial run. Evaluation using standard curves harbors the advantage of quantitative information on the expression levels of individual genes that can be compared. To prepare the PCR standards, six qRT-PCR samples per primer were selected that showed the same peak in the melting curve analysis characteristic for the respective primer. The selected samples were first combined in a 1.5 mL reaction tube (90 µL in total) and then purified using the QIAquick PCR Purification Kit (Qiagen, #28104) according to the manufacturer's instructions. A volume of 450 µL PB buffer was first added to the sample. The sample was then transferred to a column and centrifuged at maximum speed (31,514 g) for 1 min. The flow-through was discarded and the column was washed with 750 µL PE buffer by first adding the buffer solution to the column and then centrifuging at 31,514 g for 1 min. To dry the membrane, the column was centrifuged for 1 min at 31,514 g. The column was then transferred to a 1.5 mL reaction tube and 50 µL RNase-free water was added to the membrane for elution. After

centrifugation for 1 min at 31,514 g, the concentration of the obtained DNA was determined photometrically using a NanoDrop Microvolume Spectrophotometer. Based on the determined concentration, the number of molecules per µL was calculated using the Avogadro constant implemented in Equation 1.

Equation 1: Calculation of molecules per µL of a qRT-PCR sample for generating standard curves.

$$\frac{x\,\frac{g}{\mu L}\,\mathrm{DNA}}{\text{Product length in bp}\cdot 660\,\frac{g}{mol}}\cdot 6.022\cdot 10^{23}\,\frac{\text{molecules}}{\text{mol}} = y\,\frac{\text{molecules}}{\mu L}$$

A stock solution with a concentration of 3.75×10^{10} molecules/µL was prepared by dilution with RNase-free water. Starting from this stock solution, a serial dilution series (1:10) was prepared. Dilutions in the concentration range from 3.75×10^{7} to 3.75×10^{2} molecules/µL were used for the generation of the standard curves. A qRT-PCR run was performed as described above whereas the dilutions were handled as cDNA templates. After amplification of the dilutions, a threshold was calculated by the software Rotor-Gene Q Series at which the R^2-value is the closest to 1 resulting in specific Ct values of the dilution concentrations. Calculating the mean Ct values of three independent runs per primer and plotting them against the mentioned dilutions results in a linear equation. Melting points of qRT-PCR products using the same primer did not differ by more than 0.3 °C and the difference between the determined Ct values of the individual standards per primer was not greater than three cycles. Additionally, the mean value of the three obtained thresholds was calculated. Applying the calculated mean value of the threshold to a qRT-PCR run with experimental samples results in specific Ct values per sample. The Ct values of the samples were used to solve the linear equation to obtain the copy numbers of the respective gene. Afterward, the copy numbers of the target genes were normalized to those of the reference gene *CANX*.

3.8 Immunocytochemical staining of cardiomyocytes

Immunocytochemistry is used to visualize proteins or antigens of cells. An antibody binds to a specific intracellular or extracellular antigen of a cell. For detection of the antibody, it is labeled directly or indirectly with reporter conjugates e.g. fluorochromes, enzymatically convertible chromogens, or immunogold particles (used in electron microscopy). In this work, the first method was used. The primary antibody can be directly conjugated with a fluorochrome (direct staining) or is unconjugated. Indirect staining uses an unconjugated primary and a species-specific conjugated secondary antibody that binds to the primary antibody (Figure 6). The advantage of the latter method is that multiple secondary antibodies can bind to the primary antibody amplifying the signal. The stained cells are detected by excitation of the fluorescent conjugate with a specific wavelength using a fluorescence microscope. Extracellular antigens on the cell membrane can be stained without permeabilization. For

intracellular antigens, the cell membrane has to be permeabilized allowing the antibodies to pass into the cell.

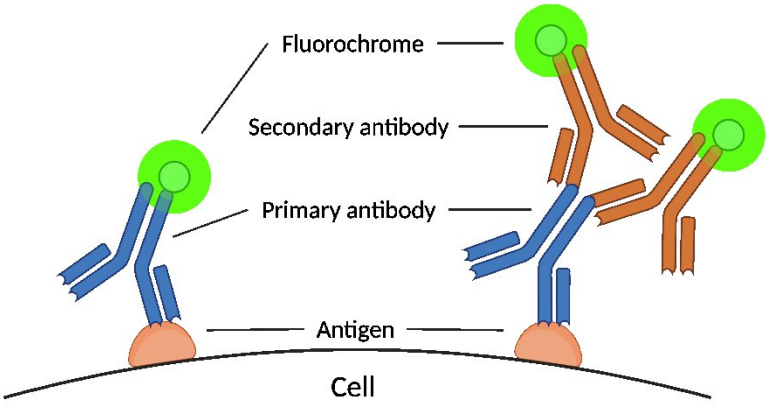

Figure 6: Schematic depiction of the direct and indirect staining principle in immunocytochemistry.

On the left, the primary antibody binds to the antigen and is directly conjugated to a fluorochrome. On the right side, the unconjugated primary antibody binds to the antigen and is bound by multiple secondary antibodies that are conjugated with fluorochromes. Created with BioRender.com.

For immunocytochemistry, cardiomyocytes were differentiated according to the protocol described in section 3.4. On day ten, cells were replated to 96-wells coated with Matrigel. For this, a single-cell suspension was prepared as described in section 3.3.2. For replating, 6×10^4 cells per well were seeded in 200 µL TS medium. After 24 h of incubation, immunocytochemical analysis was performed using an antibody against cTnT. First, 100 µL of the medium was removed and 50 µL of 12 % paraformaldehyde (PFA) (Merck, #P6148) was added to the remaining 100 µL medium resulting in a 4 % PFA solution. After incubation at 37 °C for 30 min, the supernatant was carefully removed and the cells were washed three times with 300 µL PBS $^{-/-}$ per well. For permeabilization, cells were treated with 0.1 % Triton X 100 (Merck, # T8787) in PBS $^{-/-}$ (PBS-T) for 5 min at RT. Afterward, cells were washed with 300 µL PBS $^{-/-}$ once. To avoid non-specific binding, cells were treated with 50 µL of a blocking reagent consisting of 10 % goat serum (GS) (Merck, #G9023) in PBS-T for 30 min at 37 °C. For the staining, the primary antibody Mouse Anti-Cardiac Troponin T antibody [1C11] (Abcam, #ab8295) was diluted 1:200 in PBS-T supplemented with 10 % GS. To detect any non-specific binding of the second antibody, two wells were dedicated as secondary antibody control wells, which were treated with PBS-T and 10 % GS, but without the primary antibody. A volume of 50 µL per well of the antibody solution was applied and incubated for 60 min at 37 °C. Three washing steps applying 300 µL of PBS $^{-/-}$ per well for 5 minutes and removing it afterward were performed. Then, the secondary antibody Goat anti-Mouse IgG (H+L) Cross-Adsorbed Secondary Antibody, Alexa Fluor 488 (Thermo Fisher Scientific, #A-11001) was prepared by diluting it 1:200 in PBS $^{-/-}$ supplemented with 2 % GS and 1 % bisbenzimide H33258 (Hoechst 33258) (Merck, #B1155) for nuclear staining. A volume of 50 µL of the secondary antibody solution was applied to each well and incubated for 30 min at 37 °C. Subsequently, the cells were

washed three times with 300 µL of PBS $^{-/-}$ for 5 minutes each. Fluorescence imaging was performed using an automated microscope system for high-content imaging (CellInsight CX7 LZR Platform).

3.9 Beating analysis of cardiomyocytes

On day ten, the medium was replaced with 600 µL of TS medium to ensure an equal amount of nutrition supply throughout the wells, followed by a 2 h incubation at 37 °C and 5 % CO_2 to allow floating particles to settle. Afterward, the 48-plate was placed on a heating plate integrated into the binocular Leica DMS1000 B set to 37 °C. The lid of the respective 48-well plate was removed to ensure a high quality of recorded videos. The plate was equilibrated for 10 min to the ambient environment. Videos were recorded for 10 sec or at least until the occurrence of two contractive motions using the binocular (magnification 1×). Beating frequency and beating area were analyzed using the in-house-developed software CardioVision (Dönmez et al. in preparation).

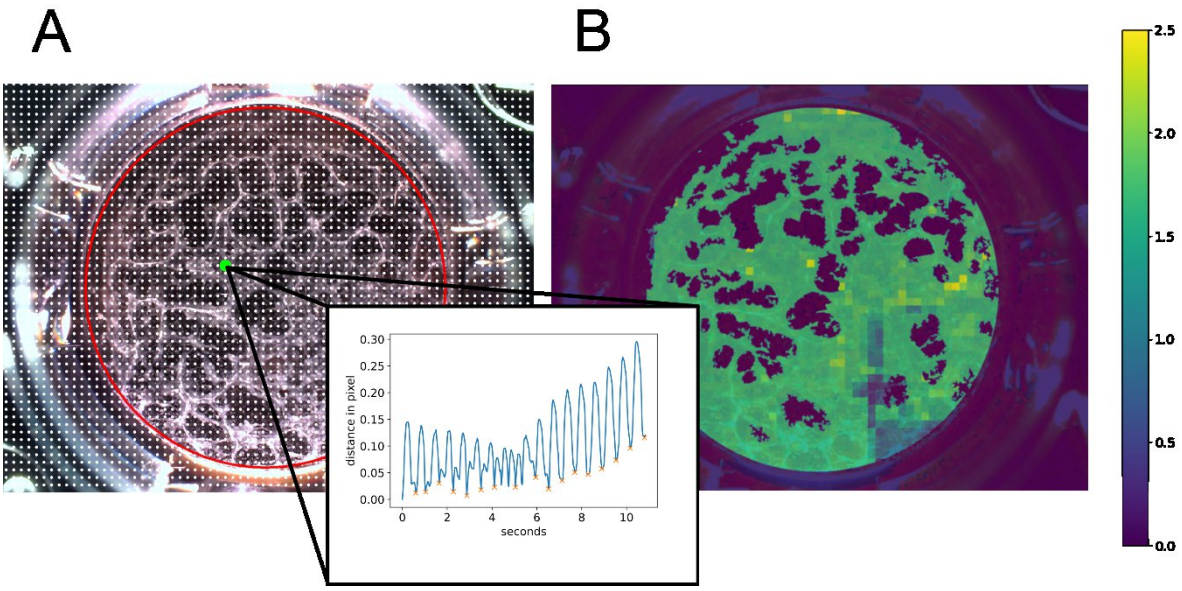

Figure 7: Visualization of video processing steps used in the in-house developed software CardioVision.

The software includes different video processing steps to determine the beating frequency and beating area of a recorded video. **A:** Reference points (white dots) were placed over the video in a grid of 20 pixels next to each other. Reference points within the region of interest (ROI), depicted as a red circle, were analyzed. The motion profile of a single reference point marked in green is depicted inside the black frame. Peaks marked with an orange X are counted as a beat. **B:** Heatmap representing the beating area color-coded with the respective beating frequency in beats/second calculated at each reference point.

The following steps were applied to each video. First, the motion profile was determined. For this, reference points were placed on the video as a grid with a distance of 20 pixels next to each other (Figure 7 A). For every reference point, the motion was tracked using the Lukas Kanade function, provided in the OpenCV library (Bradski, 2000), evaluating the function frame by frame. All frames of a video were used for analysis. As every motion is tracked in this step, it is crucial to further distinguish

between the motion of cells and artifacts, e.g., floating particles. Each motion of a reference point creates a distance profile (Figure 7 A, black frame) that reflects how far the reference point moved from the starting point (first frame) at time t. A threshold alpha was applied to the calculated distance from one frame to another for each reference point to exclude extremely small distances. This threshold enables a noise reduction for the analysis. Next, a region of interest (ROI) reflecting the total area of the well is determined with a padding of 10 pixels (Figure 7 A) performing the Hough transformation using the 'HoughCircles' function of the OpenCV library (Bradski, 2000). To distinguish between the cell layer and dead cells or small artifacts, a cell mask was created. The first frame of a video was converted to HSL (hue, saturation, lightness) color representation. Afterward, the mean value of lightness was calculated within the ROI. Based on the average lightness, thresholds were assigned to certain value ranges. This is used to optimize the binarization of the ROI to predict the cell layer. After binarization, connected components were determined using the OpenCV function 'connected-ComponentsWithStats' excluding small areas which represent dead cells or artifacts. Thus, the cell mask is the upper bound for further analysis of the beating area and beating frequency. The endpoint beating frequency was determined by performing peak analyses on the distance profile curves of the reference points within the cell mask. The result was visualized by creating a heat map using color codes for the individual beating frequency results (Figure 7 B). The total area of the beating frequency represents the beating area.

3.10 Cell viability assay for the hiPS Test

Cell viability was assessed on day ten of the differentiation protocol using the CellTiter-Blue (CTB) Cell Viability Assay (Promega Corporation, #G8081). The assay is based on the reduction of resazurin to resorufin. Resazurin is a cell-permeable redox indicator that is converted to resorufin by metabolically active, viable cells. The amount of resorufin formed is proportional to the number of viable cells and can be quantified either by measuring the absorbance or the fluorescence. Due to the lower sensitivity of absorbance measurement, quantification of the resorufin product via its fluorescence intensity is usually preferred (Riss et al., 2004).

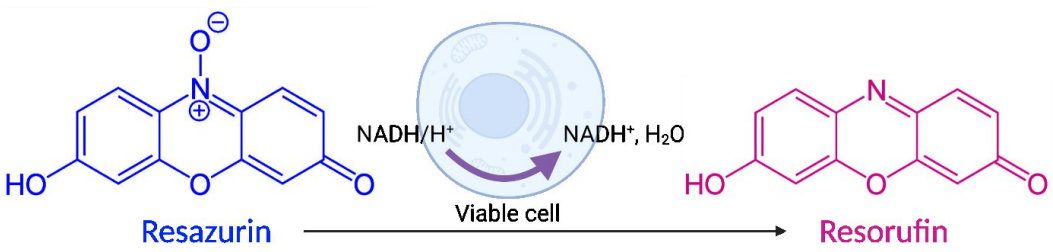

Figure 8: Scheme of the reduction of the low-fluorescent resazurin to the fluorescent resorufin in viable cells.

The reaction is used to examine cell viability as the amount of metabolized resazurin is proportional to the number of viable cells. The fluorescence of resorufin can be quantified at an emission wavelength of 590 nm after excitation at a wavelength of 540 nm (540Ex/590Em). Created with BioRender.com

The CTB reagent was mixed 1:3 with TS medium and warmed to 37 °C. After recording the videos as described in section 3.9, dedicated lysis control wells were treated with 0.2 % Triton X-100 (diluted in dH_2O) for 20 min at 37 °C and 5 % CO_2. Afterward, 200 µL of the CTB mixture was added to each well. A background control with no cells was used to detect possible effects influencing the results due to the medium used. These effects were taken into account in the subsequent evaluation of the results by subtracting the background value from the sample measurement values obtained. Plates were incubated for 1 h at 37 °C and 5 % CO_2, before analysis. Analysis was performed by measuring the fluorescence in a multimode microplate reader (Tecan, Infinite M200 PRO) at an excitation wavelength of 540 nm and an emission wavelength of 590 nm (540Ex/590Em).

3.11 Substance testing

3.11.1 Experimental setup

One substance was tested on one 48-well plate. A solvent control was implemented in the setup that represents cells cultured in the normal media used for cardiomyocyte differentiation but supplemented with the solvent used to dissolve the substance that is tested. The solvent control was implemented to exclude the possibility that the solvent used had a cytotoxic effect per se. The concentration of the solvent was the same in all concentrations of the substance of interest, as well as in the solvent and lysis control. A DMSO concentration of 0.1 % was not exceeded as it shows a cytotoxic effect in higher concentrations. A lysis control was cultured under the same conditions as the solvent control until day ten of the differentiation protocol and served as a positive control in the cell viability assay. A background control with TS medium but no cells was necessary for the cell viability assay as well (see 3.10). Substances were tested in six concentrations. The concentration range was based on literature research or was determined experimentally by preliminary tests. To obtain a concentration-response curve for the data of the cell viability assay, the lowest two concentrations of the substance should show no effect on the viability and at least one concentration should show an effect on cell viability. Every condition was tested in four technical replicates. The plating scheme follows the suggestions of Crofton et al. (2011). It is designed to identify potential edge effects as the control and the lowest concentrations both occupy one well on the edge which can be compared with the other three replicates not located on the edge.

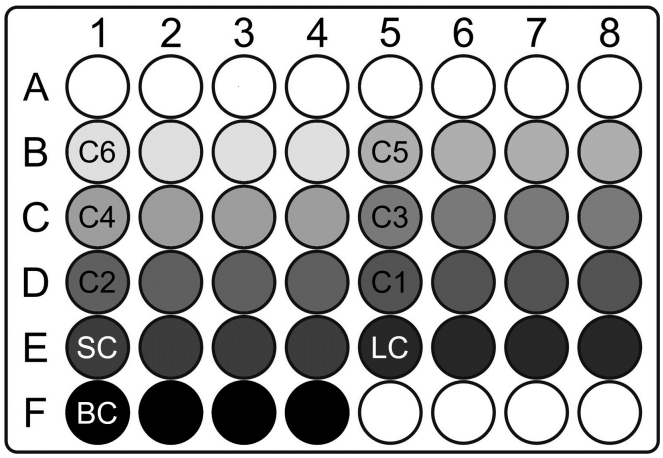

Figure 9: Pipetting scheme for substance testing.

The scheme is designed for 48-well plates including six concentrations of the substance of interest, a solvent control, lysis control, and background control, all in quadruplicates. Wells depicted in white were filled with dH_2O. C6–1 = concentration 6 (lowest)–1 (highest), SC = solvent control, LC = lysis control, and BC = background control.

For substance exposure, cells were dissociated as described in section 3.3.2. For one 48-well 2.75×10^5 cells were used. As the setup was designed in quadruplicates the respective cell number of 1.1×10^6 for four wells was transferred into eight 15 mL conical tubes each per condition. Beforehand, a dilution series of the substance of interest was prepared from the highest concentration (C1) by serial 1:3 dilution in ITS medium to the lowest concentration C6. The media were warmed to 37 °C in a water bath. After centrifugation of the cells at 200 g for 2 min, the supernatant was aspirated using a vacuum pump. Cells of six conical tubes were each resuspended in 3.2 mL (equivalent to 4×800 µL) of the dilutions C1–C6 accordingly. The two other conditions (solvent and lysis control) were resuspended in 3.2 mL ITS medium supplemented with the solvent used for substance dissolving. The cell suspension obtained from the individual preparations was distributed to four wells each (800 µL per well). The exposure of the cells to the substance took place over the entire protocol of ten days freshly applying the substance on every feeding day (days two, three, four, six, and eight). Consequently, it was necessary to prepare the dilution series described above in the medium required (ITS, TS, or TS + IWP2) for the respective differentiation days. The progress of the differentiation, as well as potential substance effects on morphology, were recorded by photo documentation on each working day with a phase-contrast microscope (magnification: 40x).

3.11.2 Substances for cell exposure

Based on the EST, 5-Fluorouracil (5-FU) was selected as a positive control, and Penicillin G (PenG) as a negative control (Genschow et al., 2004; Seiler and Spielmann, 2011). Both substances were tested for their suitability as appropriate controls for the herein-developed hiPS Test method. Triclabendazole (TCBZ), triclabendazole sulfoxide (TCBZSO), and nocodazole (NCDZ) were further tested in a collaboration with the University of Barcelona. Table 18 shows an overview of the substances tested

in this work indicating the CAS number, the respective stock concentrations, the solvent used, and the concentration range tested.

Table 18: Substances used to study their embryotoxic potential on human induced pluripotent stem cells differentiating into cardiomyocytes.
The respective CAS number, stock concentration, solvent used for dissociation, and concentration range studied are indicated.

Substance	CAS number	Stock-concentration and solvent	Exposure concentrations
5-Fluorouracil	51-21-8	10 mM in DMSO	0,01 µM–3 µM
Penicillin G	61-33-6	1 M in H_2O	1,23 µM–300 µM
Triclabendazole	68786-66-3	20 mM in DMSO	0,04 µM–10 µM
Triclabendazole sulfoxide	100648-13-3	20 mM in DMSO	0,04 µM–10 µM
Nocodazole	31430-18-9	5 mM in DMSO	0,004 µM–1 µM

3.12 Data analysis and statistics

Statistical analyses were performed using GraphPad Prism 8 for Windows 64-bit, version 8.4.3. All data are presented as the mean of ≥3 N ± SEM as not stated otherwise and analyzed with a one-way ANOVA followed by a Dunnett or Tukey multiple comparisons test; $p \leq 0.05$ was considered significant. Data for substance testing were excluded from this procedure.

For analyzing the results of the substance tests, R was used which is a free software environment for statistical computing and graphics (R Core Team, 2022). Statistical computing is based on the R package CRStats a framework for the analysis of *in vitro* data that relies on the established R packages drc (Ritz et al., 2015) and mvtnorm (Genz et al., 2021) paired with the step-down multiple test procedure of Dunnett and Tamhane (Dunnett and Tamhane, 1991). All data are presented as the mean of ≥3 N ± SEM, $p \leq 0.05$ was considered significant. Furthermore, the packages were adapted for concentration-response data analysis calculating the BMR, BMCL, BMCU, BMC, and CI band. The best curve-fitting model for the respective data sets was chosen from a large pool of 13 mathematical concentration-response functions according to robust statistical criteria. Fitted curves can follow linear, sigmoidal, monotonic, and non-monotonic trends. The estimation method assumes continuous response data. The web application framework Shiny for R (Chang et al., 2022) was used to display concentration-response curves in a browser enabling the possibility to select different curve-fitting models, check for individual data points, and view the BMRs of all endpoints (Dönmez et al. in preparation).

For compound classification in the hiPS Test, the benchmark dose approach recommended by the EFSA Scientific Committee (Hardy et al., 2017) was used. Matching the terminology for *in vitro* toxicity testing, the term benchmark concentration (BMC) was determined which is based on the same

calculation principle (Krebs et al., 2020). First, a benchmark response (BMR) was determined at which the BMC was calculated. Data sets for the compound classification were control-normalized resulting in the control always being represented as 100 %. The calculation of the benchmark response takes the variability of the test system into account by considering the variance of the first two concentrations for every endpoint evaluated of all substances tested. For this, the coefficient of variation (CoV) was determined for all data points of the first two concentrations, regardless of the substance tested as the first two concentrations should not display any effect on the evaluated endpoints. Furthermore, the CoV was multiplied by 1.5 to obtain the BMR. Thus, a higher variability within the two first concentrations results in a higher BMR.

For cell viability, the CoV was 18 %, therefore, the BMR_{20} was used for this endpoint. For beating frequency, the CoV was 32 % resulting in BMR_{30} by rounding. The calculated CoV of 21 % for the beating area resulted in a BMR_{20}. For *ACTN2* and *TNNT2* expression, the BMR_{50} and BMR_{35} were determined as the CoV was at 48 % and 33 %, respectively. For all endpoints, the BMC at the respective BMR plus confidence intervals (CI) at 95% and 5% quantile were calculated (Table 19). The confidence interval is defined as the range between the benchmark concentration lower limit (BMCL) and the benchmark concentration upper limit (BMCU). The classification model used for the hiPS Test is based on the comparison between the confidence intervals (CI) of the calculated BMC values of the viability and the cardiomyocyte differentiation-specific endpoints. A specific hit is identified if the BMCL of the cell viability and the BMCU of the specific endpoint do not overlap. If the CI of cell viability and the specific endpoint overlap it is an unspecific hit. In case no BMC could be calculated the substance is classified as no hit (Masjosthusmann et al., 2020).

4 Results

4.1 Characterization of the hiPSC culture

The quality of the hiPSC culture is of utmost importance for downstream applications and should be evaluated and documented using defined standards. For the hiPS Test, a quality control routine during the cultivation of hiPSCs was implemented. The quality control included a visual assessment of cell morphology, proliferative behavior, and detection and evaluation of specific pluripotency-associated markers expressed in hiPSCs.

4.1.1 Matrix comparison

To reduce animal-based products in the hiPS Test, it was examined if hiPSCs cultured on LN521 or Matrigel exhibit the same appearance as well as proliferation behavior.

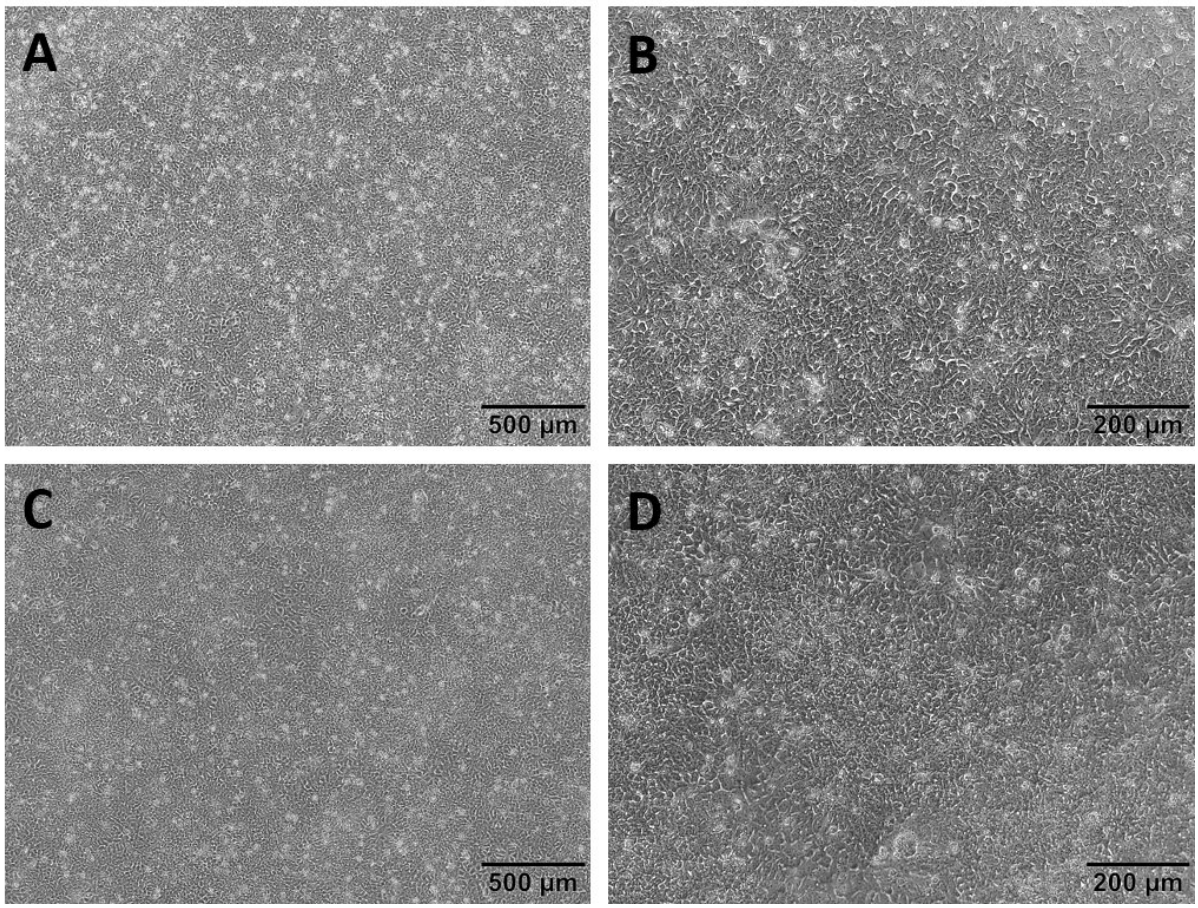

Figure 10: Comparison of human induced pluripotent stem cells grown on Laminin (LN521) and Matrigel.

Representative phase-contrast microscopic images of cultivated hiPSC line iPS11 grown in FTDA medium for three days on **A, B:** LN521 or **C, D:** Matrigel. Images were taken with an Olympus CKX53SF and integrated camera SC50.

Cells grew to 100 % confluence after three days on Matrigel or LN521 (Figure 10), and the morphology does not differ between the coatings. Cells are small in size, densely grown, and show a low cytoplasm-to-nucleus ratio (Figure 10). Further experiments were performed using LN521 for the hiPSC culture.

4.1.2 Morphology and proliferative behavior of hiPSCs

Cells in culture were quality-controlled by daily microscopic photo documentation. Human iPSCs were evaluated regarding their cell size, cytoplasm-to-nucleus ratio, the number of nucleoli, and the presence of intercellular space.

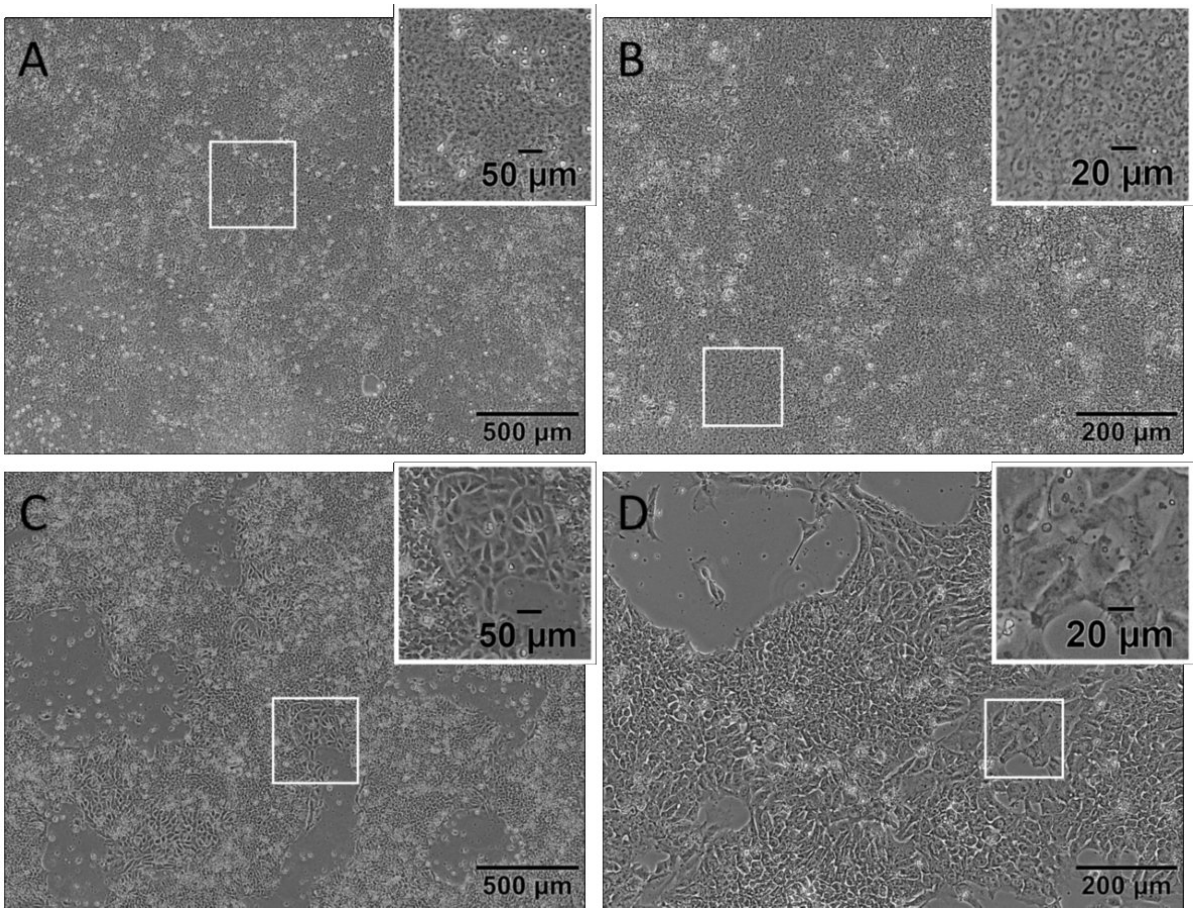

Figure 11: The human induced pluripotent stem cell (hiPSC) line iPS11 displaying pluripotent and differentiated morphology.

Representative phase-contrast microscopic images of cultivated iPS11 grown on Laminin521 (LN521) in FDTA medium were taken with an Olympus CKX53SF and integrated camera SC50 after three (D) or four (A, B, C) days of cultivation. **A, B**: Human iPSCs with a pluripotent morphology indicated by a small cytoplasm-to-nucleus ratio, multiple nucleoli, and small cell size (40x and 100x magnification, respectively). **C**, **D**: Human iPSC culture including differentiated cells showing a high cytoplasm-to-nucleus ratio, a large size, flattened morphology, and so-called differentiation cracks seen as white lines (40x and 100x magnification, respectively) (Galanjuk et al., 2022).

Cells in Figure 11 A and B exhibit a uniform small size with multiple nucleoli and no intercellular space. In comparison, cells in Figure 11 C and D are different in size within the same cell culture, partially with a flattened morphology, nucleoli are almost unnoticeable or not visible in some cells, and the intercellular space is noticeable as a white line between cells. The differences between a cell culture

with pluripotent morphology on the top row (Figure 11 A and B) and differentiated morphology on the bottom row (Figure 11 C and D) are especially seen in the magnifications on the top right of each image, illustrating, for instance, the difference in size. On the day of cell passaging, a confluence of 90–100 % should be reached resulting in a distinct cell proliferation scheme, depending on whether cells are confluent after three or four days. Cells were observed and photo-documented every working day to recognize deviant proliferative behavior.

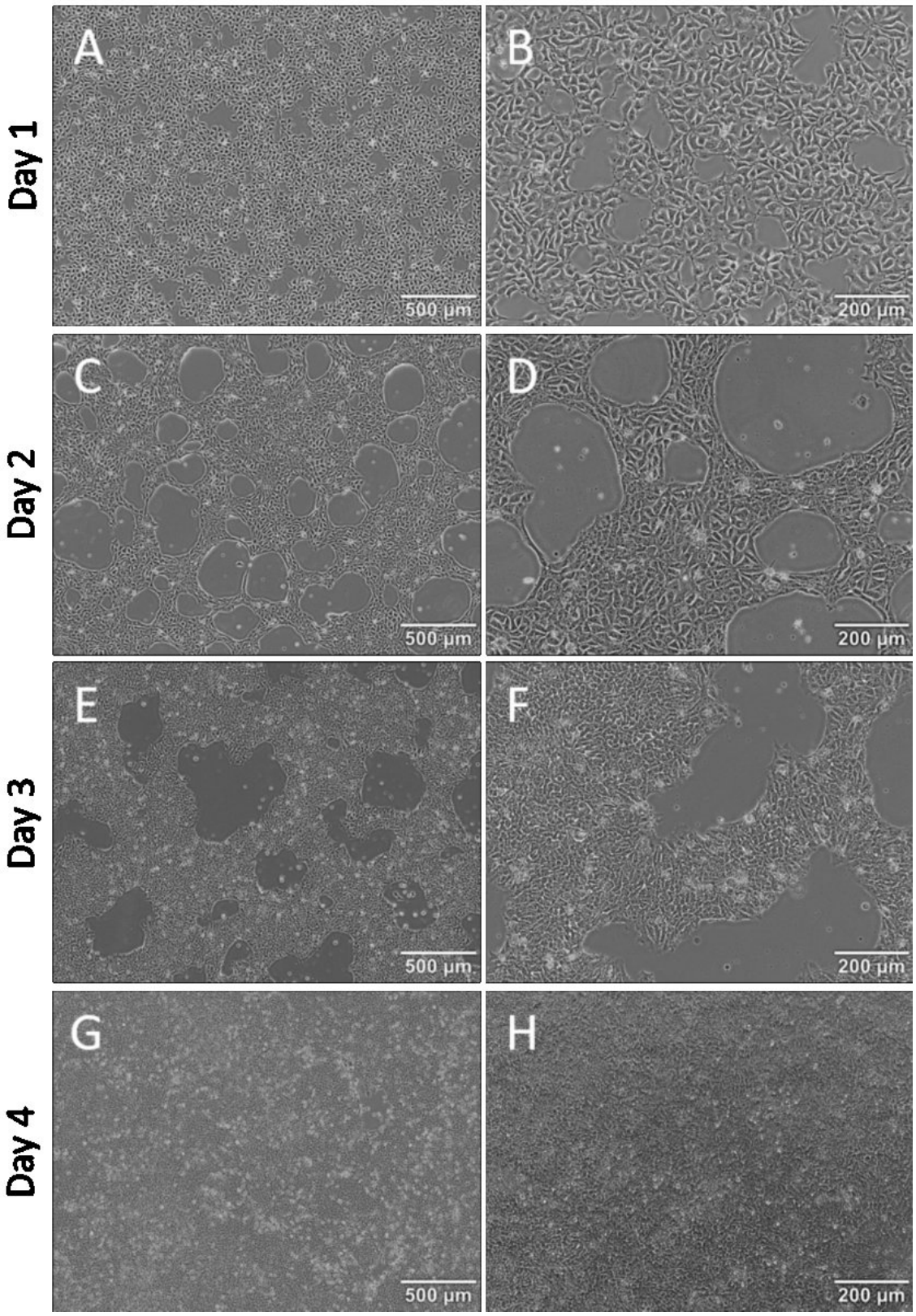

Figure 12: Exemplary phase-contrast images of the human induced pluripotent stem cell (hiPSC) line iPS11 as a function of culture time.

Human iPSCs were seeded with a density of 3×10^5 cells per Laminin521 (LN521)-coated 6-well and cultured in FTDA for four days. Cells were in passage six after thawing. Images of the same well were taken with an Olympus CKX53SF with an integrated camera SC50 on days one, two, three, and four. **A, C, E, G:** 40x magnification **B, D, F, H:** 100x magnification (Galanjuk et al., 2022).

On day one, 24 h after single-cell splitting, cells were enlarged showing a high cytoplasm-to-nucleus ratio and the intercellular space was noticed as white lines. Additionally, cells have built thin branches and no identifiable border was visible between cells and the matrix (Figure 12 A and B). On day two, some cells were still enlarged but at the same time, some cells already had a reduced cytoplasm-to-nucleus ratio. The intercellular space was still visible but branches were retrieved. Instead, a clear border between cells and the matrix was visible resulting in the formation of round holes (Figure 12 C and D). On day three, cells were uniform in their small cytoplasm-to-nucleus ratio compared to days one and two. Additionally, the white lines were not as prominent as the days before (Figure 12 E and F). On day four, cells were confluent to 90–100 %, were small in size with a small cytoplasm-to-nucleus ratio, and displayed no white lines in the intercellular space (Figure 12 G and H). The morphology was comparable to the cells in Figure 11 A and B. Before cardiomyocyte differentiation, hiPSCs were cultured for three days instead of four as shown in Figure 12, still reaching 90–100% confluence. To achieve a better understanding of how long cells can be kept in culture for the downstream application of cardiomyocyte differentiation, cells were photo-documented on day three for 20 passages to observe the morphology over time and passages.

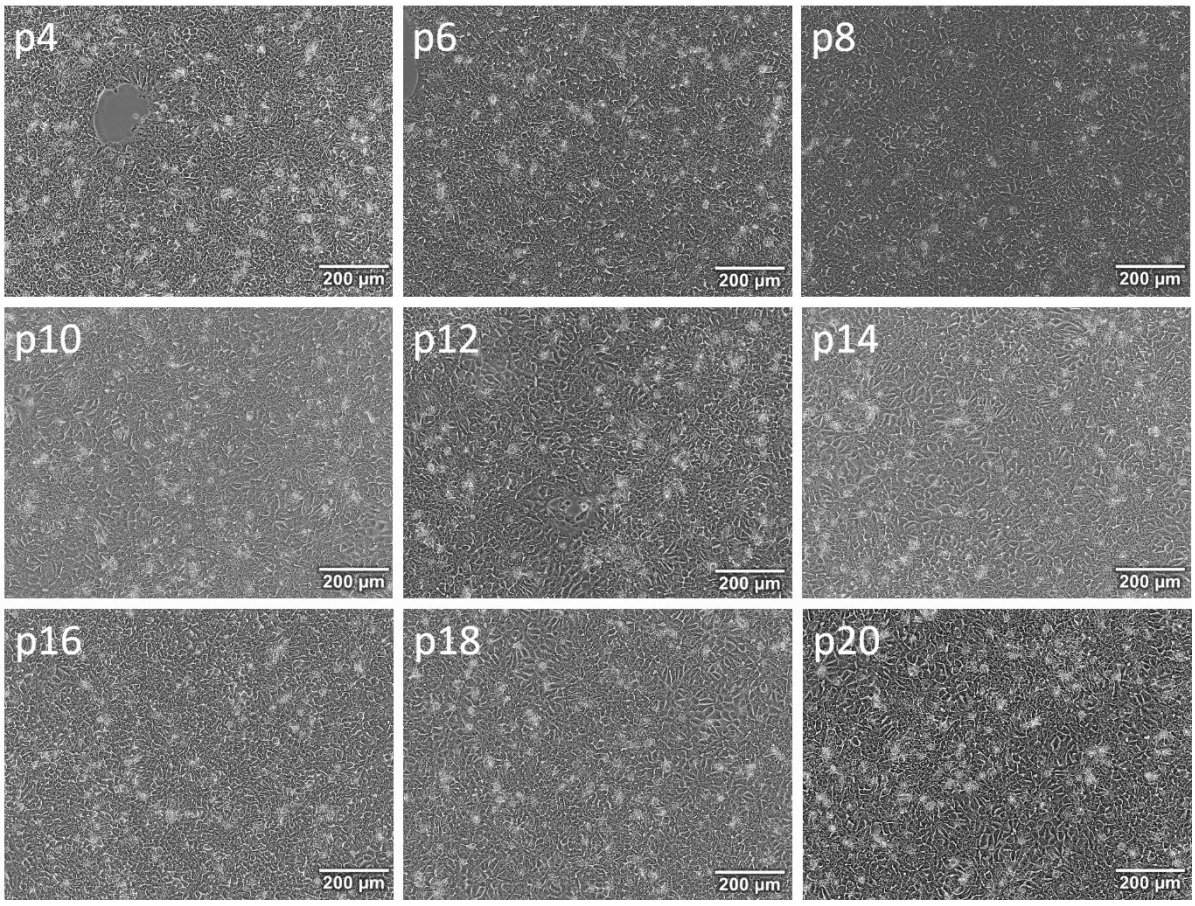

Figure 13: Exemplary phase-contrast images of human induced pluripotent stem cells (hiPSCs) from passages 4 to 20 after three days of cultivation.

Human iPSCs (cell line iPS11) were seeded with a density of 4×10^5 cells per Laminin521 (LN521)-coated 6-well and cultured in FTDA for three days. A confluence of 90–100 % was reached after three days. Images were taken with an Olympus CKX53SF with an integrated camera SC50. 40x magnification, p = passage.

The morphology of cells almost did not change from p4 to p20 (Figure 13). However, from p12 onwards, more cells appear larger within the culture compared to p4–10. It is noteworthy that cells growing confluent over three days (Figure 13) partially show a white line in the intercellular space compared to cells growing confluent over four days (Figure 12 G and H). Besides daily photo documentation, quality control on protein level was performed to further characterize and evaluate the hiPSC culture over time. For this purpose, flow cytometry was performed using four specific pluripotency-associated markers expressed in hiPSCs, namely, NANOG, SOX2, OCT4, and SSEA4.

4.1.3 Flow cytometry analysis of human induced pluripotent stem cells

Flow cytometry analysis was performed to evaluate the percentage of proteins marked with fluorochrome-conjugated antibodies in iPS11 cells. The pluripotency markers NANOG, SOX2, OCT4, and SSEA4 were examined in every other passage from p4 to p20.

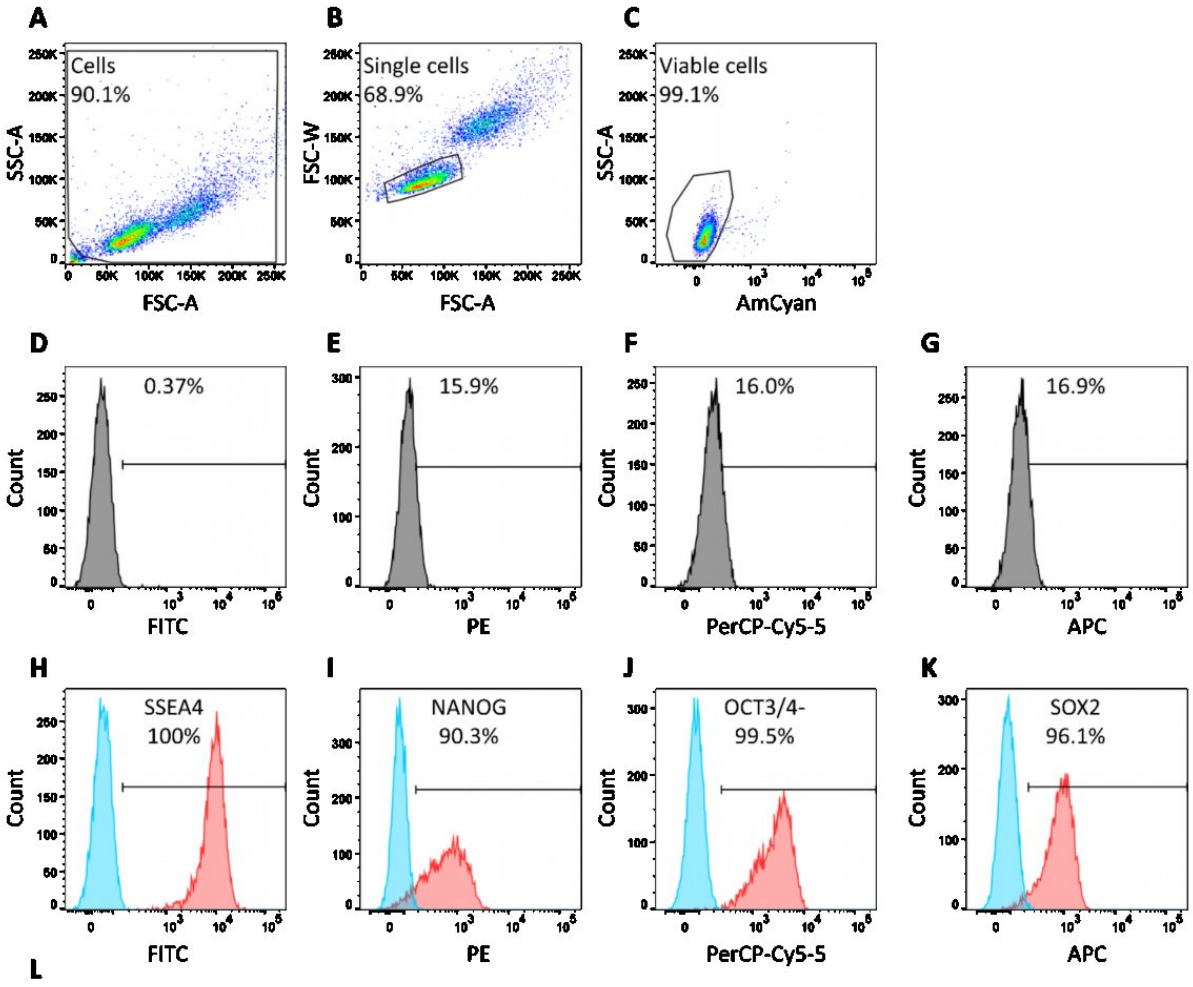

L

	p4	p6	p8	p10	p12	p14	p16	p18	p20
SSEA4 $^{+}$ (%)	100	99	99	99	94	99	97	99	87
NANOG $^{+}$ (%)	90	83	78	80	2	93	85	94	82
OCT3/4 $^{+}$ (%)	100	97	98	97	95	95	90	97	91
SOX2 $^{+}$ (%)	96	93	96	92	86	91	88	95	86

Figure 14: Flow cytometry analyses of human induced pluripotent stem cell (hiPSC) line iPS11 analyzed for stem cell markers NANOG-PE, OCT3/4-PerCP-Cy5.5, SOX2-Alexa Fluor 647, and SSEA-4-FITC, plus fixable viability stain 510 (FVS510) as a live/dead discriminator.

The human iPSC line iPS11 was cultured in FTDA on Laminin521 (LN521)-coated 6-well plates in a single-cell-based culture and analyzed every other passage (p) from p4 to p20 after three days of cultivation. The acquisition was performed using a BD FACSCanto II system operated with the BD FACSDiva software. Further analysis was conducted with FlowJo. **A–K:** Exemplary flow cytometry results of hiPSCs in p4. Alexa Fluor 647 was detected in the channel for APC. **A:** Gating strategy for the relevant cell population. **B:** Gating strategy to ensure analyses of single cells. **C:** Gating strategy to discriminate between live and dead cells. **D–G:** Isotype controls for the respective antibodies. Gating was performed based on the unstained control with a maximum of 0.49 % positively marked cells in the unstained control, every signal above was counted as positively stained. **H–K:** The gate (black line) was set to a maximum of 0.49 % positive cells in the unstained control (blue peak), every signal above was counted as a positive signal (red peak). **L:** Percentages of positively stained cells (indicated by "+") of the flow cytometry analyses from p4 to p20 for the indicated markers. p = passage (Galanjuk et al., 2022).

The gating strategy for flow cytometry analysis is shown exemplarily in Figure 14 A–C. The first gate excluded the debris analyzing only the relevant cell population which was 90.1 % of all detected signals

(Figure 14 A). Afterward, a gate was set to exclude doublets resulting in a single-cell population of 68.9 % (Figure 14 B). Viable cells (99.1 %) were gated for further analysis, excluding dead cells (Figure 14 C). For analysis of the markers of interest, further gating was performed based on the viable cell population. For this, a gate was created within the unstained sample that excludes all unstained cells only displaying detected signals. The gate allowed to include a maximum of 0.49 % detected signals within the unstained control. All signals detected above this threshold were counted as positive staining. As a result, isotype controls showed a slight shift leading to a positive signal of 0.37, 15.9, 16.0, and 16.9 % of the respective antibodies for SSEA4, NANOG, OCT3/4, and SOX2, respectively (Figure 14 D–G). Positively stained cells depicted in red exhibited a distinguishable peak compared to the unstained cell population in blue (Figure 14 H–K). Of all viable cells analyzed, 100, 90.3, 99.5, and 96.1 % were positively stained for SSEA4, NANOG, OCT3/4, and SOX2, respectively (Figure 14 H–K) in p4. The percentages of positively stained cells for the mentioned markers in p4 to p20 are listed in Figure 14 L. The percentage of SSEA4 positively stained cells ranged from 100 to 94 % within p4 to p18, however, in p20 the percentage of positively stained cells decreased to 87 % (Figure 14 L). Positively stained cells for marker NANOG followed no trend over the different passages ranging from 80 to 93 % from p4 to p20. The NANOG-positive population of 2 % determined in p12 (Figure 14 L) was identified as a statistical outlier (Grubbs' test), which can probably be attributed to an error in protocol execution. The marker OCT3/4 was stained in 90 to 100 % of the cells from p4 to p20 (Figure 14 L). The marker SOX2 was detected in 86–96 % of cells from p4 to p20 (Figure 14 L). It is noteworthy that the highest expression of SSEA4, OCT3/4, and SOX2 were detected in p4, the earliest evaluated passage. Additionally, the three highest percentages for these markers were measured in the first three evaluated passages p4, p6, and p8. The highest expression of marker NANOG, however, was detected in p18 (Figure 14 L). The lowest measured percentage 87, 90, and 86 % of the respective markers SSEA4, OCT3/4, and SOX2 was detected between p16 and p20, and also p12 for SOX2. An exception is the marker NANOG which displayed the lowest measured percentage (78 %) in p8 (Figure 14).

4.2 The cardiomyocyte differentiation protocol

The differentiation protocol described in section 3.4 is based on the publication of Zhang et al. (2015) describing a method to differentiate hiPSCs into cardiomyocytes in a 2D and 3D culture system by modeling the WNT and BMP signaling pathways. The 2D protocol was slightly adapted in the following points: For TS medium 250 µM 2-phospho-L-ascorbic acid was used, which is of optional use in the protocol of Zhang et al. (2015). The medium replacement was altered from daily to every other day from day four onwards. The system was transferred from a 24-well to a 48-well format. The first step in using the adapted protocol was the determination of the optimal concentrations of CHIR and BMP4 to achieve the most confluent beating structure of cardiomyocytes. The concentrations of CHIR and

BMP4 are given as a range in the protocol of Zhang et al. (2015) which was tested and expanded in a grid scheme.

4.2.1 Concentration grid of CHIR and BMP4

The titration of CHIR and BMP4 was performed in a grid with concentrations of CHIR and BMP4 ranging from 1 to 1.75 µM and 0.75 to 2 ng/mL, respectively. The initial range-finding experiment was performed in the original 24-well format used for experiments in the protocol of Zhang et al. (2015), however, the plate format was changed to 48-well plates afterward to allow for testing of the concentrations of interest in triplicates.

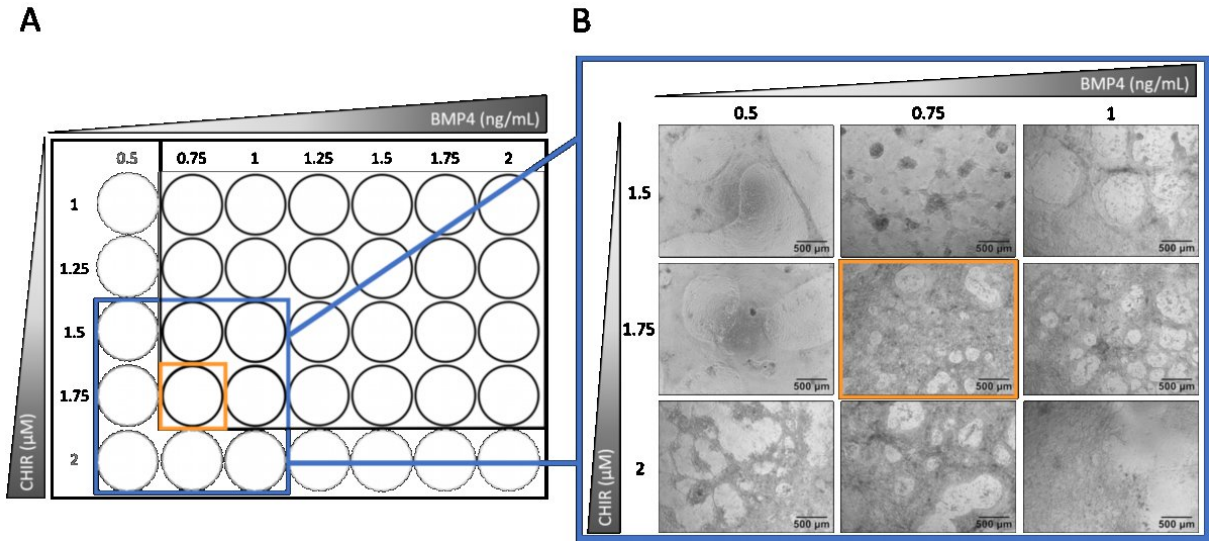

Figure 15: Scheme of the range-finding experiment of CHIR99021 (CHIR) and bone morphogenetic protein 4 (BMP4) concentrations.

A: The concentrations of CHIR and BMP4 were examined in a grid of 1 to 1.75 µM CHIR and 0.75 to 2 ng/mL BMP4 in increments of 0.25 µM and ng/mL, respectively. For this, the protocol described in section 3.4 was used but seeding 5×10^5 cells per Matrigel-coated 24-well in 1.5 mL ITS or TS each with the respective concentrations of CHIR and BMP4. In case the first results showed an optimal concentration combination at the edge of the grid (orange square in A), the grid was extended framing the optimal concentration (blue square in A), and tested again. **B:** Exemplary phase-contrast images of the grid testing for iPS11 cells. The grid was extended to 2 µM CHIR and 0.5 ng/mL BMP4 as shown in A (blue square). Concentrations of interest were tested in triplicates seeding 2.75×10^5 cells per Matrigel-coated 48-well following the protocol described in section 3.4 with the respective concentrations of CHIR and BMP4. Exemplary images were taken on day ten using an Olympus CKX53SF with an integrated camera SC50. Magnification: 40×, (Galanjuk et al., 2022).

The results of the first grid in the 24-well format following the scheme shown in Figure 15 A indicated an optimal concentration of 1.75 µM CHIR and 0.75 ng/mL BMP4 as cardiomyocytes displayed a confluent layer of beating cells. However, the initial grid contained only one well per concentration combination, in addition, the concentration combination of choice was located on the edge of the grid. To confirm the results, the grid was extended as shown in Figure 15 A (blue square), and transferred to a 48-well format that allows for testing in triplicates to evaluate the reproducibility of the previous results. Exemplary phase-contrast images of the extended grid are shown in Figure 15 B. Additionally, video recordings of each concentration combination shown in Figure 15 B were

performed to evaluate the beating area visually (Video 1 on CD). As a result, all concentration combinations tested did lead to beating cardiomyocytes, except for 1.5 µM CHIR and 0.5 ng/mL BMP4. However, the area of the well covered with beating cardiomyocytes and beating behavior differed between the concentrations. The concentration combination of 1.75 µM CHIR and 0.75 ng/mL BMP4 was the only one where the whole well area was covered with beating cardiomyocytes that were beating in a uniform synchronous wave (Video 1 on CD, orange square), confirming the results of the initial range-finding experiment. Based on these results, the differentiation protocol for the hiPSC line iPS11 was performed using 1.75 µM CHIR and 0.75 ng/mL BMP4 for all following experiments.

4.3 Characterization of hiPSC-derived cardiomyocytes

For the final application of substance testing, cardiomyocytes were first characterized to ensure a quality-controlled basis and to have a better understanding of the differentiation process and maturity stage of the generated cardiomyocytes on day ten of the protocol. Additionally, the results of the characterization were used to evaluate if the protocol can be shortened.

4.3.1 Morphological changes during differentiation from hiPSCs to cardiomyocytes

Human iPSCs change in morphology and proliferative behavior during the ten-day differentiation protocol until they reach their typical cardiomyocyte morphology. In Figure 16, images of the same well were taken over the ten-day differentiation protocol to document these changes.

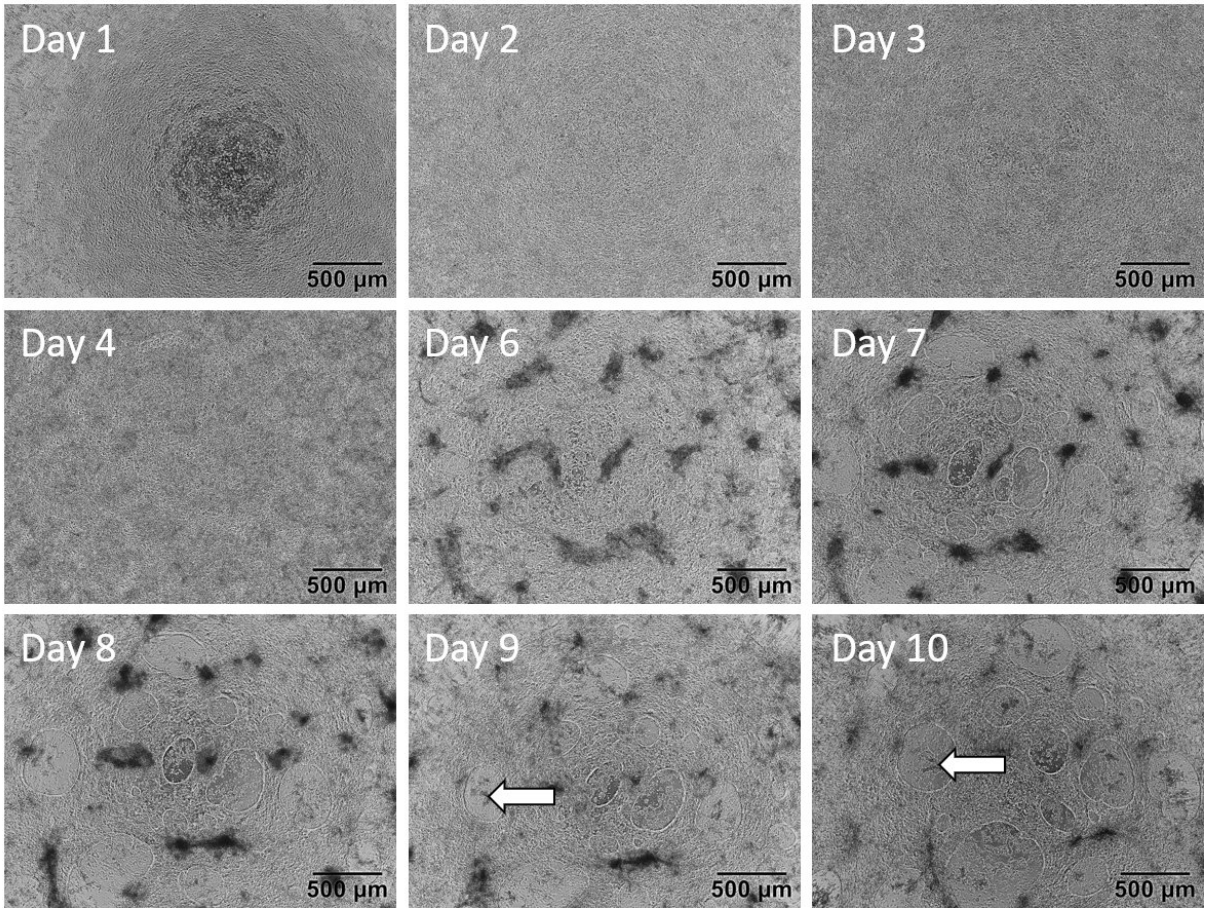

Figure 16: Exemplary phase-contrast images of the same well of human induced pluripotent stem cells (hiPSCs) differentiating into cardiomyocytes over a time course of ten days.

First, 2.75×10^5 cells per Matrigel-coated 48-well were plated on day zero in ITS medium. **Day 1**: 24 h after seeding, the medium was completely replaced with TS medium. Cells grew on top of each other. **Day 2 and 3**: Medium was replaced with TS medium supplemented with 2 µM IWP2. Cells grew to uneven heights. **Day 4**: Medium was replaced with TS medium. Only slight changes in the heights of the cell layer are visible. On day five, cells were not fed and not photo-documented. **Day 6**: TS medium was removed and fresh TS medium was applied. Cells started to form holes but were still attached to the matrix. **Day 7**: Cells formed multiple holes and further detachment from the matrix was observed. The first areas of beating cardiomyocytes were observable. **Day 8**: TS medium was removed and freshly applied. Cells started to beat in a wave motion. **Day 9–10**: The morphology of cells did not alter noticeably. The beating developed into a synchronous wave contracting over the entire well on day ten. Dead cells were trapped under the beating cells and did not get sucked in during medium replacement, staying in place up to day ten (white arrows). Images were taken with an Olympus CKX53SF and an integrated camera SC50. Magnification: 40x, ITS = Insulin, Transferrin, Selenous acid, TS = Transferrin, Selenous acid, IWP2 = Inhibitor of WNT production 2 (Galanjuk et al., 2022).

During the differentiation period of ten days, cells displayed a typical morphology and specific features on certain days. On day one, cells had grown on top of each other after culturing the cells in ITS medium for 24 h (Figure 16, Day 1) which is not observable in the hiPSC culture (Figure 12 G and H and Figure 13). On day two, cells have been cultured with no modulation of signaling pathways for 24 h. During this time, cells have further grown on top of each other. After the addition of IWP2 on days two and three, cells continued to proliferate and built multiple layers with uneven levels of height (Figure 16, Days 3 and 4). After the application of TS medium containing IWP2, cell death was a normal phenomenon that sometimes appeared stronger on days three and four. On day four, IWP2

supplemented TS medium was completely replaced with TS medium. The medium was not changed on day five, nor was the culture photo-documented. On day six, denser areas of cells were present appearing darker on phase-contrast images and the typical mesh with holes already started to form, yet cells were still attached to the matrix (Figure 16, Day 6). Holes were not always visible on day six but appeared on day seven at the latest (Figure 16, Day 7). Multiple contracting areas were observable on day seven when cells started to lift from the matrix. At this point, the typical mesh structure consisted of multiple cell layers (Figure 16, Day 7). From day eight to ten, the morphology did not change noticeably (Figure 16, Day 8–10). Cells started beating latest on day eight, additionally, some cells started beating at multiple points in small waves. On days nine and ten of differentiation, not only did the beating intensity increase, but it resulted in a uniform wave motion as shown in Video 2 on CD. Beating cardiomyocytes were connected to the matrix with only a few cell-matrix contacts. Dead cells were trapped under the mesh and did not get sucked in during medium replacement, staying in place up to day ten (Figure 16, Days 9 and 10, white arrows). Cells were photo-documented every working day to ensure a high quality of cardiomyocyte differentiation and to notice deviations from the development shown in Figure 16. After reproducibly differentiating cardiomyocytes, the next step was to examine how the passage number of the hiPSC culture influenced the outcome of cardiomyocyte differentiation.

4.3.2 Cardiomyocyte differentiation outcome in relation to hiPSC passages

Human iPSCs were differentiated into cardiomyocytes every other passage from p4 to p20 to establish a cut-off on how long hiPSCs can be cultured for a successful cardiomyocyte differentiation ensuring a stable and reproducible outcome for substance exposure experiments. For this, videos of cardiomyocytes derived from hiPSCs in p4 to p20 were recorded on day ten (Video 3). Beating area and beating frequency were analyzed using the in-house developed software CardioVision.

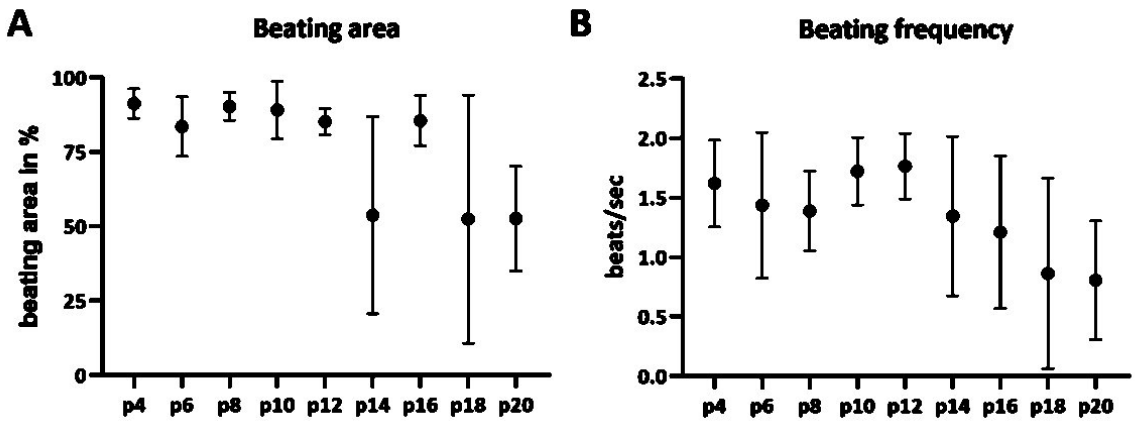

Figure 17: Beating area and beating frequency analysis of cardiomyocytes derived from human induced pluripotent stem cells (hiPSCs) in different passages (p).

For cardiomyocyte differentiation, 2.75×10^5 cells per Matrigel-coated 48-well were plated and cultured according to the protocol described in section 3.4. The hiPSCs used for differentiation were in different passages ranging from p4 to p20. Results from p6 to p12 included video recordings of control wells of substance testing from different experiments (N=2), while results from p4 and p14 to p20 were derived from only one experiment. For each passage, 10–18 videos were evaluated. No statistical analysis was performed due to n<3, mean ± SD of technical replicates from one or two experiments.

The beating area in p4, p6, p8, p10, and p12 was at 91, 84, 90, 89, and 85 %, respectively. In passage 14, however, the average beating area was reduced to 54 % followed by 86 % in passage 16. Passages 18 and 20 showed a beating area of 52 and 53 %, respectively. It is noteworthy that results from passages resulting in reduced beating areas (p14, p18, and p20) also displayed a high standard deviation (Figure 17 A). The reduced beating area is also seen in Video 3 on CD showing exemplary videos of cardiomyocytes differentiated from hiPSCs in different passages. The beating frequency was at 1.6, 1.4, 1.4, 1.7, and 1.8 beats/sec in p4, p6, p8, p10, and p12, respectively. From p14 onwards, a trend towards a decreasing beating frequency was observed resulting in 1.3, 1.2, 0.9, and 0.8 beats/sec in p14, p16, p18, and p20. Again, the standard deviation was higher in higher passages. Interestingly, although the beating area is at 86 % in p16, the beating frequency is the third lowest (1.2 beats/sec) with a high standard deviation (Figure 17 B) which is also seen in Video 3 on CD. Due to these results hinting towards a higher variability in later passages, experiments were only performed with hiPSCs in p4 to p12. Besides the documentation of the morphological development of cardiomyocytes and evaluation of their beating area and beating frequency, gene expression of developing cardiomyocytes was assessed.

4.3.3 Gene expression analysis of hiPSCs differentiating into cardiomyocytes

Gene expression of markers across the developmental stages of cardiomyocytes was examined for multiple purposes. First, to gain information to which extent the differentiation of *in vitro* hiPSC-based cardiomyocytes is comparable to the physiological development of cardiomyocytes *in vivo*, and second, to identify suitable marker genes for endpoint analysis that might change upon substance

exposure. Third, it gives information on when genes were stably expressed and if the protocol could potentially be shortened which would be convenient for large-scale substance screening.

A suitable reference gene for expressing qRT-PCR results as mean copy numbers of the target gene per copy numbers of the reference gene was chosen. Preliminary results showed that the reference gene β-Actin was differently expressed in cells during differentiation from hiPSCs into cardiomyocytes. Based on literature research, N-Acylsphingosine Amidohydrolase 2 (*ASAH2*)*, CAPN10*, and *CANX* were identified as the top three most stably expressed genes in cells of the mesodermal lineage (Holmgren et al., 2015). Analyzing the qRT-PCR results of cardiomyocytes on day ten and hiPSCs, the marker *ASAH2* did not show a specific signal as the amplification curves raised together with the negative control resulting in Ct values of around 30 when assuming a threshold of 0.1. However, the markers *CANX* and *CAPN10* both showed an expression. Standards were established for both markers leading to the result that the gene *CANX* was expressed in tremendously higher copy numbers than *CAPN10* which led to the decision of *CANX* as a suitable reference gene in anticipation that the markers of interest could reach similar copy numbers (Figure 18 A).

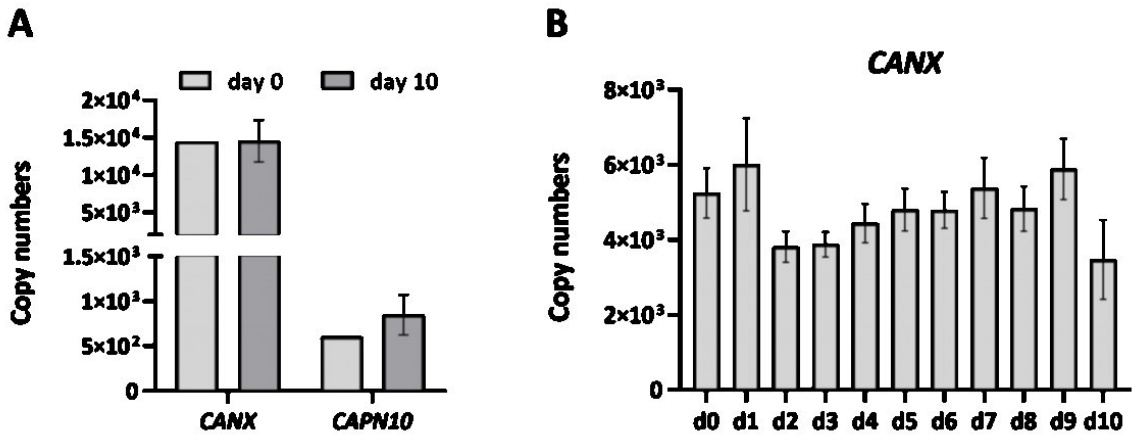

Figure 18: Expression of the genes *CANX and CAPN10.*

A: Expression of the genes *CANX* and *CAPN10* in hiPSCs (day 0) and cardiomyocytes on day ten (day 10) of the differentiation protocol. For day zero, 1–2 million hiPSCs were collected during the passaging procedure. For day 10, six replicates of 2.75×10^5 hiPSCs/well were seeded onto Matrigel-coated 48-well plates and differentiated according to the protocol described in section 3.4. On day ten, samples were collected for qRT-PCR and prepared together with the hiPSC sample as described in section 3.7. N = 1; mean ± SD. **B:** Triplicates of 2.75×10^5 hiPSCs/well were seeded onto Matrigel-coated 48-well plates and differentiated according to the protocol described in section 3.4. Each day a triplicate was collected and pooled for qRT-PCR analysis of the reference gene *CANX*. For the time point named "d0", 1–2 million hiPSCs were collected during the splitting procedure of the respective experiment. N = 4; mean ± SEM; one-way ANOVA followed by a Tukey multiple comparisons test; $p \leq 0.05$ was considered significant. Each data set was compared to the other. *CANX* = calnexin, *CAPN10* = calpain10. D = day.

The reference gene *CANX* was stably expressed in hiPSCs as well as in samples on every day of the protocol up to differentiated cardiomyocytes on day ten (Figure 18 B). No significant difference in expression was detected comparing all days with each other. Therefore, *CANX* was used as the

reference gene for all further gene expression analyses. Gene expression analysis was performed evaluating markers that reflect different stages from hiPSCs differentiating into cardiomyocytes, namely, *OCT4*, *MESP1*, *ISL1*, *GATA4*, *TNNT2*, and *ACTN2*.

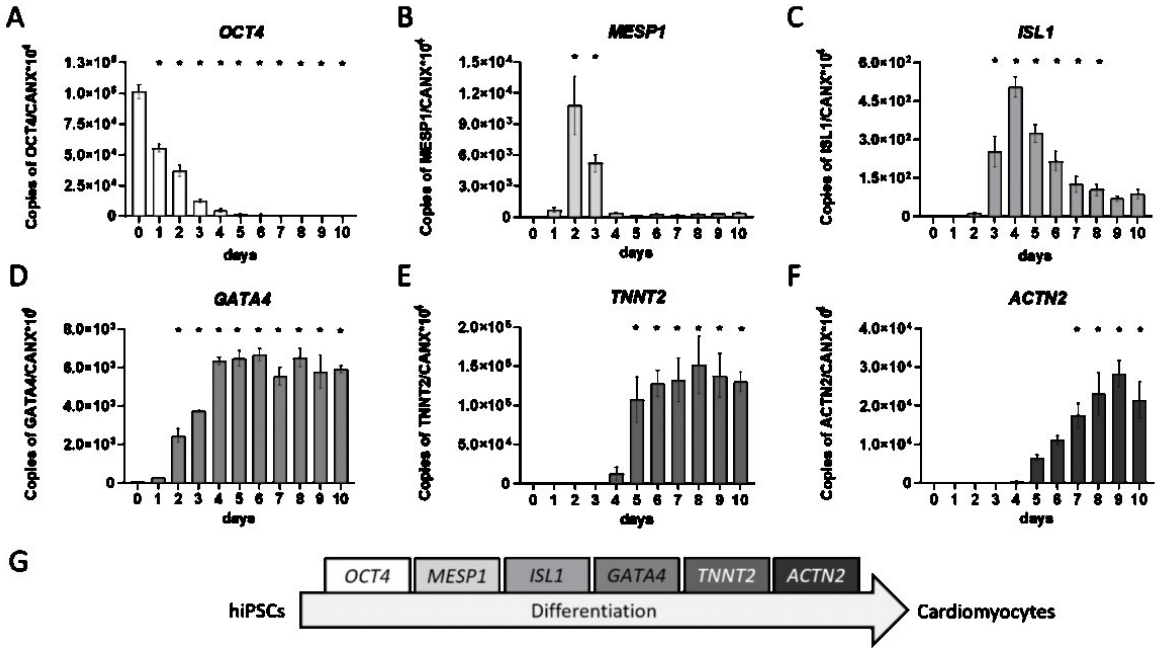

Figure 19: Quantitative real-time PCR (qRT-PCR) analyses of differentiating human induced pluripotent stem cell (hiPSC)-derived cardiomyocytes over a time course of ten days.

Triplicates of 2.75×10^5 cells per well were seeded onto Matrigel-coated 48-well plates and differentiated according to the protocol described in section 3.4. On each day of the protocol, a triplicate of samples was collected and pooled for qRT-PCR analysis of marker genes for **A**: stem cells, **B**: cardiac mesoderm, **C** and **D**: cardiac progenitor cells, and **E** and **F**: functional cardiomyocytes. **G**: Depiction of chosen markers related to the differentiation stages from hiPSCs to cardiomyocytes. Day 0 represents hiPSCs used for the respective differentiation collected during the cell passaging procedure ($1–2\times10^6$ cells). Mean values of copy numbers of the target genes *OCT4*, *MESP1*, *ISL1*, *GATA4*, *TNNT2*, and *ACTN2* were normalized to the reference gene *CANX*. N=3; mean ± SEM; one-way ANOVA followed by a Dunnett multiple comparisons test; $p \leq 0.05$ was considered significant, * = significant compared to day 0. *CANX* = calnexin, *CAPN10* = calpain 10, *OCT4* = octamer-binding protein 4, *MESP1* = mesoderm posterior 1, *ISL1* = Insulin gene enhancer protein 1, *GATA4* = GATA-binding protein 4, *TNNT2* = cardiac troponin T, *ACTN2* = α actinin2 (Galanjuk et al., 2022).

The expression of the stem cell marker *OCT4* significantly decreased from day one with almost no expression detectable from day five onwards. The expression of the early mesoderm marker *MESP1* was significantly increased on days two and three with a peak expression on day two. From day three onwards, the expression decreased. Slightly time-shifted, the expression of the progenitor marker *ISL1* arose being significantly expressed from day three onwards with a peak expression on day four. Afterward, the expression decreased but was still significantly increased compared to day zero until day eight. Concomitantly, the progenitor cell marker *GATA4* was expressed significantly higher compared to day zero from day two onwards, reaching a plateau on day four. The expression of early cardiomyocyte marker *TNNT2* was significantly increased compared to day zero from day five onwards being stably expressed up to day ten. The expression of the later cardiomyocyte marker *ACTN2* slowly

arose from day five onwards being significantly higher expressed from day seven onwards compared to day zero. The cardiomyocyte markers *TNNT2* and *ACTN2* were chosen for further analysis using flow cytometry as these markers were highly expressed on day ten compared to the other evaluated markers and, therefore, were possible candidates for endpoint analysis in later substance testing.

4.3.4 Flow cytometry analysis of hiPSC-derived cardiomyocytes

To perform reproducible experiments, a cell population as uniform as possible should be present, which ideally is subjected to only minor interexperimental variations. Flow cytometry analysis of hiPSC-derived cardiomyocytes was performed on culture days eight, nine, and ten evaluating the markers cTnT, α-actinin2, and GATA4. An evaluation of to which extent cardiomyocytes were positively stained for the mentioned markers was performed as well as how stable these proteins were expressed among different experiments. Additionally, it was evaluated if the protocol can be shortened in case a stable expression of cardiomyocyte-specific markers is reached earlier than day ten.

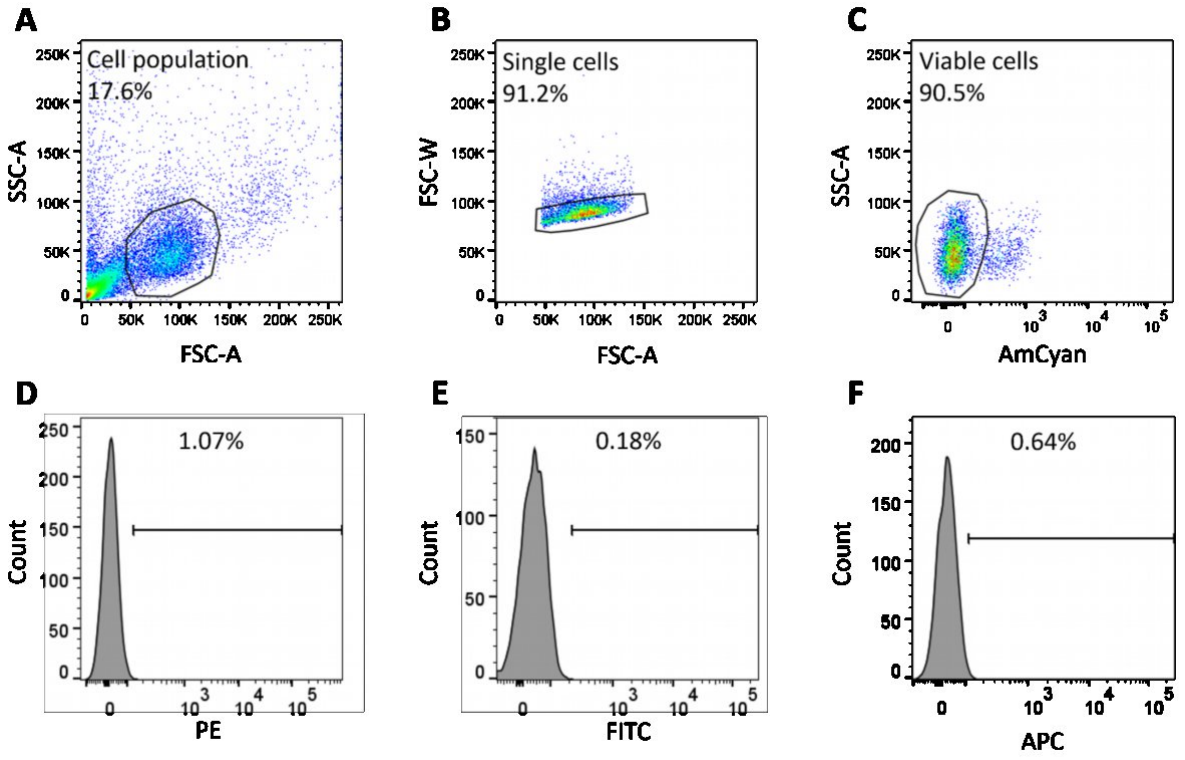

Figure 20: Exemplary gating strategy for flow cytometry analysis and results of isotype controls of human induced pluripotent stem cell (hiPSC)-derived cardiomyocytes.

Human iPSCs were differentiated into cardiomyocytes as described in section 3.4 in replicates of 16 for every day of analysis and pooled on the respective days. Flow cytometry analyses were performed using a BD FACSCanto II system operated with the BD FACSDiva software. Further analyses were conducted with FlowJo. **A:** Gating strategy for the relevant cell population. **B:** Gating strategy to ensure analyses of single cells. **C:** Gating strategy to discriminate between live and dead cells. **D, E, F:** Isotype controls for the respective antibodies cTnT (PE), α-Actinin2 (FITC), and GATA4 (APC) were used for analysis. Adapted from Galanjuk et al. (2022).

The gating strategy for flow cytometry analysis is shown exemplarily for a day ten sample in Figure 20 A–C. The first gate excluded debris analyzing only the relevant cell population representing 17.6 % of all measured signals (Figure 20 A). Based on the gated cell population, a gate was set to exclude doublets resulting in a single-cell population of 91.2 % (Figure 20 B). Viable cells (90.5 %) were gated for further analysis, excluding dead cells (Figure 20 C). Based on the viable cell population, a gate was set to discriminate between unstained and stained cells. For this, a gate was created within the unstained sample that excluded all unstained cells only detecting signals above a threshold of 0.49 %. As a result, isotype controls of the antibodies for cTnT, α-Actinin2, and GATA4 of the examined sample on day ten were negative with a minimal signal of 1.07, 0.18 %, and 0.64 % respectively (Figure 20 D, E, F).

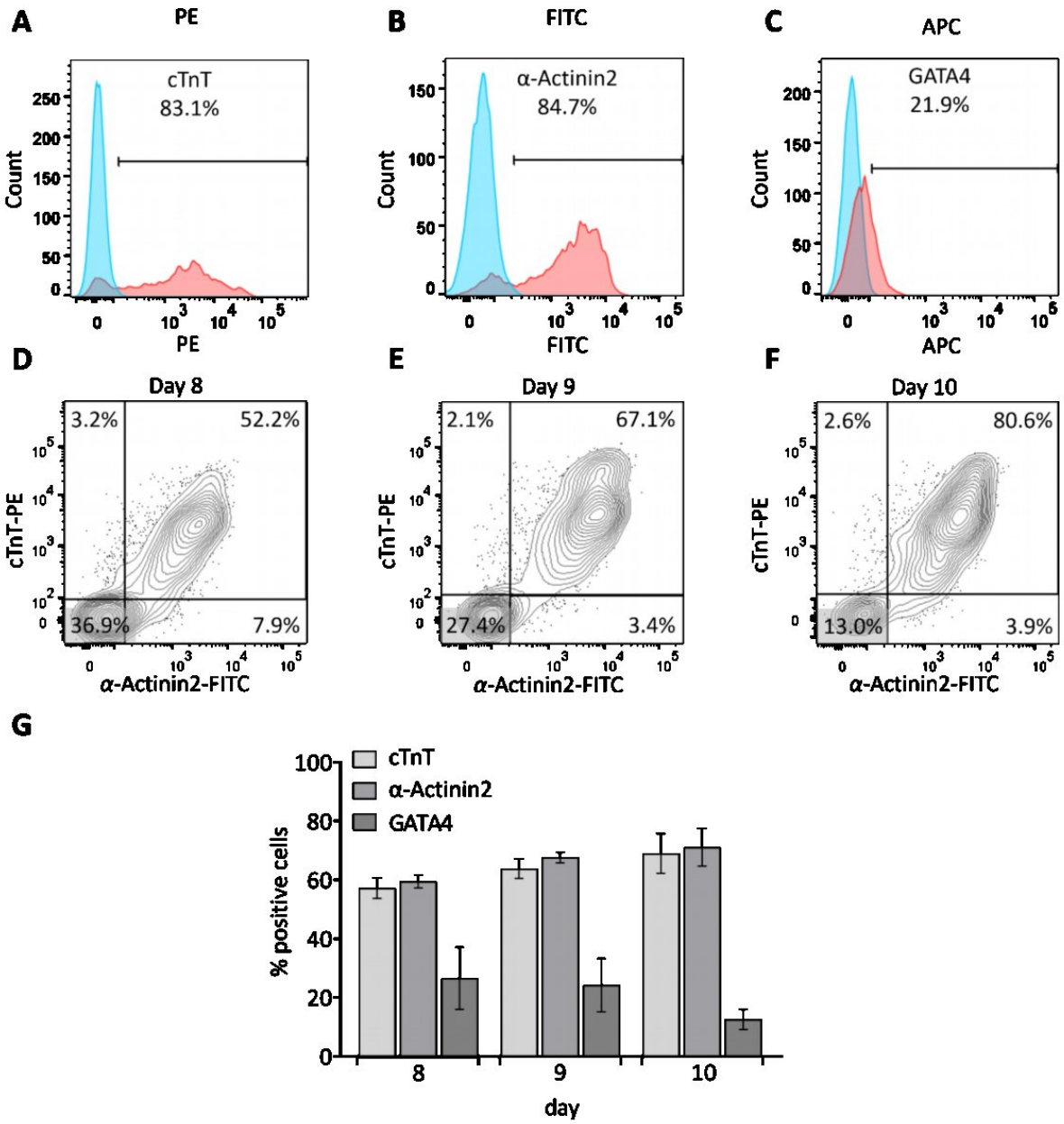

Figure 21: Flow cytometry analysis of human induced pluripotent stem cell (hiPSC)-derived cardiomyocytes analyzed for cardiac-specific proteins cTnT-PE, α-Actinin2-FITC, and GATA4-APC.

Analysis was performed on days eight, nine, and ten of the differentiation protocol including fixable viability stain 510 (FVS510) as a live/dead discriminator.

Human iPSCs were differentiated into cardiomyocytes as described in section 3.4 in replicates of 16 for every day of analysis and pooled on the respective days. Flow cytometry analyses were performed using a BD FACSCanto II system operated with the BD FACSDiva software. Further analyses were conducted with FlowJo. **A, B, C:** Exemplary flow cytometry results of day ten for the markers cTnT-PE, α-Actinin2-FITC, and GATA4-APC; blue peak: unstained cells, red peak: positively stained cells. **D, E, F:** Dot plot diagrams depicting the percentage of negative, single, or double positive stained cells for markers cTnT-PE and α-Actinin2-FITC on days eight, nine, and ten of one experiment. **G:** Results of positively stained cells for the markers cTnT-PE, α-Actinin2-FITC, and GATA4-APC on days eight, nine, and ten. N = 4, mean ± SEM; one-way ANOVA followed by a Dunnett multiple comparisons test; $p \leq 0.05$ was considered significant, compared to day 8. Adapted from Galanjuk et al., 2022.

Positively stained cells depicted in red show a distinguishable peak compared to the unstained cell population in blue resulting in a percentage of 83.1 and 84.7 % positively stained cells for the marker cTnT and α-Actinin2, respectively, of the day-ten sample (Figure 21 A, B). In the day-ten sample of

GATA4, the red curve representing stained cells is only slightly shifted compared to the unstained sample depicted in blue resulting in 21.9 % positively stained cells. (Figure 21 C). This was the case for the other examined samples of GATA4 for all replicates. The majority of cells were double positive on days eight, nine, and ten for cTnT and α-Actinin2, and only a small population expressed only one of the markers (Figure 21 D, E, F). As a result, cTnT and α-Actinin2 expression slightly increased from day eight (57.2 ± 3.5 % and 59.5 ± 2.2 %) to day nine (63.8 ± 3.3 % and 67.6 ± 1.8 %), and finally reaching the highest expression on day ten (69 ± 6.8 % and 71.1 ± 6.4 %) but was not statistically different compared to day eight (Figure 21 G). In contrast, GATA4 expression decreased over time from 26.5 ± 10.6 % on day eight to 24.2 ± 9.1 % on day nine, and 12.5 ± 3.5 % on day ten (Figure 21 G). The maturity stage of the obtained cardiomyocytes was evaluated by performing immunocytochemistry (ICC).

4.3.5 Immunocytochemical staining of hiPSC-derived cardiomyocytes

Immunocytochemical staining for the marker cTnT was established and performed on cardiomyocytes one day after performing the cardiomyocyte differentiation protocol for ten days.

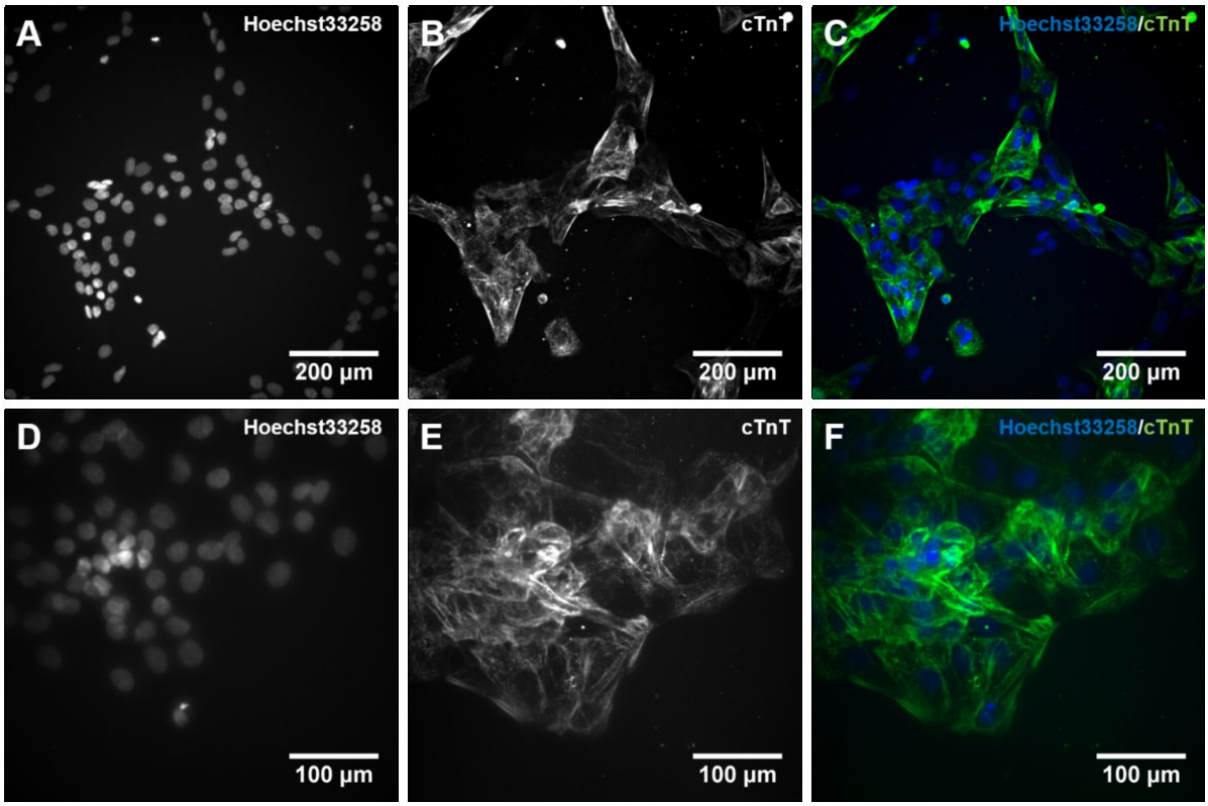

Figure 22: Immunocytochemical (ICC) staining for cardiac muscle Troponin T (cTnT) of human induced pluripotent stem cell-derived cardiomyocytes.

Human iPSCs were differentiated into cardiomyocytes according to the protocol described in section 3.4. On day ten, cells were dissociated with Accutase supplemented with 10 µM Y-27632, and 6×10^4 cells were plated on a 96-well plate coated with Matrigel. Cells were cultivated for an additional 24 h and subsequently stained with an antibody against cTnT together with Hoechst 33258. **A, D:** cell nuclei stained with Hoechst33258; **B, E:** cTnT staining, **C, F:** merged pictures. The visualization was performed with an automated microscopic system

for high-content imaging (CellInsight CX7 LZR Platform). Magnification: **A–C:** 100x, **D–F:** 200x (Galanjuk et al., 2022).

The staining confirmed the presence of cTnT after eleven days of differentiation. It also revealed that almost every stained nucleus was attributable to a cell stained with cTnT (Figure 22 C, F). Furthermore, cardiomyocytes showed immature features as they did not exhibit bi- or multinucleation (Figure 22 C, F) and no clear striated banding was observable (Figure 22 B, E). Additionally, cells display a more rounded than elongated shape. These features would be present in mature cardiomyocytes (Bedada et al., 2016). The characterized cardiomyocyte culture was then challenged with substances.

4.4 Substance testing

Analysis of the endpoints cell viability, beating frequency, beating area, and gene expression was performed on day ten. First, a potential positive and negative control was tested. In addition, substance testing as a proof of concept was performed in collaboration with the University of Barcelona.

4.4.1 Establishment of a potential positive and negative control

The substance 5-FU was chosen as a potential positive control and PenG as a potential negative control as the effect of these substances is well known and also served as a positive and negative control in the EST (Genschow et al., 2004). Both substances were tested according to the method described in section 3.11. The benchmark concentration approach was used for compound classification in the hiPS Test calculating benchmark concentration (BMC) values of a certain benchmark response (BMR), see section 3.12 for more details of the BMC approach for substance classification.

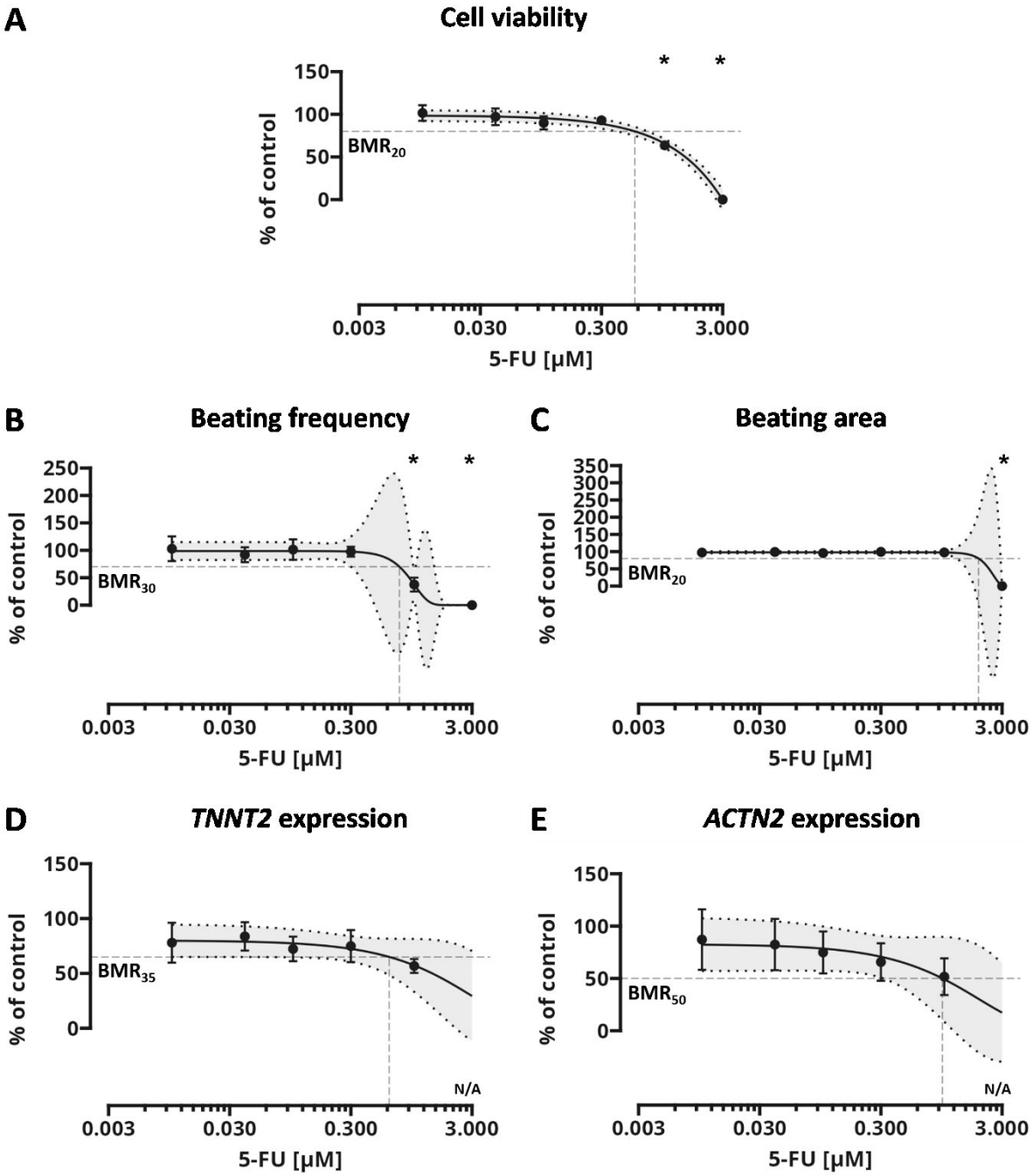

Figure 23: Substance testing of 5-Fluorouracil (5-FU) in the hiPS Test.

Human iPSCs were exposed to 0.012–3 µM 5-FU as described in section 3.11. On day ten, endpoints were analyzed. **A–E:** Concentration-response curves normalized to the control of cell viability, beating frequency, beating area, *TNNT2*, and *ACTN2* expression. The filled area with a dotted border represents the confidence band. The horizontal line indicates the benchmark response (BMR) calculated for each endpoint individually (see section 3.12). The vertical line demonstrates the point at which the curve intersects the BMR representing the benchmark concentration (BMC). **A:** A cell viability assay (Alamar blue assay) was performed and analyzed using a multimode-microplate reader (TECAN, Infinite 200 PRO). Model selection: linear. **B, C:** Videos of every well were recorded using a Binocular (Leica DS100B) with an integrated heating plate set to 37 °C. Beating frequency and beating area were evaluated with the software CardioVision. Model selection: Weibull type 1 with lower limit at 0 (A) and Weibull type 2 (B). **D, E:** For qRT-PCR, quadruplicates were collected and pooled for expression analysis of *TNNT2*, an early cardiomyocyte marker, and *ACTN2*, a later cardiomyocyte marker. Mean values of copy numbers of *TNNT2* and *ACTN2* were normalized to the reference gene calnexin (*CANX*). Model selection: Exponential decay with lower limit at 0 (D, E). N = 3, mean ± SEM, R packages CRStats, drc, and mvtnorm were

used for statistical analyses; $p \leq 0.05$ was considered significant, * = significant compared to the solvent control. N/A = not applicable. *TNNT2* = cardiac troponin T, *ACTN2* = α-Actinin2

The substance 5-FU exerted an effect on multiple endpoints. Cell viability and beating frequency were significantly reduced at 1 and 3 µM resulting in a BMC_{20} value of 0.57 µM and BMC_{30} value of 0.75 µM, respectively (Figure 23 A, B). The beating area was reduced significantly only at 3 µM resulting in a BMC_{20} value of 1.92 µM (Figure 23 C, Table 19). It is noteworthy that almost all cells treated with 3 µM 5-FU were already washed off during medium replacement steps before day ten. Although *TNNT2* and *ACTN2* expression was not altered significantly, a trend in decreased expression was notable and a BMC_{35} of 0.62 µM and a BMC_{50} value of 0.97 µM were calculated, respectively (Figure 23 D, E, Table 19). The BMR as well as the BMC including the benchmark concentration lower limit (BMCL) and benchmark concentration upper limit (BMCU) per endpoint are listed in Table 19.

Table 19: Benchmark concentration (BMC) values including the benchmark concentration lower limit (BMCL) and benchmark concentration upper limit (BMCU) calculated with the respective benchmark response (BMR) for the substance 5-Fluorouracil tested in the hiPS Test at different endpoints.

Endpoint	BMR	BMC in µM	BMCL - BMCU in µM
Cell viability	20	0.57	0.40 – 0.72
Beating frequency	30	0.75	0.30 – 0.99
Beating area	20	1.92	1.26 – 2.92
TNNT2 expression	35	0.62	N/A – 3.58
ACTN2 expression	50	0.97	0.31 – 3.87

N/A = not applicable

For a better comparison between the hiPS Test and other *in vitro* developmental toxicity assays, the BMC_{50} value was calculated for all endpoints for 5-FU as it is comparable to the IC_{50} value which is often used in publications. However, these values were not used for compound classification in the hiPS Test. The following BMC_{50} values were calculated for the different endpoints; cell viability: 1.47 µM, beating frequency: 0.91 µM, beating area: 2.34 µM, and *TNNT2* expression: 1.41 µM.

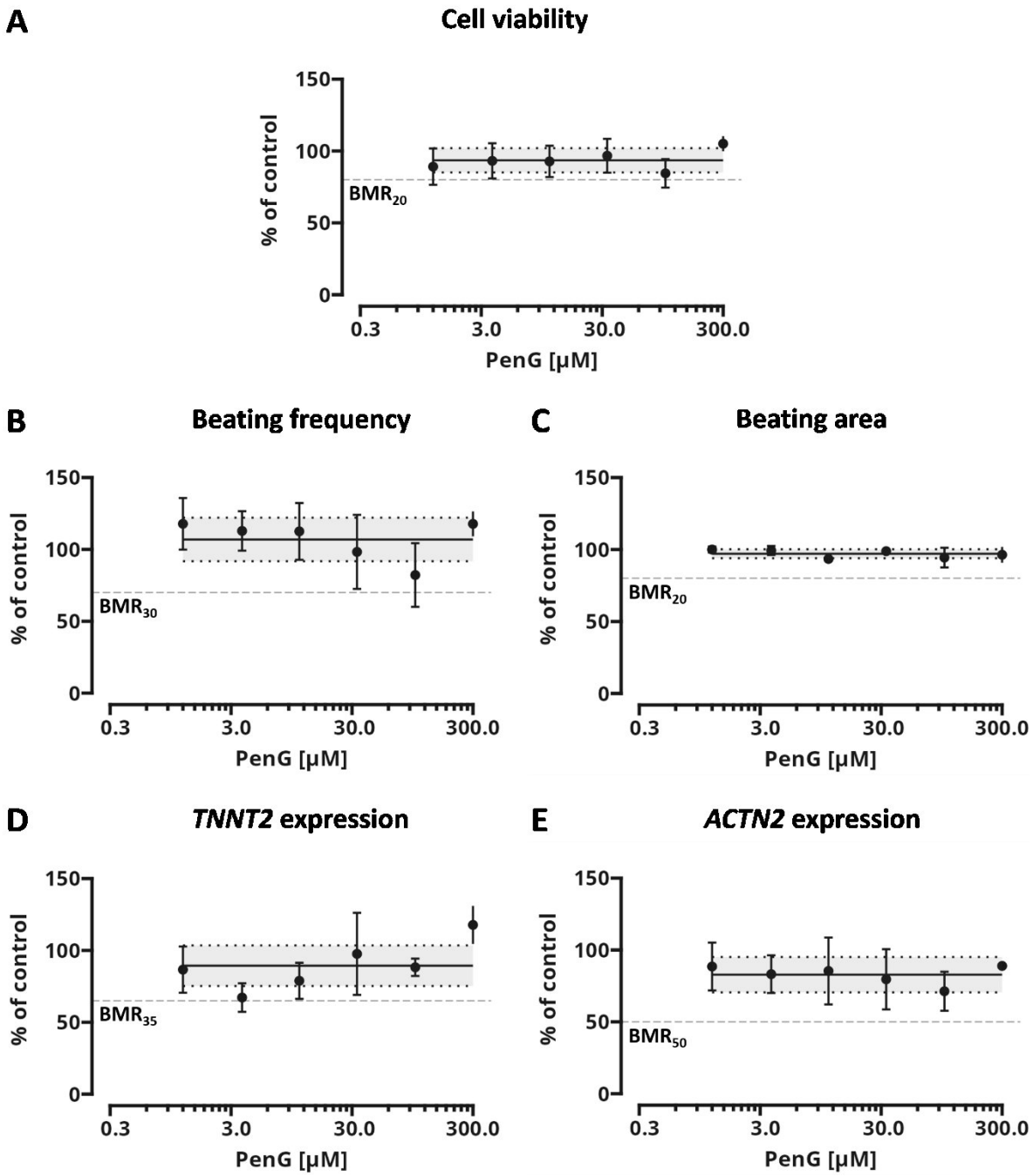

Figure 24: Substance testing of Penicillin G (PenG) in the hiPS Test.

Human iPSCs were exposed to 1.2–300 µM PenG as described in section 3.11. On day ten, endpoints were analyzed. **A–E:** Concentration-response curves normalized to the control of cell viability, beating frequency, beating area, *TNNT2*, and *ACTN2* expression. The filled area with a dotted border represents the confidence band. The horizontal line indicates the benchmark response (BMR) calculated for each endpoint individually (see section 3.12). The vertical line demonstrates the point at which the curve intersects the BMR representing the benchmark concentration (BMC). **A:** A cell viability assay (Alamar blue assay) was performed and analyzed using a multimode-microplate reader (TECAN, Infinite 200 PRO). Model selection: 1-Paramter. **B, C:** Videos of every well were recorded using a Binocular (Leica DS100B) with an integrated heating plate set to 37 °C. Beating frequency and beating area were evaluated with the in-house developed software CardioVision. Model selection: 1-Paramter. **D, E:** For qRT-PCR, quadruplicates were collected and pooled for expression analysis of *TNNT2*, an early cardiomyocyte marker, and *ACTN2*, a later cardiomyocyte marker. Mean values of copy numbers of *TNNT2* and *ACTN2* were normalized to the reference gene calnexin (*CANX*). Model selection: 1-Paramter. N = 3, mean ± SEM, R packages CRStats, drc, and mvtnorm were used for statistical analyses; $p \leq 0.05$ was considered significant, * = significant compared to the solvent control. *TNNT2* = cardiac troponin T, *ACTN2* = α-Actinin2.

Endpoint analyses in the hiPS Test revealed that PenG did not affect the cell viability, beating frequency, or beating area (Figure 24 A, B, C), nor the expression of *TNNT2* or *ACTN2* (Figure 24 D, E) as no BMC was calculated for the specific endpoints and no statistical significance was detected.

4.4.2 Proof of concept testing

As a proof of concept, the substances triclabendazole (TCBZ), triclabendazole sulfoxide (TCBZSO), and nocodazole (NCDZ) were chosen in collaboration with the University of Barcelona. TCBZSO is the main metabolite of TCBZ which is an antihelmintic used in veterinary medicine and in humans for the treatment of fasciolosis. NCDZ was chosen as a positive control as it is thought to influence the WNT pathway (Li et al., 2013).

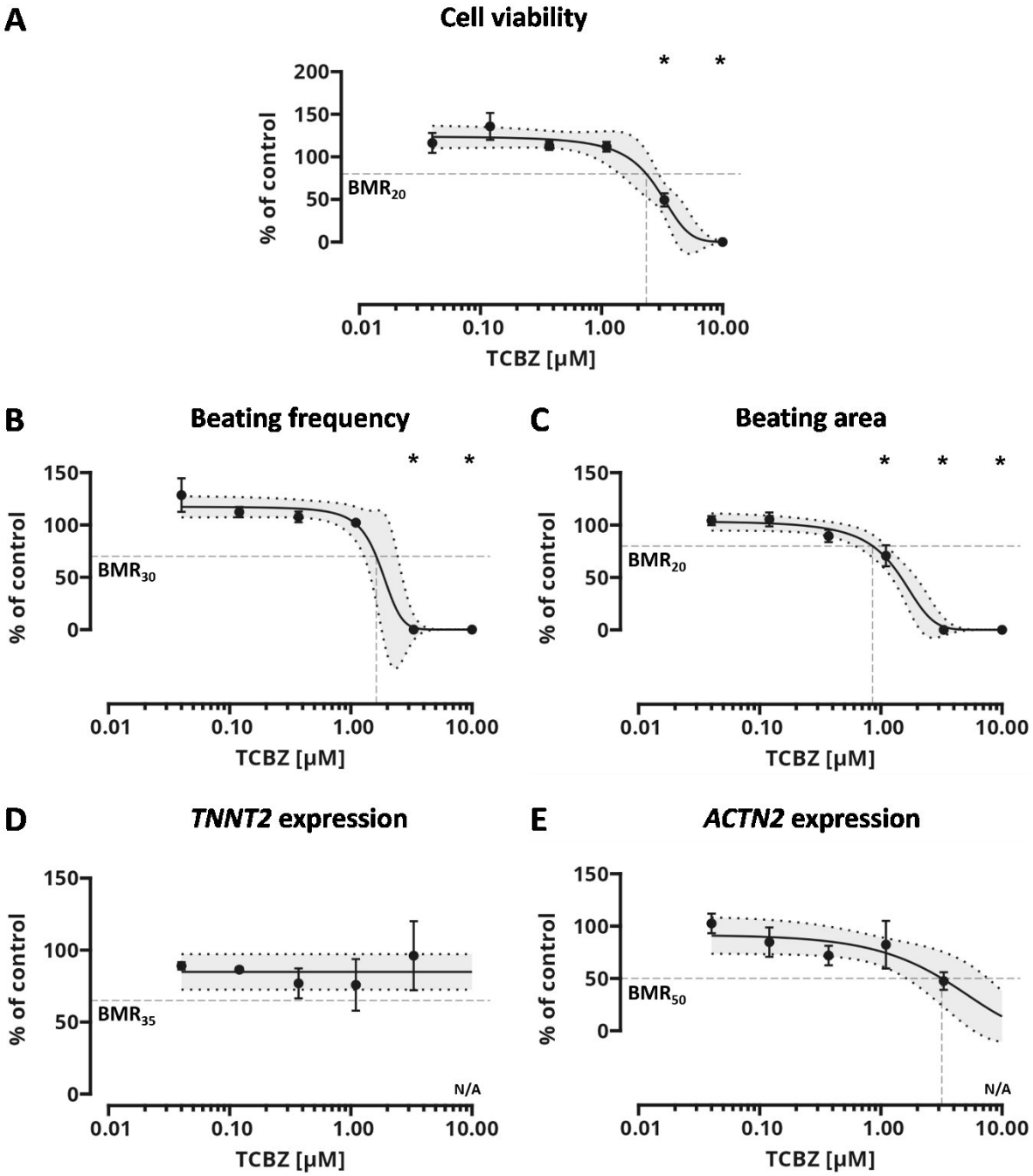

Figure 25: Substance testing of Triclabendazole (TCBZ) in the hiPS Test.

Human iPSCs were exposed to 0.04–10 µM TCBZ as described in section 3.11. On day ten, endpoints were analyzed. **A–E:** Concentration-response curves normalized to the control of cell viability, beating frequency, beating area, *TNNT2*, and *ACTN2* expression. The filled area with a dotted border represents the confidence band. The horizontal line indicates the benchmark response (BMR) calculated for each endpoint individually (see section 3.12). The vertical line demonstrates the point at which the curve intersects the BMR representing the benchmark concentration (BMC). **A:** A cell viability assay (Alamar blue assay) was performed and analyzed using a multimode-microplate reader (TECAN, Infinite 200 PRO). Model selection: Logistic (ED50 as parameter) with lower limit fixed at 0. **B, C:** Videos of every well were recorded using a Binocular (Leica DS100B) with an integrated heating plate set to 37 °C. Beating frequency and beating area were evaluated with the in-house developed software CardioVision. Model selection: Logistic (ED50 as parameter) with lower limit fixed at 0. **D, E:** For qRT-PCR, quadruplicates were collected and pooled for expression analysis of *TNNT2*, an early cardiomyocyte marker, and *ACTN2*, a later cardiomyocyte marker. Mean values of copy numbers of *TNNT2* and *ACTN2* were normalized to the reference gene calnexin (*CANX*). Model selection: 1-Paramter (D) and Exponential decay with lower limit at 0 (E). N = 3, mean ± SEM, R packages CRStats, drc, and mvtnorm were used for statistical analyses; $p \leq 0.05$

was considered significant, * = significant compared to the solvent control. N/A = not applicable. *TNNT2* = cardiac troponin T, *ACTN2* = α-Actinin2.

After TCBZ treatment performing the hiPS Test, cell viability and beating frequency were significantly reduced at 3 and 10 µM (Figure 25 A, B) resulting in a BMC_{20} and BMR_{30} of 2.34 and 1.62 µM, respectively. The beating area, however, was already reduced at 1 µM onwards leading to a BMC_{20} of 0.85 µM (Figure 25 C). Exposure to 3 µM TCBZ affected cell viability to a lesser extent than the beating area as no cells started beating up to day ten although a cell layer covering the entire well was present also representing typical cardiomyocyte morphology seen in the hiPS Test. Quantitative RT-PCR analysis revealed no significant effect of TCBZ on the expression of *TNNT2* (Figure 25 D). Although not defined as significant, *ACTN2* expression was gradually reduced resulting in a BMC_{50} value of 3.18 µM. At 10 µM no samples could be collected as dead cells were already washed off during medium replacement beforehand. BMR, BMC, BMCL, and BMCU are summarized in Table 20 for all endpoints analyzed.

Table 20: Benchmark concentration (BMC) values including the benchmark concentration lower limit (BMCL) and benchmark concentration upper limit (BMCU) calculated with the respective benchmark response (BMR) for the substance triclabendazole tested in the hiPS Test at different endpoints.

Endpoint	BMR	BMC in µM	BMCL - BMCU in µM
Cell viability	20	2.34	1.40 – 2.96
Beating frequency	30	1.62	1.28 – 2.44
Beating area	20	0.85	0.61 – 1.11
TNNT2 expression	35	N/A	N/A
ACTN2 expression	50	3.18	1.63 – 7.64

N/A = not applicable

The BMR_{50} value for cell viability (3.28 µM) was calculated for comparison with published data expressing the IC_{50} value.

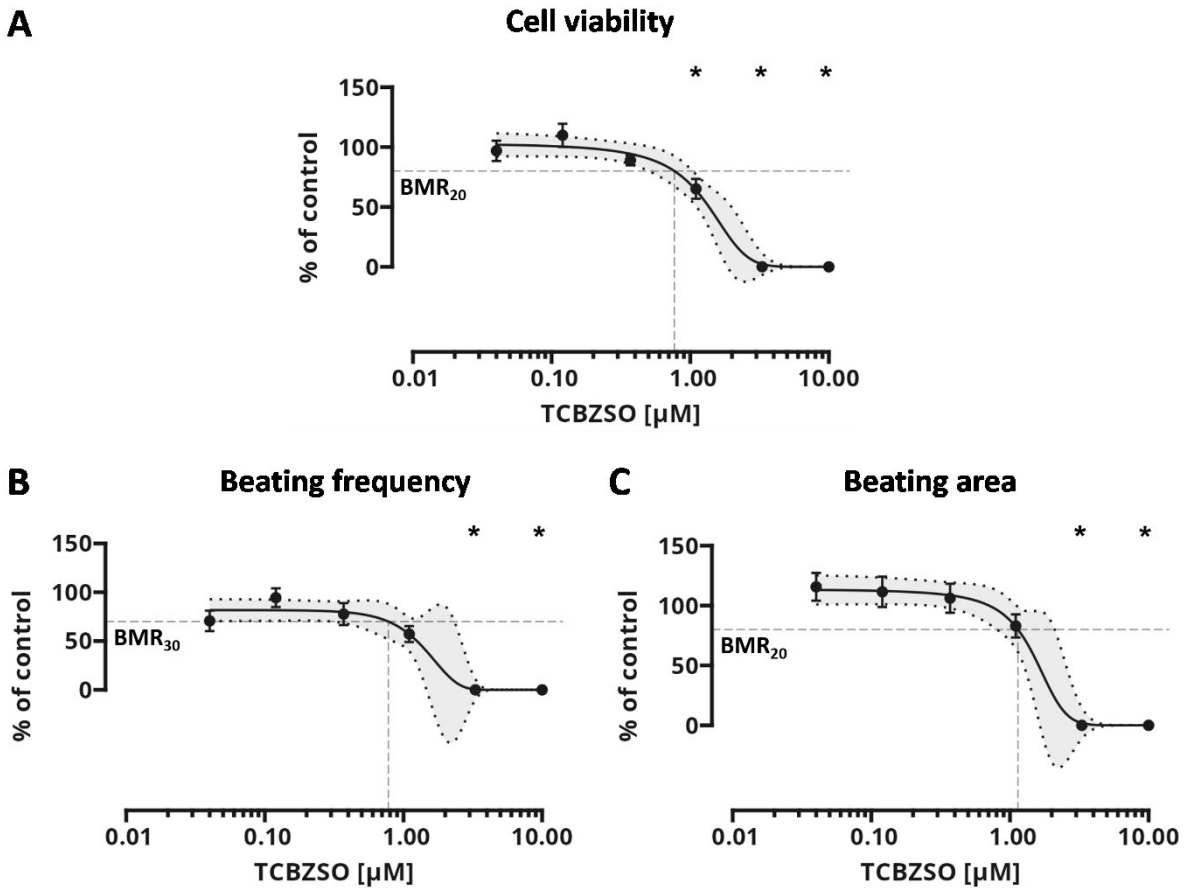

Figure 26: Substance testing of Triclabendazole sulfoxide (TCBZSO) in the hiPS Test.

Human iPSCs were exposed to 0.04–10 µM TCBZSO as described in section 3.11. On day ten, endpoints were analyzed. **A–C:** Concentration-response curves normalized to the control of cell viability, beating frequency, and beating area. The filled area with a dotted border represents the confidence band. The horizontal line indicates the benchmark response (BMR) calculated for each endpoint individually (see section 3.12). The vertical line demonstrates the point at which the curve intersects the BMR representing the benchmark concentration (BMC). **A:** A cell viability assay (Alamar blue assay) was performed and analyzed using a multimode-microplate reader (TECAN, Infinite 200 PRO). Model selection: Logistic (ED50 as parameter) with lower limit fixed at 0. **B, C:** Videos of every well were recorded using a Binocular (Leica DS100B) with an integrated heating plate set to 37 °C. Beating frequency and beating area were evaluated with the in-house developed software CardioVision. Model selection: Weibull (type 1) with lower limit at 0 (B) and Logistic (ED50 as parameter) with lower limit fixed at 0 (C). N = 4, mean ± SEM, R packages CRStats, drc, and mvtnorm were used for statistical analyses; $p \leq 0.05$ was considered significant, * = significant compared to the solvent control, BMR = benchmark response.

The substance TCBZSO significantly reduced cell viability at 1, 3, and 10 µM resulting in a BMC_{20} of 0.77 µM. Although cell viability was significantly reduced at 1 µM, beating frequency and beating area were both only significantly reduced at 3 and 10 µM with a BMC_{30} and BMC_{20} of 0.78 and 1.14 µM, respectively. Gene expression samples were not collected. BMR, BMC, BMCL, and BMCU are summarized in Table 21 for all endpoints analyzed.

Table 21: Benchmark concentration (BMC) values including the benchmark concentration lower limit (BMCL) and benchmark concentration upper limit (BMCU) calculated with the respective benchmark response (BMR) for the substance triclabendazole sulfoxide tested in the hiPS Test at different endpoints.

Endpoint	BMR	BMC in µM	BMCL - BMCU in µM
Cell viability	20	0.77	0.50 – 1.04
Beating frequency	30	0.78	0.31 – 2.33
Beating area	20	1.14	0.81 – 2.10

The BMR_{50} value for cell viability (1.36 µM) was calculated for comparison with published data expressing the IC_{50} value.

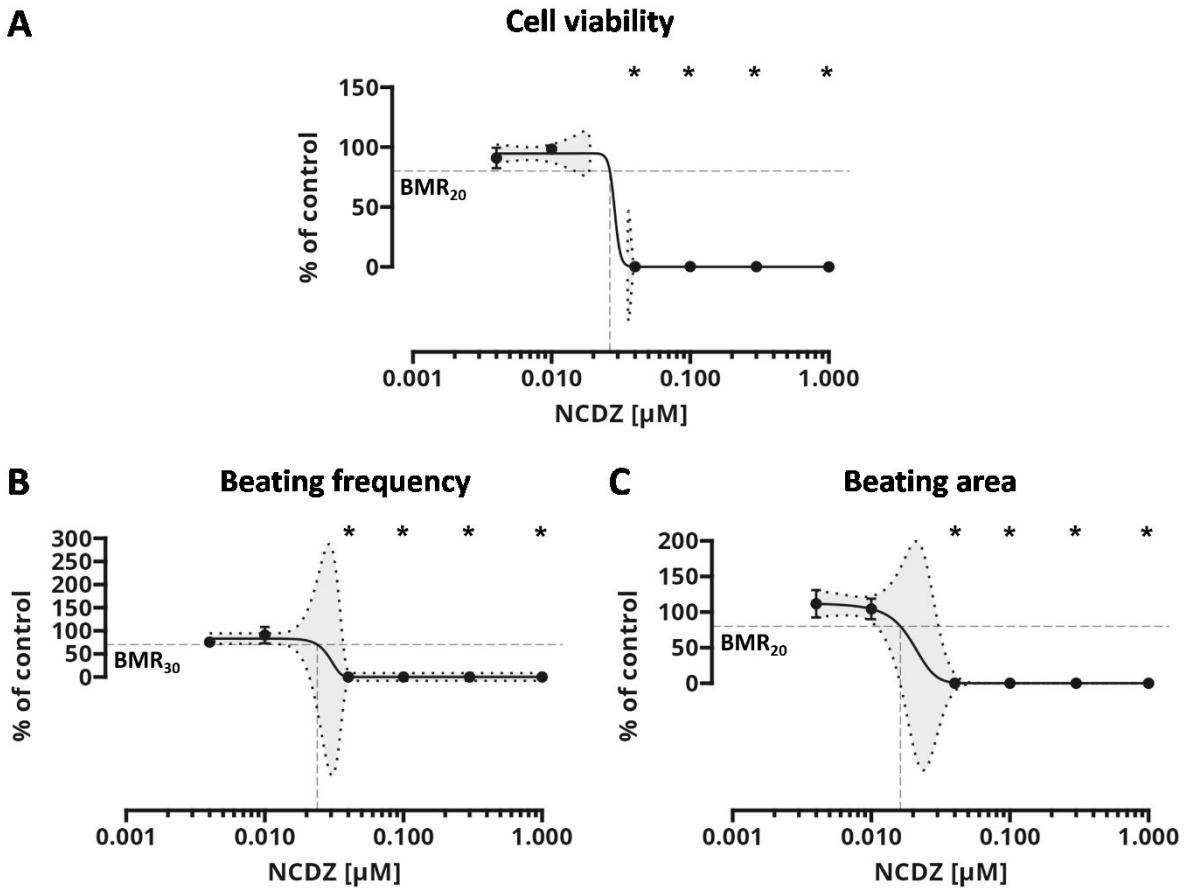

Figure 27: Substance testing of Nocodazole (NCDZ) in the hiPS Test.

Human iPSCs were exposed to 0.004–1 µM NCDZ as described in section 3.11. On day ten, endpoints were analyzed. **A–C:** Concentration-response curves normalized to the control of cell viability, beating frequency, and beating area. The filled area with a dotted border represents the confidence band. The horizontal line indicates the benchmark response (BMR) calculated for each endpoint individually (see section 3.12). The vertical line demonstrates the point at which the curve intersects the BMR representing the benchmark concentration (BMC). **A:** A cell viability assay (Alamar blue assay) was performed and analyzed using a multimode-microplate reader (TECAN, Infinite 200 PRO). Model selection: Brain-Cousens (hormesis) with lower limit fixed at 0. **B, C:** Videos of every well were recorded using a Binocular (Leica DS100B) with an integrated heating plate set to 37 °C. Beating frequency and beating area were evaluated with the in-house developed software CardioVision. Model selection: Weibull (type 1) (B) and Logistic (ED50 as parameter) with lower limit fixed at 0 (C). N = 3, mean ± SEM, R packages CRStats, drc, and mvtnorm were used for statistical analyses; $p \leq 0.05$ was considered significant, * = significant compared to the solvent control, BMR = benchmark response.

The substance NCDZ significantly reduced cell viability at 0.04, 0.1, 0.3, and 1 µM which represent four of six concentrations tested while the first two concentrations did not exert a significant effect. Due to the data gap between two concentrations that resulted in similar values to the control and the next four concentrations leading to values of around zero, no continuous CI could be displayed (Figure 27 A) but a BMC_{20} of 0.026 µM was determined (Table 22). The same set of problems was present for values of the beating frequency and beating area as these endpoints were also significantly reduced at 0.04, 0.1, 0.3, and 1 µM with values close to zero as cells were already washed off during medium replacement steps until day ten resulting in a high CI due to the data gap (Figure 27 B, C). The

BMC values calculated were 0.024 at BMR_{30} and 0.016 µM at BMR_{20} for the beating frequency and beating area, respectively (Table 22).

Table 22: Benchmark concentration (BMC) values including the benchmark concentration lower limit (BMCL) and benchmark concentration upper limit (BMCU) calculated with the respective benchmark response (BMR) for the substance Nocodazole tested in the hiPS Test at different endpoints.

Endpoint	BMR	BMC in µM	BMCL - BMCU in µM
Cell viability	20	0.026	0.015 – 0.035
Beating frequency	30	0.024	0.014 – 0.037
Beating area	20	0.016	0.011 – 0.031

The BMR_{50} value for cell viability (0.028 µM) was calculated for comparison with published data expressing the IC_{50} value.

5 Discussion

5.1 Characterization of the hiPSC culture for cardiomyocyte differentiation

The hiPSC culture was established with the goal to establish a human cell-based system and to optimize the throughput of testing substances compared to the EST which uses 24 EBs per plate per condition (Genschow et al., 2004). Additionally, it was aimed at avoiding the use of animal-origin-based products like FBS or Matrigel to achieve a xeno-free hiPSC culture. Coating of culture vessels with a protein matrix is especially important in FBS-free cell cultures as in the hiPS Test to provide cells with a suitable matrix for adhesion, migration, and differentiation (Gstraunthaler et al., 2013). The still often used Matrigel is a mixture of multiple proteins extracted from the Engelbreth-Holm-Swarm mouse sarcoma, a tumor rich in extracellular matrix proteins with the main components laminin, collagen IV, entactin, and heparin sulfate proteoglycan perlecan. In addition to the matrix proteins, Matrigel also contains several growth factors produced by the tumor cells, namely, TGFβ, epidermal growth factor (EGF), insulin-like growth factor 1 (IGF1), FGF, and others (Corning Incorporated Life Sciences, 2022). However, the composition of Matrigel varies from batch to batch resulting in a similarity of the protein composition of only 53 % (Hughes et al., 2010). Despite its disadvantages of being variable in its composition, being of animal origin, and bearing ethical concerns for its production, Matrigel is still widely used as a coating. Alternatives e.g. different types of laminins, vitronectin, or fibronectin are often recommended for specific culture conditions e.g. the combination of vitronectin and E8 medium (Thermo Fisher Scientific, 2022), and are often not characterized well for other conditions. Additionally, recombinant proteins are often higher in price (Murphy et al., 2022) which might hinder their use. The alternative coating to Matrigel used in this work is LN521, a chemically defined human recombinant protein (Biolamina, 2022). Laminins are predominantly found in basement membranes (Timpl et al., 1979). The morphological comparison of iPS11 grown on LN521 or Matrigel did not reveal a difference in morphology or proliferation (Figure 10), therefore, the alternative coating LN521 was used in favor of Matrigel. In a comparison between Geltrex which is also obtained from Engelbreth-Holm-Swarm mouse sarcoma, LN521, LN511, and vitronectin, it was shown that the alternative coatings do not differ in terms of stem cells expressing stem cell markers on protein and mRNA level as well as their ability to differentiate into podocytes. Additionally, stem cells cultured on these alternative coatings did not show altered karyotypes compared to cells cultured on Geltrex (Murphy et al., 2022). The overall morphology of the hiPSCs as single-cell culture depicted in Figure 12 is in line with the literature describing the morphology of pluripotent stem cells (Smith et al., 2009; Wakui, 2017). In addition, the altered morphology after culturing cells in a medium supplemented with Y-27632 (Figure 12 A, B) is also described in the literature (Emre et al., 2010; Stover and Schwartz, 2011) and is a well-known phenomenon. However, extended

cultivation of hiPSCs is not recommended as cell cultures in higher passages combined with enzymatic passaging are prone to develop chromosomal abnormalities (Maitra et al., 2005; Ben-David et al., 2010; Mayshar et al., 2010; Laurent et al., 2011; Bai et al., 2015). Therefore, testing for genomic integrity is recommended at least every 12 weeks (WHO, 2013; Assou et al., 2018) or 15 passages (WHO, 2013; Pamies et al., 2017) during hiPSC culture. Therefore, hiPSCs were only used for a maximum of 12 passages over a time course of 6 weeks in the hiPS Test to prevent genomic aberrations and to ensure stable and reproducible cardiomyocyte differentiation.

For flow cytometry analysis, the gating strategy shown in Figure 14 A–C allows for the analysis of single viable cells reducing the possibility of analyzing false positive stained apoptotic cells in which antibodies might accumulate without binding their intended target. With the use of isotype controls, any influence on the staining due to the non-specific binding of the antibodies used could be excluded. One reason for the detected shift in the isotype controls for NANOG, OCT3/4, and SOX2 (Figure 14 E–G) can be the naturally occurring differences between isotype controls and antibodies due to their different production leading to a non-specific binding that would not be present in the antibody sample. Additionally, differences in protein concentrations and fluorochrome to protein ratio can be present between antibody and isotype control resulting in different outcomes during fluorescence measurement (Keeney et al., 1998; Cossarizza et al., 2017). While it is debatable if isotype controls should still be used for all flow cytometry experiments (Keeney et al., 1998; O'Gorman and Thomas, 1999) there are situations in which isotype controls are helpful tools serving as a negative control, e.g. when staining for intracellular markers. Sample preparation like fixation or permeabilization might affect autofluorescence and non-specific antibody binding. In case the antibody stays in the cell but without binding to its target antigen, an isotype control would detect that problem as it would be trapped within the cell as well. Since NANOG, OCT3/4, and SOX2 are intracellular markers, trapped antibodies within the cells are, therefore, a possible reason for the slight shift seen in the respective isotype controls (Figure 14 E–G). For the reasons mentioned above and the fact that the shift is minor, it was concluded that the small percentages of positive isotype controls are in a tolerable range of natural variability. While the recommended threshold of >70 % (Pamies et al., 2017; Sullivan et al., 2018; Tigges et al., 2021) for the markers examined was reached, the downstream application of cardiomyocyte differentiation was considered as well. Lian et al. (2013) defined a threshold of ≥ 95 % OCT4-positive cells as a criterion for the absence of differentiated cells and successful cardiomyocyte differentiation. The threshold of ≥ 95 % OCT4-positive cells was reached for all passages, except for p16 (90 %) and p20 (91 %). It is noteworthy that in passages 12 and 14 this threshold was exactly reached. In consistency with these findings, cardiomyocyte differentiation was gradually hampered and highly variable from p14 onwards in terms of the beating area, except for p16 (Figure 17 A) and beating frequency (Figure 17 B). Although not meeting the threshold of ≥ 95 %

OCT4-positive cells was partially in line with a reduced cardiomyocyte differentiation it is reasonable to assume that the differentiation success is not exclusively dependent on the pluripotency of the hiPSCs used, but is influenced by other factors as well as cells in p12 and 14 both expressed OCT4 to 95 % while only cells in p12 lead to a successful cardiomyocyte differentiation (Figure 17). In addition, cells in p18 reached the threshold but lead to a hampered cardiomyocyte differentiation in terms of beating area and frequency (Figure 17).

In this work, differentiation was achieved by modulation of the WNT signaling pathway. For this purpose, the WNT pathway was first activated by temporary application of the GSK-3β inhibitor CHIR on day zero and subsequently inactivated by application of IWP2 on days two and three. In this context, attention should be paid to cultivation intervals that should be as consistent as possible since the cell culture density influences the cell cycle state and required CHIR application (Laco et al., 2018). Thus, in addition to the pluripotency of the hiPSCs, the cell cycle profile is a crucial factor for successful cardiomyocyte differentiation. A high proportion of cells in S-, G2- and M-phase (> 20 % each) and a high differentiation capacity of the cells (measured by the expression of the stem cell markers NANOG and OCT4 > 85 %) were identified by Laco et al. (2018) as indicative markers for cell lines with high suitability for cardiomyocyte differentiation via modulation of the WNT signaling pathway. A small reduction of 5–7 % in the proportion of cells in the S-, G2-, and M-phase (regulated by initial cell density) already resulted in a substantial loss of differentiation capacity. Thus, implementing cell cycle analysis as part of the regular quality control of hiPSCs could be beneficial to provide a basis for the reproducibility of the differentiation protocol.

5.2 Characterization of hiPSC-derived cardiomyocytes

5.2.1 Gene expression analysis of developing hiPSC-derived cardiomyocytes

Gene expression analysis over the ten-day differentiation period was designed to provide information on how similar the development of hiPSC-derived cardiomyocytes *in vitro* reflects the development of embryonic cardiomyocytes *in vivo*.

For this purpose, the expression levels of several specific marker genes were examined throughout the ten-day differentiation protocol by collecting samples on every day of the protocol including hiPSCs used for the respective differentiation (Figure 19). The markers chosen should indicate different developmental stages discussed herein. The decrease in *OCT4* expression is an indicator of differentiating hiPSCs (Pamies et al., 2017; Sullivan et al., 2018; Tigges et al., 2021). However, it is not an indicator in which lineage hiPSCs differentiate. Therefore, the earliest known molecular marker for cardiac mesoderm *MESP1* was chosen as an indicator for cardiac-specific differentiation. *MESP1* is expressed as early as day one and is expressed in early gastrulation *in vivo* (Saga et al., 1996; Saga,

2000). Disruption of *Mesp1* expression in mice resulted in aberrant heart morphogenesis, resulting in cardia bifida suggesting that *Mesp1*-expressing cells contribute to the formation of the heart tube (Saga et al., 1999). Additionally, *Mesp1* is directly influenced by the WNT pathway since inhibition of the pathway resulted in decreased *Mesp1* expression (Ueno et al., 2007; Lindsley et al., 2008). The WNT pathway also plays a role in the expansion of *Isl1*$^{+}$ progenitor cells. While the activation of the pathway leads to the proliferation of *Isl1*$^{+}$ cells up to a massive accumulation of *Isl1*$^{+}$ progenitor cells and outflow tract defects, a deactivation of the pathway leads to reduced numbers of progenitor cells promoting pre-specification (Qyang et al., 2007). After the integration of *Isl1*$^{+}$ cells into the developing heart, there is a decrease in *Isl1* expression (Cohen et al. 2008; Cai et al. 2003). After the initial increase in *ISL1* expression, the application of IWP2 resulted in a continuous decrease in *ISL1* gene expression *in vitro* in the hiPS Test as well. The decrease in *ISL1* expression during cardiomyocyte differentiation is an important regulatory event. It has been demonstrated that the use of cell lines (e.g. the hESC line H9) showing consistently high *ISL1* expression during differentiation was associated with a low yield of cTnT-positive cardiomyocytes. Consequently, it is assumed that cell lines exist that show more or less aptitude for differentiation toward the myocardial lineage (Balafkan et al., 2020). A possible rationale may be found in the lack of ability to reduce *ISL1* expression, keeping the cells in a progenitor cell stage or preferentially embarking on differentiation toward other cardiac cell types (Sepac et al., 2012; Balafkan et al., 2020). In the context of cardiogenesis, the transcription factor *GATA4* represents an important early regulatory gene that is expressed in cardiac progenitor cell populations and plays an important role in the formation of the linear heart tube (Mummery et al., 2012; Brade et al., 2013). *GATA4* is also expressed in adult cardiomyocytes and the endo- and epicardium. During organogenesis, null mutations of the *Gata4* gene in mice can be embryonically lethal. Deletion of *Gata4* early in cardiac development resulted in a thinning of the myocardium due to reduced cardiomyocyte proliferation. In addition to the phase-dependent influence of *Gata4* on cardiomyocyte proliferation, it has been demonstrated that expression of this gene is also required in the formation of the endocardial cushions, formation of the right ventricle, and septation of the outflow tract. Thus, during cardiogenesis, the expression of *Gata4* is essential for the proper formation of the heart and the survival of the embryo (Zeisberg et al., 2005). Expression of *GATA4* is also induced in hiPSCs after activation of the WNT signaling pathway by application of CHIR (Laco et al., 2018) which is consistent with the results presented here (Figure 19 D). For further lineage-specific differentiation of cardiac progenitor cells, the activity of canonical Wnt signaling has to be reduced (Ueno et al. 2007; Naito et al. 2006). In this context, the WNT signaling pathway is often referred to as having a biphasic role, as activation leads to positive regulation of gene expression of the early precardiac mesoderm (pro-cardiogenic effect), but exerts an inhibitory effect on later differentiation toward the final cardiac cell types (Naito et al., 2006; Tian et al., 2010). Application of IWP2 at differentiation days two and three

resulted in the inactivation of the WNT signaling pathway and further myocardial lineage specification, which was characterized by the expression of *TNNT2* and *ACTN2* (Figure 19 E, F). These genes encode key myofilament structural proteins in cardiac sarcomeres and are, therefore, essential for cell contractility (Mummery et al., 2012). The results of gene expression analysis over the full differentiation period of ten days showed that the differentiated iPS11 cells undergo developmental stages during their differentiation into cardiomyocytes that are very similar to the cardiac lineage specification of the growing human or mouse embryo. Additionally, the results are consistent with gene expression analysis over time of other groups (Seki et al., 2014; Zhang et al., 2015; Balafkan et al., 2020). Based on gene expression results alone, a shortening of the protocol down to as soon as cardiomyocytes start beating on day eight would be possible as from day eight onwards gene expression of *TNNT2* and *ACTN2* is not altered.

5.2.2 Flow cytometry analysis of hiPSC-derived cardiomyocytes

Flow cytometry analysis was performed on days eight, nine, and ten of the differentiation protocol to determine the percentage of cTnT-, α-Actinin2-, and GATA4-positive cardiomyocytes in the total cell population. The generated hiPSC-derived cardiomyocytes should be as reproducible as possible and ideally subject to only minor inter-experimental variations. A consideration of shortening the protocol was not only based on gene but also protein expression.

The staining of the marker GATA4 never lead to a defined signal with only a slight shift of the whole cell population (Figure 21 C). Additionally, compared to a high expression on mRNA level, protein expression was low on all examined days. Although a translation of mRNA is not guaranteed, the high SEM and also the decreased expression from days eight to ten hint toward an error during protocol execution or a protocol that is not suitable for the evaluated antibody. Interestingly, a percentage of 69 % and 71 % for cTnT and α-Actinin2, respectively, revealed an undefined cell population of around 30 % of the total cell population. During cardiac lineage specification, smooth muscle and endothelial cells are formed as major cell types in addition to cardiomyocytes (Sturzu and Wu, 2011). In the study of Balafkan et al. (2020), the proportion of cardiomyocytes, endothelial, and smooth muscle cells was evaluated in one ESC and two hiPSC lines via flow cytometry using the markers cTnT, CD144, and CD140b, respectively. The differentiation protocol to generate cardiomyocytes was also based on the modulation of the WNT signaling pathway as in this study, however, cells were differentiated for 15 days in the study of Balafkan et al. (2020). As a result, ESC line H1-derived cardiomyocytes expressed 74.5 ± 8 % cTnT, 9.5 ± 2.94 % CD140b (smooth muscle cell marker), and 3.71 ± 0.81 % CD144 (endothelial cell marker). Cardiomyocytes derived from the two hiPSC lines Detroit 551-A and AG05836B-15 expressed 77 ± 0.18 % and 67.2 ± 0.2 % cTnT positive cells, respectively. Smooth muscle cell marker CD140b was expressed in 18.45 ± 0.1 % of cardiomyocytes derived from cell line Detroit

551-A and 21 ± 0.1 % from cell line AG05836B-15. Also similar was the expression of endothelial cell marker CD144 with 5.53 ± 0.02 % and 2 ± 0.007 %, respectively. Since the differentiation protocol used in this study is also based on the modulation of the WNT signaling pathway differentiating hiPSCs into cardiomyocytes, it is reasonable to assume that the method used for the hiPS Test also leads to a partial differentiation into smooth muscle and endothelial cells. Considering the observed increase of cardiomyocyte markers cTnT and α-Actinin2 over days eight, nine, and ten it remains unclear whether the percentage of cells expressing these markers would further increase and when to expect a plateau in their expression. It remains debatable if it is desirable to achieve a mixed culture to better simulate the natural environment or if a mixture of cardiac and non-cardiac cells poses a problem in terms of unknown interactions between these cell types. This may have an impact on the functionality of desired differentiated cells or lead to an interference with the cellular response to chemical stimuli and thus may not accurately represent the physiological context (Smith et al., 2017). Although the expression of the markers cTnT and α-Actinin2 slightly increased over time, their expression is stable and exibit a low variability indicated by a low SEM (Figure 21 G) which further supports the possibility to shorten the protocol.

5.2.3 Beating behavior of hiPSC-derived cardiomyocytes

Differentiated cardiomyocytes exhibited the same beating behavior (Video 1 on CD, orange square) as cardiomyocytes produced in the study by Zhang et al. (2015) but with a more prominent mesh structure including more holes. Any changes in the normal beating behavior would be unfavorable for the developing embryo, hence it is desired to evaluate changes during compound exposure. One method to assess endpoints for the beating is via multi-electrode arrays (MEA). For this method, cardiomyocytes are plated on a surface that consists of multiple electrodes which can detect field potentials. Endpoints that can be evaluated are electrophysiological and can include e.g. field potential duration, beat period, beat rate, and spike amplitude (Clements and Thomas, 2014). However, MEAs are often used to detect cardiotoxicity (Braam et al., 2010; Abassi et al., 2012; Zwartsen et al., 2019) or to characterize cardiomyocytes (Seki et al., 2014) rather than for developmental toxicity assays. Additionally, MEAs do not give information on the whole cardiomyocyte culture but only on the cells in contact with the electrodes with no information on e.g. the beating area of the entire well. Furthermore, cardiomyocytes of the hiPS Test detach from the matrix rendering MEAs an unsuitable test method for the hiPS Test. Another method widely used is fluorescent imaging which makes use of voltage-sensitive dyes or calcium indicators to give information on voltage changes or ion fluctuations (Entcheva et al., 2004; Walter et al., 2015), but again giving no information on mechanical beating behavior. In the EST, the beating of differentiated EBs is evaluated manually using a yes or no principle. Peters et al. (2008) developed an automated analysis recording EBs for 9 seconds with 3.33 frames per second (fps). The software then compared each frame with the one before and after recognizing

changes between them. However, no beating frequency or beating area was evaluated. Kamgoué et al. (2009) developed an optical flow method where the contraction wave was computed also being able to image the starting point of the contraction but on a single-cell basis. Mapping the block-matching algorithm described in Ghanbari (1990) on beating cardiomyocytes, Hayakawa et al. (2012) analyzed sections of a well evaluating the propagation of impulses and velocity of cardiomyocytes motion. However, up to date, no method evaluated the entire well of beating cardiomyocytes. In the hiPS Test, the beating behavior changes over time starting with multiple beating points on day seven until a uniform wave motion developed on day ten. The aim was to evaluate the beating frequency and area of the whole cardiomyocyte layer. For this, the software CardioVision was developed that can quantitatively evaluate beating frequency and beating area considering the entire well with all beating and non-beating areas. The only endpoint comparable with other assays, however, is the beating frequency. Measuring single hiPSC-derived cardiomyocytes, even the one with the highest frequency of 66.34 beats per minute (bpm) in the study of Ahola et al. (2014) is much slower compared to the measured average of 1.6 beats/second which equals 96 bpm (average from p4 to p12, see Figure 17 B) of the cardiomyocytes in the hiPS Test. Similar results were only achieved in hiPSCs-derived cardiomyocytes stimulated with 2 Hz for seven days in the study of Eng et al. (2016). In a human embryo, the embryonic heart rate (EHR) can usually be measured at around 6 weeks of gestational age which would translate to 4 weeks of embryonic age, about one week after heart tube formation. The average EHR was shown to be around 117.6 ± 14.2 bpm at gestational week 6–6.4 (Hyer et al., 2004) or 110 ± 15 bpm at gestational week ≤ 6.2 (Doubilet and Benson, 1995), which is close to 96 bpm measured in the hiPS Test. Taking into account that cardiomyocytes in the hiPS Test resemble an even earlier state of development, the beating rate probably reflects the one of human embryonic cardiomyocytes *in vivo*.

Taking into account the results of gene expression analysis, flow cytometry analysis, and assessment of the beating of hiPSC-derived cardiomyocytes, it was decided not to shorten the protocol and to evaluate the endpoints on day ten for compound testing. An important criterion for this was the increasing synchronization of the occurring cell contractions observed towards the end of the differentiation protocol between days eight and ten (Video 2 on CD), which is a crucial factor for the reproducibility of the video analyses with the software CardioVision.

5.2.4 Immunocytochemical staining of hiPSC-derived cardiomyocytes

Visualization of the hiPSC-derived cardiomyocytes in this study with an antibody against cTnT revealed that hiPSC-derived cardiomyocytes of the hiPS Test display immature features. Embryonic/ fetal cardiomyocytes are smaller in size and more rounded and also only mononucleated at this time (Snir et al., 2003) while mature cardiomyocytes are elongated (approximately 150 µm x 10 µm) with a

cylindrical shape and can be binucleated or even multinucleated accounting for approximately 26 % of adult cardiomyocytes (Olivetti, 1996). Additionally, in mature cardiomyocytes sarcomeres are organized in parallel resulting in a striated structure when stained with filament-specific markers (Robertson et al., 2013) which is not the case for the herein differentiated cardiomyocytes (Figure 22 B, E). These findings are in line with stainings of *in vitro* differentiated cardiomyocytes performed by others although cardiomyocytes have been differentiated for up to 15 days (Lian et al., 2012; Burridge et al., 2014; Zhang et al., 2015). In general, it has been shown that *in vitro*-induced cardiomyocytes cultured for a short period show higher similarity to embryonic or fetal cardiomyocytes (Fijnvandraat et al., 2003).

5.3 Establishment of a potential positive and negative control for the hiPS Test

Based on the previously ECVAM-validated EST, 5-FU and PenG were chosen as a potential positive and negative control, respectively (Genschow et al., 2004; Seiler and Spielmann, 2011) for the hiPS Test. A compound serving as a positive control should have a known and reproducible effect on the evaluated endpoints. However, the effect should not be exerted together with reduced viability as that would make it impossible to distinguish between a general toxic effect or compound specific effect. Carrying a positive control serves as methodological evidence that the test system is capable of detecting the effect under investigation (Johnson and Besselsen, 2002). In contrast, a negative control should not exert an effect on any endpoint up to the highest concentration tested.

The compound 5-FU is a chemotherapeutic agent used for different types of cancer with the most treated cancers being colorectal and anal carcinoma, pancreatic adenocarcinoma, and esophageal carcinoma in 2018 (Chalabi-Dchar et al., 2021). 5-FU is a nucleobase analog of uracil with a fluorine atom attached at the C5 position instead of a hydrogen atom. The mechanism of action of 5-FU is, therefore, based on the replacement of uracil exerting effects on processes where usually uracil would play an important role. As 5-FU acts as a pyrimidine antagonist, it enters cells via a facilitated transport system for purine and pyrimidine bases. Once 5-FU has entered the cell, it is converted into Fluorouridine-monophosphate (FUMP) and Fluorodeoxyuridine-monophosphate (FdUMP). FUMP can be triphosphorylated and then incorporated into RNA causing RNA damage or faulty transcription. FdUMP in turn inhibits thymidylate synthase which is essential for the synthesis of deoxythymidine triphosphate (dTTP) usually incorporated into DNA. This leads to an imbalance of nucleotide availability. In addition, FdUMP can also be triphosphorylated and incorporated into DNA directly. Both exerted effects of FdUMP lead to DNA damage. The therapeutic effect is especially effective in fast-proliferating cells leading to cell death after incorporation (reviewed in Grem, 2000; Longley et al., 2003; Zhang et al., 2008). The C_{max} for patients differs depending on the administered dosage which is dependent on the indication 5-FU is used for. In the study of Bocci et al. (2000) colorectal cancer

patients received either 250 or 370 mg/mg² resulting in a C_{max} of 18.15 ± 1.35 and 48.41 ± 7.69 µg/mL which equals 139.53 and 372.16 µM which is well above the tested concentrations. Developmental toxic effects of 5-FU were shown in studies where pregnant rats were administered 5-FU subcutaneously. 5-FU negatively affected fetus weight which was correlated with an increased incidence of malformations, e.g. anasarca, hindlimb defects, or cleft palate (Shuey et al., 1994; Lau et al., 2001). Teratogenic effects of 5-FU have been shown in numerous laboratory species including rat, mouse, hamster, chick, and even the common sand dollar (Dagg, 1960; Karnofsky and Basch, 1960; Shah and MacKay, 1978; Shuey et al., 1994). Case reports of women being treated with 5-FU during pregnancy within the first trimester identified congenital anomalies in the fetuses, however, the treatment regimen also included radiation, therefore, it is uncertain if the observed anomalies are solely due to the treatment of 5-FU (Stephens et al., 1980; Leyder et al., 2011). Since the developmental toxic effects of 5-FU are known for a few decades, it is contraindicated during pregnancy (Schaefer et al., 2006). Nevertheless, 5-FU has been classified as pregnancy category D by the FDA, meaning that despite potential risks related to fetal harm, the potential benefits of the drug may justify its use during pregnancy (FDA, 2016).

In the hiPS Test, 5-FU showed an effect on cell viability, beating frequency, beating area, *TNNT2* expression, and *ACTN2* expression (Figure 23 A, B, C, D, E). Calculating the IC_{50} is commonly used to express the concentration of a substance at which 50 % of the cells are viable. The half maximal inhibitory concentration of differentiation (ID_{50}) is used to refer to a concentration at which only 50 % of cells differentiated into e.g. cardiomyocytes. However, for compound classification in the hiPS Test, the BMC approach was used, for further details see section 3.12. Results for 5-FU in the hiPS Test are shown in Table 19. In the hiPS Test, no endpoint is classified as a specific hit for 5-FU, as the BMC of every specific endpoint lies within or above the CI of the endpoint cell viability. Interestingly, the BMCL of the beating area (1.26 µM) lies above the BMCU of cell viability (0.72 µM) meaning that the viability is reduced while beating cardiomyocytes still cover the whole well area. However, the beating frequency is affected at a similar BMC (0.75 µM) as cell viability (0.57 µM). A possible reason for this phenomenon could be a reduced mitochondrial activity of cardiomyocytes upon exposure to 5-FU. That would affect the outcome of the cell viability assay used as it is based on mitochondrial activity. Cardiomyocytes by nature have a high number of mitochondria to maintain their contracting behavior (Zhao et al., 2019). A reduced mitochondrial activity would, therefore, also explain the reduced beating frequency. 5-FU was recently found to decrease mitochondrial membrane potential, increase mitochondrial fragmentation and decrease the number of cells with a mitochondrial fusion of hiPSCs also at 1 µM (Yamada et al., 2018) making adverse effects on mitochondria a plausible mode of action for the observed toxicity *in vitro*. Furthermore, the beating area was not significantly reduced at 1 µM hinting towards a decreased viability, not due to fewer cells but impaired mitochondrial activity while

the beating frequency was significantly reduced at 1 µM. In addition, the decreased expression of *TNNT2* and *ACTN2* following 5-FU exposure points to hampered differentiation of cardiomyocytes, however, this is only an observed trend and statistically not significant. In the hiPS Test, 5-FU does not serve as a suitable positive control since no specific hit distinguishable from cell viability could be observed.

Still, the significantly reduced cell viability itself can be compared to other assays interpreting the results concerning possible species differences or similarities between other assays. Since the BMC approach was not used in assays comparable to the hiPS Test, the BMC at BMR_{50} for cell viability was calculated (1.47 µM) as it equals the IC_{50} value of other assays enabling a comparison between different assays. In the EST, the IC_{50} of cell viability and the ID_{50} were calculated. 5-FU also reduced cell viability in the EST, resulting in an IC_{50} of 0.42 µM which does not differ much from the ID_{50} of 0.36 µM (Genschow et al., 2004), listed in Table 23. Since both values are very close, it is questionable if 5-FU is the best option as a positive control in the EST as well. In the hESC-based EST, the assay design of the EST was adapted to use hESCs instead of mESCs. There, exposure to 5-FU resulted in IC_{50} values of 1.4 and 0.5 µM (Table 23) for the cell lines MRC-5 and H1, respectively (Adler et al., 2008). No beating analysis was performed. The same assay design but substituting mESCs or hESCs with hiPSCs, called the iPST resulted in an IC_{50} value of 13 µM and ID_{50} of 4.2 µM (Table 23) with the ID_{50} value being three times lower than the IC_{50} (Aikawa, 2020). Combining hiPSCs with a 2D assay called the hiPSC-based EST an IC_{50} value of 0.4 nM and an ID_{50} value of 0.018 nM was demonstrated which differ in one order of magnitude compared to each other. Comparing the human-cell-based assays among each other the hiPS Test BMC_{50} value of cell viability (1.47 µM) was in the same order of magnitude as the IC_{50} value of the hESC-based EST (1.4 µM for cell line MRC-5) (Adler et al., 2008). The hiPS Test is more sensitive compared to the iPST with a difference in BMC_{50}/IC_{50} values of one order of magnitude (1.47 and 13 µM, respectively). The hiPSC-based EST, however, is more sensitive than all other compared assays with an IC_{50} value five orders of magnitude lower compared to the iPST (13 µM). These differences might be due to different protocols used for cardiomyocyte differentiation. While Aikawa, (2020) formed EBs that grew in a 3D structure, Walker et al., (2021) chose a 2D protocol resulting in contracting clusters. This led to a different exposure of cells to the substances tested which might explain the higher IC_{50} and ID_{50} values for 5-FU in the study of Aikawa, (2020). Furthermore, different hiPSC lines were used which already showed different IC_{50} values within the same test system, 1.4 and 0.5 µM for the cell lines MRC-5 and H1, respectively in the study of Adler et al. (2008). Additionally, both assays used FBS but in different concentrations, 5 % (Aikawa, 2020) and 18 % (Walker et al., 2021) which represents a fluctuating variable in cell cultures. Additionally, 5-FU is bound to proteins to a degree of 10 % (Liston and Davis, 2017) which means a high FBS concentration could lead to a more inactive percentage of 5-FU resulting in a higher concentration necessary to exert an effect. In

summary, 5-FU has an effect on cell viability and differentiation in the hiPS Test as well as comparable assays using mESCs, hESCs, or hiPSCs in a 3D or 2D format.

Table 23: Comparison of IC_{50} and ID_{50} or BMC_{50} values for 5-FU of *in vitro* embryotoxicity assays based on human stem cell differentiation into cardiomyocytes and the embryonic stem cell test.

Assay	IC_{50} / BMC_{50}	ID_{50} / BMC_{50}
Embryonic stem cell test (EST) (Genschow et al., 2004)	0.42 µM	0.36 µM
hESC-based EST (Adler et al., 2008)	1.4 µM (cell line MRC-5) 0.5 µM (cell line H1)	X
iPST (Aikawa, 2020)	13.3 µM	4.2 µM
hiPSC-based EST (Walker et al., 2021)	0.36 nM	0.018 nM
hiPS Test (Galanjuk et al., 2022)	1.47 µM	Beating frequency: 0.91 µM Beating area: 2.34 µM *TNNT2* expression: 1.41 µM *ACTN2* expression: 0.97 µM

PenG has been used as an antibiotic against group B streptococcus in pregnant women without exerting embryotoxic effects (Nathan et al., 1993; Weeks et al., 1997) and therefore, renders useful as a negative control compound in the hiPS Test. The results of the hiPS Test revealed no effect of the negative control PenG as it did not alter cell viability, beating frequency, beating area, *TNNT2* expression, or *ACTN2* expression of differentiating hiPSCs up to 300 µM (Figure 9B-E) as no BMC value was determined. In the EST, PenG did not affect any endpoint up to 1000 µg/mL equaling 2990 µM (Genschow et al., 2004). However, 1000 µg/mL is well above the mean value of the serum concentration of 0.38 ± 0.27 µg/mL (~ 1 µM) at delivery, measured in pregnant women who took PenG as an antibiotic against group B streptococcus (Weeks et al., 1997). In the study of Nathan et al., (1993) half of the PenG concentration was used which resulted in a serum concentration of 0.14 µg/mL (0.4 µM) after 1 day of injection. It was confirmed that PenG is a suitable negative control for the hiPS Test.

5.4 Proof of concept testing

Proof of concept testing was performed with the substances TCBZ, TCBZSO, and NCDZ. TCBZ is an anthelmintic primarily used to treat fasciolosis and paragonimiasis. Both are foodborne, zoonotic diseases caused by trematode infestation in cattle. TCBZ is a benzimidazole derivative only approved for veterinary use except in Egypt, Venezuela, and France, where it is also approved for human use for the treatment of fasciolosis (Boix et al., 2015), however, since 2019 it was also approved by the FDA for the US (Novartis, 2022). Nevertheless, TCBZ has been included in the essential medicines list by the world health organization since 2006 (WHO, 2006). Despite most compounds of the benzimidazole

family being teratogenic, TCBZ is considered safe during pregnancy, but the assessment is based primarily on data from extrapolation with other benzimidazole compounds (Boix et al., 2015). Human exposure to TCBZ other than direct treatment is through the consumption of dairy products, especially in a fasciola endemic area (Boix et al., 2016). Potential adverse effects of TCBZ and TCBZSO on human embryonic development are poorly studied. However, detailed information regarding possible adverse effects during the embryonic developmental period is needed for a risk-benefit assessment, especially concerning TCBZ treatment during pregnancy (Boix et al., 2015). In the study by Lecaillon et al. (1998), the maximum plasma concentration (C_{max}) for TCBZ and TCBZSO was evaluated depending on food intake before administration. Since it is recommended to administer TCBZ with food (Novartis, 2022), the values after food intake were considered for comparison. The C_{max} of TCBZ was 1.16 µM and for TCBZSO 38.6 µM after two single doses of 10 mg/kg which is due to the fast metabolism of TCBZ to TCBZSO (Keiser et al., 2005). While in the hiPS Test the BMC_{50} of cell viability for TCBZ (3.28 µM) was above the C_{max}, the BMC_{50} value of cell viability for TCBZSO (1.36 µM) was 30 times lower than the C_{max}. However, these results are not in line with the study results of Boix et al. (2015) regarding the postimplantation WEC. In their study, a zebrafish embryo test (ZFET), a preimplantation, and a postimplantation rodent whole embryo culture (WEC) were used to examine potential embryotoxicity or teratogenicity. Both compounds, TCBZ and TCBZSO did not induce any adverse effects in gestational days (GD) 9.5–11.5 rat embryos after exposure for 48 h at 140 µM and 267 µM, respectively. However, the test evaluates a later stage in development compared to the hiPS Test when mapping to human development as GD 9.5–11.5 rat embryos correlate to about week 7 gestational age in humans (Yun Liu et al., 2013) while the hiPS Test is covering the human embryonic development up to week 5 gestational age. More suitable for comparison is the ZFET where the compound is present at an early stage of development. In the ZFET, TCBZ showed 100 % lethality at 5 µM and 0 % lethality at 2.5 µM. The BMC_{50} value of 3.28 µM in the hiPS Test aligns with these findings ranging between these values. TCBZSO however, showed 35 % lethality at 10 µM and 100 % lethality at 50 µM. In the hiPS Test, the BMC_{50} value of 1.36 µM lies drastically below any significant effect on the lethality in the ZFET. In the preimplantation WEC, neither TCBZ nor TCBZSO showed an effect on lethality up to 3 µM, covering GD 0–4, which is approximately the same developmental time covered in the hiPS Test. However, in the hiPS Test, the BMC_{50} was already reached at 3.28 and 1.36 µM for TCBZ and TCBZSO, respectively. These results possibly show the first indication of a higher sensitivity of the human cell system (hiPS Test) compared to the animal-based assay models (ZFET, WEC) used by (Boix et al., 2015). Additionally, at 3 µM TCBZ cardiomyocytes did not display a beating despite covering the entire well area. In the compound classification system of the hiPS Test, this leads to a specific hit as the cell viability BMCL value 1.40 µM does not overlap with the BMCU value 1.11 µM of the endpoint beating area (Table 20). All other endpoints including beating frequency, *TNNT2* expression and *ACTN2*

expression were classified as no specific hit.

The third substance of interest NCDZ is used in cancer treatment as an antineoplastic compound. NCDZ exerts its effect by affecting the dynamics of spindle microtubules inhibiting the tubulin exchange at microtubule ends (Jordan et al., 1992). Additionally, activation of the mitotic checkpoint leads to the accumulation of cells in the metaphase which results in cell cycle arrest. In male mice, it was shown that administration of NCDZ results in aneuploidy in sperm (Attia et al., 2008). It is estimated that about 35 % of all spontaneous abortions are caused by aneuploidy (Fritz et al., 2001). Besides its known interfering effect on microtubule polymerization, it was also demonstrated that NCDZ reduces the oncogenic potential of cancer cells by stimulating the expression of large tumor suppressor kinase 2 (LATS2), which exerts an inhibitory influence on the WNT signaling pathway. In many cancer types, the WNT signaling pathway is activated atypically resulting in abnormal transcription activity (Li et al., 2013). Especially the effect on the WNT pathway is important for NCDZ to serve as a potential positive control eventually interfering with the normal development of cardiomyocytes in the test system relying on the correct modeling of this pathway. Study results from an *in vitro* investigation on differentiating embryonic rat cells in the micromass cell culture system for midbrain and limb bud are available, which suggests a developmental toxic potential of NCDZ (Whittaker and Faustman, 1992). In the study, the IC_{50} value for cytotoxicity was at 0.76 µM for the micromass limb bud and 0.037 µM for the micromass midbrain test. In the hiPS Test, the toxic potential of NCDZ was confirmed resulting in a BMC_{50} value of 0.028 µM for cell viability. Interestingly, NCDZ did not exert an effect in the lowest two concentrations (0.004 and 0.012 µM) on cell viability, beating frequency, or beating area while the next higher concentration (0.037 µM) already lead to a total loss of cells until day ten. For a complete concentration-response curve values between the concentration with no effect and the concentration that leads to almost no cell viability are needed to calculate a reliable BMC value, CIs, and CI band. As NCDZ influences the WNT pathway an adjusted concentration range including a concentration with no effect on cell viability but on the beating frequency and beating area would make NCDZ a suitable positive control.

5.5 The hiPST in comparison with other *in vitro* embryotoxicity assays

The heart is the first functional organ in a developing embryo which is one reason why attention has been focused on this process over the last decades of developing alternative methods for embryotoxicity testing. The EST was the first method to produce beating mouse cardiomyocytes through EB formation for assessing developmental toxicity (Scholz et al., 1999) and was later validated by ECVAM (Genschow et al., 2002, 2004). However, it was not approved for regulatory purposes. One limitation of the EST was a low accuracy in differentiating weak and non-teratogens (Chapin et al., 2007). After the development of the EST, various additions were made by other groups

to enhance the system which is summarized in Table 24. Very early after the validation by ECVAM, Pellizzer et al. (2004) added RT-PCR as an endpoint to the EST evaluating Brachyury, *NKX2.5*, *α-MHC*, and *OCT4* expression. The studies of van Dartel et al. (2010) revealed differential gene expression in EBs exposed to different compounds via microarrays. Seiler and Spielmann (2011) included the endpoint flow cytometry analysis evaluating the marker MHC or α-Actinin. Another method was developed by Suzuki et al. (2011), evaluating the luciferase activity of reporter cell lines for heart and neural crest derivatives expressed 1 (*HAND1*) and cardiomyopathy associated 1 (*CMYA1*). Besides the addition of endpoints to improve the predictivity of the EST, multiple groups developed methods to facilitate the handling of cell culture e.g. the generation of EBs using 96-well plates instead of hanging drops (Peters et al., 2007) or by automation of handling steps during the protocol. Peters et al. (2008) developed an automated contractility assessment minimizing experimenter-dependent evaluation. Witt et al. (2021) additionally automated cell seeding, compound dilution and transfer, media exchange as well as the cell viability assay and EB transfer to imaging plates. In addition, they added marker expression analysis by imaging as an endpoint. Still, even with these numerous additions and enhancements, the EST was not re-evaluated by ECVAM.

Table 24: Additions or changes to the ECVAM-validated EST to improve the original test system (Galanjuk et al., 2022)**.**

Authors	Additions/ Changes	Supposed benefits
Pellizzer et al., 2004	• RT-PCR	• Additional endpoint
Peters et al., 2007	• EB formation in 96-well plate • Introduction of Relative Embryotoxic Potency (REP) values	• Higher throughput • Omission of 3T3 cells
Peters et al., 2008	• Automated contractility assessment	• Minimizing experimenter-dependent evaluation
van Dartel et al., 2010	• Transcriptomics (Microarray)	• Additional endpoint
Seiler and Spielmann, 2011	• Molecular marker analysis using flow cytometry	• Additional endpoint
Suzuki et al., 2011	• Evaluation of luciferase activity of reporter cell lines for *HAND1* and *CMYA1*	• Additional endpoint
Witt et al., 2021	• Automation of cell seeding, compound dilution, and transfer, media exchange and cell viability assay, EB transfer to imaging plates • Marker expression analysis by imaging	• Higher throughput • Additional endpoint

Although cells used in the EST are devoid of ethical concerns since they are derived from permanent mouse cell lines, there are species differences in cardiac development between mice and humans

which are unfavorable for the predictivity in humans. Besides the timing of development, there is for example a switch from a high expression of the gene *MYH6* in human embryonic hearts to a high expression of *MYH7* in adult human hearts, while in mice it is vice versa (Uosaki and Taguchi, 2016). Additionally, the EST makes use of FBS which should be omitted in an *in vitro* method due to scientific reasons concerning the non-defined nature and batch variability and its ethical concerns owing to its production (Gstraunthaler et al., 2013). Besides the attempt to improve the EST, multiple human-based *in vitro* assays for developmental toxicity were developed. To better compare their similarities, differences, strengths, and weaknesses, currently available assays for embryotoxicity evaluation based on cardiomyocyte differentiation are listed in Table 25, including the hiPS Test developed within this thesis.

Table 25: Published human *in vitro* embryotoxicity assays based on stem cell differentiation into beating cardiomyocytes compared to the EST (Galanjuk et al., 2022)

Assay	Species	Cell type	2D/3D	Endpoints	Advantages	Disadvantages
Embryonic stem cell test (EST) (Genschow et al., 2004)	Mouse	• Mouse embryonic stem cells • Mouse fibroblasts	3D	• Cell viability • Beating evaluation (yes/no principle)	• 3D cell system • ECVAM validated	• Rodent cells • FBS in medium • Low throughput due to high number of technical replicates • Experienced staff needed for visual evaluation of beating
hESC-based EST (Adler et al., 2008)	Human	• hESCs • Human embryonic lung fibroblasts	3D	• Cell viability	• 3D cell system	• FBS in fibroblast medium • Low throughput due to high number of technical replicates • Ethical concerns using hESCs • Only viability evaluation
iPST (Aikawa, 2020)	Human	• hiPSCs • Adult human dermal fibroblasts	3D	• Cell viability • Beating evaluation (yes/no principle) as a function of time	• 3D cell system • No ethical concerns using hiPSCs	• FBS in medium • Low throughput due to high number of technical replicates • Experienced staff needed for visual evaluation of beating
Pluri Beat Assay (Lauschke et al., 2020)	Human	• hiPSCs	3D	• Cell viability • Beating evaluation with 'beat score' • EB volume	• 3D cell system • No FBS • No ethical concerns using hiPSCs	• Low throughput due to high number of technical replicates • Experienced staff needed for visual evaluation of beating
hiPSC-based EST (Walker et al., 2021)	Human	• hiPSCs • Human foreskin fibroblasts	2D	• Cell viability • Beating evaluation (yes/no principle) • mRNA expression	• No ethical concerns using hiPSCs	• FBS in medium • Low throughput due to high number of technical replicates • Experienced staff needed for visual evaluation of beating • 2D cell system • Long assay duration
hiPS Test (Galanjuk et. al, 2022)	Human	• hiPSCs	2D	• Cell viability • Beating area • Beating frequency • mRNA expression	• No FBS • No ethical concerns using hiPSCs • Defined percentage of cardiomyocytes • Low number of replicates • No human-based evaluation	• Low throughput • 2D cell system

Replacing mESCs in the EST with hESCs was the first attempt to overcome species differences in the hESC-based EST (Adler et al., 2008). Although the hESC-based EST is mimicking the EST, only a cell viability assay was performed, while the beating of cardiomyocytes was not evaluated. In addition, the assay is raising ethical concerns as working with hESCs underlies restrictions due to ethical issues in many countries worldwide (Bobbert, 2006; Lo and Parham, 2009). Over ten years later, after the discovery of hiPSCs, mESCs or hESCs were replaced with hiPSCs in the iPST (Aikawa, 2020). While this assay overcomes possible species differences and raises no ethical concerns, the drawbacks of the EST remain present. Like the EST the iPST includes FBS (5 %) in the medium and needs a high number of replicates (24 EBs per concentration) making it low throughput. Additionally, for the visual evaluation of beating EBs experienced staff is needed. While also using hiPSCs, Lauschke et al. (2020) took a step further not only mimicking the EST but omitting FBS from their protocol called the Pluri Beat Assay advancing towards an animal-free method. Lauschke et al., (2020) also changed the yes and no principle-based evaluation of beating EBs introducing a new scoring method called beat score which aims to distinguish between different degrees of beating in terms of the area. In addition, they added the endpoint of measuring the EB volume to their assay. Besides these changes, the low throughput due to a high number of replicates (32) remains as well as the need for experienced staff for the visual evaluation of beating EBs. While the hESC-based EST, the iPST, and the Pluri Beat Assay are based on the formation of 3D EBs (Adler et al., 2008; Aikawa, 2020; Lauschke et al., 2020) mimicking the EST, Walker et al. (2021) developed another approach using a 2D cell system. The use of 2D versus 3D cell systems is always debatable. During a comparison of 2D versus 3D cardiomyocyte differentiation of hESCs and hiPSCs, the 2D method yielded a higher purity of cardiomyocytes in the study of Zhang et al. (2015). It is also known that in EBs not only cardiomyocytes are present in the culture. On the other hand, the heterogeneity of cell cultures is also seen as an advantage since it better mimics the natural environment of e.g. cardiomyocytes. An argument against a heterogenous cell culture is the often unknown effect of other cell types in the culture on the substance tested, advocating for pure cell cultures for substance testing. In the hiPSC-based EST by Walker et al. (2021), a monolayer hiPSC culture is directly differentiated into cardiomyocytes. This is performed by using a high amount of FBS (18%) instead of a defined medium modulating the WNT or BMP pathways. Additionally, a higher number of 32 replicates is required compared to 24 replicates in the EST. This additionally increases the handling time as the beating is assessed manually, again, in need of experienced staff. However, the molecular readout of cardiac transcription factors *TBX5* and *MEF2c* mRNA expression was implemented adding sensitivity to the test system. The hiPS Test developed in this thesis also uses hiPSCs differentiated into cardiomyocytes in a 2D format but is completely devoid of FBS. A 2D system, however, does not necessarily mean that cells grow in a monolayer. Differentiated cardiomyocytes in the hiPS Test grow multilayered and consist of around 70 % cardiomyocytes marked by cTnT and

α-Actinin2 expression. On day ten of the protocol, cardiomyocytes developed a synchronous uniform beating area. As mentioned above, the cell composition in differentiated EBs is often not defined generating partially not beating EBs which are difficult to score requiring experienced staff. The beating of 3D EBs or beating structures in 2D cannot be evaluated quantitatively regarding the beating area or the beating frequency so far (Genschow et al., 2002; Aikawa, 2020; Lauschke et al., 2020; Walker et al., 2021). The hiPS Test aimed at overcoming the need for experienced staff to evaluate the beating as well as reducing the handling time to do so. For this, video recordings of the entire well area were recorded to fully recognize all contracting and non-contracting structures. The inhouse-developed software CardioVision was programmed to quantitatively evaluate the percentage of the beating frequency and beating area of every well. This procedure saves time and makes the assay independent of the investigator. Additionally, there is room for expanding the software to different well formats and sources of recording as well as adapting it to beating EBs. Besides that, a molecular readout was estbalished for the hiPS Test. As *TNNT2* and *ACTN2* are markers expressed later in cardiomyogenesis, a delayed development due to substance toxicity would be related with a reduced expression of these genes which can be evalauted with the standards created. Furthermore, the hiPS Test gets by with only four technical replicates resulting in the performance of the hiPS Test on only one 48-well plate per substance, eliminating plate-to-plate variability. Additionally, the handling time was decreased by using a singel-cell culture of the hiPSCs which can be propagated very quickly and in high numbers. These features enable a higher throughput of the hiPS Test compared to assays using EBs but still being considered as low throughput. However, the method is very sensitive to small disturbances especially regarding cardiomyocyte differentiation. The quality and cell density of the hiPSC culture before plating is crucial for this. Practically in the lab, this sensitivity leads to either successful differentiation or no differentiation over the whole plate hence not affecting intra-plate variability. A point to consider at further enhancing the hiPS Test is the medium for hiPSCs culture. Different media are available for culturing hiPSCs e.g. E8, mTeSR, and iPS Brew which are commercially available. Each of them was designed to support hiPSC growth and maintain their pluripotency. However, the exact composition is unknown. To achieve a fully defined medium, FTDA medium was used in this work, which consists of ten different ingredients and was characterized previously (Frank et al., 2012). Although the medium is completely defined, it bears the risk of batch-to-batch variation of its ingredients that are partially stable for only three months like the ITS Premix Universal Culture Supplement from Corning. Additionally, if one of the ingredients is suspended for any reason, an alternative has to be used which requires testing of the culture to yield the same performance as before. Overall, the risk of using a self-made medium like FTDA might be too high for projects lasting for several years increasing the risk of FTDA ingredients being suspended. In the future, it would be a better alternative for the hiPS Test to switch from FTDA to a commercially available hiPSC medium in order to receive a less variable culture

medium. Additionally, an attempt to change the matrix for cardiomyocyte differentiation from Matrigel to an alternative like LN521, vitronectin or fibronectin should be made to reduce the before mentioned drawbacks of the use of Matrigel proceeding in the development of a true animal free test system.

6 Abstract

Human development can be disrupted by a variety of substances, resulting in the need to test compounds for their embryotoxic potential. Embryonic toxicity testing for marketed and newly developed compounds is regulated worldwide by different agencies, e.g. the United States Environmental Protection Agency (US EPA) or European Chemicals Agency (ECHA) by the implementation of the Organisation for Economic Co-operation and Development (OECD) or US EPA test guidelines. Since the regulation Registration, Evaluation, Authorisation of Chemicals (REACH) went into force in 2007 stipulating that substances produced or imported over ten tonnages per year have to be tested for reproductive toxicity an increase in animal testing was inevitable. At the same time, the ECHA supports the use and development of alternative methods to comply with the 3Rs, reduction, refinement, and replacement of animal testing. The embryonic stem cell test (EST) is an alternative method validated by the European Center for Validation of Alternative Methods (ECVAM) testing for embryotoxicity making use of two permanent mouse cell lines, however, the EST was not approved for regulatory purposes. To overcome the issue of species differences, the human induced pluripotent stem cell test (hiPS Test) was established in this work which is based on human induced pluripotent stem cells (hiPSC). Human iPSCs are an auspicious tool in a variety of biological research fields as they provide an almost unlimited source of human cells, which can differentiate into almost every cell type of the human body. In contrast to embryonic stem cells (ESCs), generating hiPSCs does not require human embryos and therefore, does not raise ethical concerns. The hiPS Test was established to contribute to a future test battery of *in vitro* embryotoxicity tests by differentiating hiPSCs into beating cardiomyocytes under substance exposure. The test system was characterized and endpoints for the test method were established. For assessing the beating frequency and area of cardiomyocytes, the software CardioVision was developed. A small training set of compounds was studied as a first proof of concept. In summary, the hiPS Test exhibits a similar result in terms of cell viability for the positive control (5-Fluorouracil) compared to other human cell-based test systems. For one compound tested as a proof-of-concept (triclabendazole), the hiPS Test seems to have a higher sensitivity compared to the zebrafish embryo test, and pre-, or postimplantation rodent whole embryo culture. One drawback of the hiPS Test is its sensitivity to small disturbances due to e.g. handling or medium constituents. Hence, it is advisable to improve its robustness. Additionally, more substances have to be screened to assess the predictivity of the hiPS Test.

7 Zusammenfassung

Die menschliche Entwicklung kann durch eine Vielzahl von Substanzen gestört werden, weshalb es unerlässlich ist, diese auf ihr embryotoxisches Potenzial zu testen. Die Prüfung der Embryotoxizität von vermarkteten und neu entwickelten Substanzen wird weltweit von verschiedenen Behörden wie z. B. der United States Environmental Protection Agency (US EPA) oder der European Chemicals Agency (ECHA) geregelt und durch die Testrichtlinien der Organisation for Economic Co-operation and Development (OECD) oder der US EPA umgesetzt. Seit dem Inkrafttreten der Verordnung Registration, Evaluation, Authorisation of Chemicals (REACH) im Jahr 2007, die vorschreibt, dass Stoffe, die in einer Menge von mehr als zehn Tonnen pro Jahr hergestellt oder eingeführt werden, auf ihre Reproduktionstoxizität getestet werden müssen, war eine Zunahme von Tierversuchen unvermeidlich. Gleichzeitig unterstützt die ECHA jedoch die Verwendung und Entwicklung alternativer Methoden, um das 3R Prinzip, Replacement (Vermeidung), Reduction (Verringerung), Refinement (Verbesserung) von Tierversuchen zu erfüllen. Der vom European Center for Validation of Alternative Methods (ECVAM) validierte embryonale Stammzelltest (EST) ist eine alternative Testmethode zur Prüfung von Substanzen auf Embryotoxizität, bei der zwei permanente Mauszelllinien verwendet werden. Der EST wurde jedoch nicht für regulatorische Zwecke zugelassen. Um das Problem der Speziesunterschiede zu überwinden, wurde in dieser Arbeit der human induced pluripotent stem cell test (hiPS Test) entwickelt, der auf humanen induzierten pluripotenten Stammzellen (hiPSC) basiert. Humane induzierte pluripotente Stammzellen sind ein vielversprechendes Werkzeug in einer Vielzahl von biologischen Forschungsbereichen, da sie eine nahezu unbegrenzte Quelle menschlicher Zellen darstellen, die in fast jeden Zelltyp des menschlichen Körpers differenzieren können. Im Gegensatz zu embryonalen Stammzellen (ESC) werden für die Erzeugung von hiPSCs keine menschlichen Embryonen benötigt, so dass keine ethischen Bedenken bestehen. Der hiPS-Test wurde entwickelt, um einen Beitrag zu einer künftigen Testbatterie von *in-vitro*-Embryotoxizitätstests zu leisten, indem hiPSCs unter Substanzexposition zu schlagenden Kardiomyozyten differenziert werden. Das Testsystem wurde charakterisiert und Endpunkte definiert. Für die Bewertung der schlagenden Fläche und Schlagfrequenz der Kardiomyozyten pro Well wurde die Software CardioVision entwickelt. Ein kleines Trainingsset wurde als erster Konzeptnachweis untersucht. Zusammenfassend kann geschlossen werden, dass der hiPS-Test für die Positivkontrolle (5-Fluorouracil) ein ähnliches Ergebnis in Bezug auf die Zellviabilität zeigt wie andere auf menschlichen Zellen basierende Testsysteme. Für eine als Konzeptnachweis getestete Substanz (Triclabendazol) scheint der hiPS-Test im Vergleich zum Zebrafisch-Embryotest und zur Prä- oder Postimplantationskultur von Nagetier-Vollembryonen eine höhere Empfindlichkeit aufzuweisen. Ein Nachteil des hiPS-Tests ist seine Empfindlichkeit gegenüber kleinen Störungen, z. B. durch die Handhabung oder Bestandteile des Mediums. Daher ist es ratsam, seine Robustheit zu verbessern. Außerdem müssen mehr Substanzen untersucht werden, um die Vorhersagekraft des hiPS-Tests beurteilen zu können.

8 References

Abassi, Y. A., Xi, B., Li, N. et al. (2012). Dynamic monitoring of beating periodicity of stem cell-derived cardiomyocytes as a predictive tool for preclinical safety assessment. *Br J Pharmacol 165*, 1424–1441. https://doi.org/10.1111/j.1476-5381.2011.01623.x.

Al Abbar, A., Ngai, S. C., Nograles, N. et al. (2020). Induced Pluripotent Stem Cells: Reprogramming Platforms and Applications in Cell Replacement Therapy. *Biores Open Access 9*, 121–136. https://doi.org/10.1089/biores.2019.0046.

Adler, S., Pellizzer, C., Hareng, L. et al. (2008). First steps in establishing a developmental toxicity test method based on human embryonic stem cells. *Toxicol Vitr 22*, 200–211. https://doi.org/10.1016/j.tiv.2007.07.013.

Afrakhte, M., Morén, A., Jossan, S. et al. (1998). Induction of inhibitory Smad6 and Smad7 mRNA by TGF-β family members. *Biochem Biophys Res Commun 249*, 505–511. https://doi.org/10.1006/bbrc.1998.9170.

Ahola, A., Kiviaho, A. L., Larsson, K. et al. (2014). Video image-based analysis of single human induced pluripotent stem cell derived cardiomyocyte beating dynamics using digital image correlation. *Biomed Eng Online 13*, 39. https://doi.org/10.1186/1475-925X-13-39.

Aikawa, N. (2020). A novel screening test to predict the developmental toxicity of drugs using human induced pluripotent stem cells. *J Toxicol Sci 45*, 187–199. https://doi.org/10.2131/jts.45.187.

Assou, S., Bouckenheimer, J. and Vos, J. De (2018). Concise Review: Assessing the Genome Integrity of Human Induced Pluripotent Stem Cells: What Quality Control Metrics? *Stem Cells 36*, 814–821. https://doi.org/10.1002/STEM.2797.

Attia, S. M., Badary, O. A., Hamada, F. M. et al. (2008). The chemotherapeutic agents nocodazole and amsacrine cause meiotic delay and non-disjunction in spermatocytes of mice. *Mutat Res Toxicol Environ Mutagen 651*, 105–113. https://doi.org/10.1016/j.mrgentox.2007.10.011.

Bai, Q., Ramirez, J. M., Becker, F. et al. (2015). Temporal analysis of genome alterations induced by single-cell passaging in human embryonic stem cells. *Stem Cells Dev 24*, 653–662. https://doi.org/10.1089/scd.2014.0292.

Balafkan, N., Mostafavi, S., Schubert, M. et al. (2020). A method for differentiating human induced pluripotent stem cells toward functional cardiomyocytes in 96-well microplates. *Sci Reports 2020 101 10*, 1–14. https://doi.org/10.1038/s41598-020-73656-2.

BD Biosciences (2022). BD Human Pluripotent Stem Cell Transcription Factor Analysis Kit Instruction Manual. , 1–2. Available at: https://www.bdbiosciences.com/content/dam/bdb/products/global/reagents/flow-cytometry-reagents/research-reagents/panels-multicolor-cocktails-ruo/560589_base/pdf/23-12787.pdf [Accessed December 13, 2022].

Bedada, F. B., Wheelwright, M. and Metzger, J. M. (2016). Maturation status of sarcomere structure and function in human iPSC-derived cardiac myocytes. *Biochim Biophys Acta - Mol Cell Res 1863*, 1829–1838. https://doi.org/10.1016/J.BBAMCR.2015.11.005.

Ben-David, U., Benvenisty, N. and Mayshar, Y. (2010). Genetic instability in human induced pluripotent stem cells: Classification of causes and possible safeguards. *Cell Cycle 9*, 4603–4604. https://doi.org/10.4161/cc.9.23.14094.

Van Den Berg, G., Abu-Issa, R., De Boer, B. A. J. et al. (2009). A caudal proliferating growth center contributes to both poles of the forming heart tube. *Circ Res 104*, 179–188. https://doi.org/10.1161/CIRCRESAHA.108.185843.

Betts, G., Desaix, P., Johnson, E. et al. (2013). *Anatomy and Physiology*. Houston: Rice University. Available at: https://openstax.org/details/books/anatomy-and-physiology.

Biolamina (2022). Biolaminin 521 LN. Available at: https://biolamina.com/products/laminin-ln-521-stem-cell-matrix/ [Accessed December 13, 2022].

Bobbert, M. (2006). Ethical questions concerning research on human embryos, embryonic stem cells and chimeras. *Biotechnol J 1*, 1352–1369. https://doi.org/10.1002/biot.200600179.

Bocci, G., Danesi, R., Di Paolo, A. et al. (2000). Comparative pharmacokinetic analysis of 5-fluorouracil and its major metabolite 5-fluoro-5,6-dihydrouracil after conventional and reduced test dose in cancer patients. *Clin Cancer Res 6*, 3032–3037

Boix, N., Teixido, E., Vila-Cejudo, M. et al. (2015). Triclabendazole sulfoxide causes stage-dependent embryolethality in zebrafish and mouse in vitro. *PLoS One 10*. https://doi.org/10.1371/journal.pone.0121308.

Boix, N., Teixidó, E., Vila-Cejudo, M. et al. (2016). Risk assessment for human embryonic development of triclabendazole residues in milk and cheese in the diet of a rural population in Cajamarca (Peru): A preliminary approach. *Recent Adv Pharm Sci VI 661*, 37–47

Bondue, A. and Blanpain, C. (2010). Mesp1: A key regulator of cardiovascular lineage commitment. *Circ Res 107*, 1414–1427. https://doi.org/10.1161/CIRCRESAHA.110.227058.

von Both, I., Silvestri, C., Erdemir, T. et al. (2004). Foxh1 is essential for development of the anterior heart field. *Dev Cell 7*, 331–345. https://doi.org/10.1016/j.devcel.2004.07.023.

Braam, S. R., Tertoolen, L., van de Stolpe, A. et al. (2010). Prediction of drug-induced cardiotoxicity using human embryonic stem cell-derived cardiomyocytes. *Stem Cell Res 4*, 107–116. https://doi.org/10.1016/j.scr.2009.11.004.

Brade, T., Pane, L. S., Moretti, A. et al. (2013). Embryonic Heart Progenitors and Cardiogenesis. *Cold Spring Harb Perspect Med 3*, a013847–a013847. https://doi.org/10.1101/cshperspect.a013847.

Bradman, A., Barr, D. B., Henn, B. G. C. et al. (2003). Measurement of pesticides and other toxicants in amniotic fluid as a potential biomarker of prenatal exposure: A validation study. *Environ Health Perspect 111*, 1779–1782. https://doi.org/10.1289/ehp.6259.

Bradski, G. (2000). The OpenCV Library. *Dr Dobb's J Softw Tools*. Available at: https://www.drdobbs.com/open-source/the-opencv-library/184404319 [Accessed December 13, 2022].

Brown, M. and Wittwer, C. (2000). Flow cytometry: Principles and clinical applications in hematology. *Clin Chem 46*, 1221–1229. https://doi.org/10.1093/clinchem/46.8.1221.

Bruneau, B. G., Nemer, G., Schmitt, J. P. et al. (2001). A murine model of Holt-Oram syndrome defines roles of the T-Box transcription factor Tbx5 in cardiogenesis and disease. *Cell 106*, 709–721. https://doi.org/10.1016/S0092-8674(01)00493-7.

Burdsal, C. A., Flannery, M. L. and Pedersen, R. A. (1998). FGF-2 alters the fate of mouse epiblast from ectoderm to mesoderm in vitro. *Dev Biol 198*, 231–244. https://doi.org/10.1016/S0012-1606(98)80001-8.

Burridge, P. W., Matsa, E., Shukla, P. et al. (2014). Chemically defined generation of human cardiomyocytes. *Nat Methods 11*, 855–860. https://doi.org/10.1038/nmeth.2999.

Bustin, S. A. (2000). Absolute quantification of mRNA using real-time reverse transcription polymerase chain reaction assays. *J Mol Endocrinol 25*, 169–193. https://doi.org/10.1677/JME.0.0250169.

Cai, C.-L., Liang, X., Shi, Y. et al. (2003). Isl1 Identifies a Cardiac Progenitor Population that Proliferates Prior to Differentiation and Contributes a Majority of Cells to the Heart. *Dev Cell 5*, 877–889. https://doi.org/10.1016/S1534-5807(03)00363-0.

Cai, J., Li, W., Su, H. et al. (2010). Generation of Human Induced Pluripotent Stem Cells from Umbilical Cord Matrix and Amniotic Membrane Mesenchymal Cells. *J Biol Chem 285*, 11227–11234. https://doi.org/10.1074/JBC.M109.086389.

Chalabi-Dchar, M., Fenouil, T., Machon, C. et al. (2021). A novel view on an old drug, 5-fluorouracil: an unexpected RNA modifier with intriguing impact on cancer cell fate. *NAR Cancer 3*, 1–13. https://doi.org/10.1093/narcan/zcab032.

Chang, W., Cheng, J., Allaire, J. J. et al. (2022). shiny: Web Application Framework for R. Available at: https://cran.r-project.org/package=shiny [Accessed December 13, 2022].

Chapin, R., Stedman, D., Paquette, J. et al. (2007). Struggles for equivalence: In vitro developmental toxicity model evolution in pharmaceuticals in 2006. *Toxicol Vitr 21*, 1545–1551. https://doi.org/10.1016/j.tiv.2006.10.006.

Chen, B., Dodge, M. E., Tang, W. et al. (2009). Small molecule–mediated disruption of Wnt-dependent signaling in tissue regeneration and cancer. *Nat Chem Biol 5*, 100–107. https://doi.org/10.1038/nchembio.137.

Clements, M. and Thomas, N. (2014). High-Throughput Multi-Parameter Profiling of Electrophysiological Drug Effects in Human Embryonic Stem Cell Derived Cardiomyocytes Using Multi-Electrode Arrays. *Toxicol Sci 140*, 445–461. https://doi.org/10.1093/toxsci/kfu084.

Corning Incorporated Life Sciences (2022). Corning Matrigel Matrix Frequently Asked Questions. , 1–8. Available at: https://www.corning.com/catalog/cls/documents/faqs/CLS-DL-CC-026.pdf [Accessed December 13, 2022].

Cossarizza, A., Chang, H., Radbruch, A. et al. (2017). Guidelines for the use of flow cytometry and cell sorting in immunological studies. *Eur J Immunol 47*, 1584–1797. https://doi.org/10.1002/eji.201646632.

Crofton, K. M., Mundy, W. R., Lein, P. J. et al. (2011). Developmental neurotoxicity testing: Recommendations for developing alternative methods for the screening and prioritization of chemicals. *ALTEX 28*, 9–15. https://doi.org/10.14573/altex.2011.1.009.

Dagg, C. P. (1960). Sensitive stages for the production of developmental abnormalities in mice with 5-fluorouracil. *Am J Anat 106*, 89–96. https://doi.org/10.1002/aja.1001060202.

van Dartel, D. A. M., Pennings, J. L. A., de la Fonteyne, L. J. J. et al. (2010). Monitoring developmental toxicity in the embryonic stem cell test using differential gene expression of differentiation-related genes. *Toxicol Sci 116*, 130–139. https://doi.org/10.1093/toxsci/kfq127.

Ten Dijke, P., Yamashita, H., Sampath, T. K. et al. (1994). Identification of type I receptors for osteogenic protein-1 and bone morphogenetic protein-4. *J Biol Chem 269*, 16985–16988. https://doi.org/10.1016/s0021-9258(17)32506-1.

Doubilet, P. M. and Benson, C. B. (1995). Embryonic heart rate in the early first trimester: what rate is normal? *J Ultrasound Med 14*, 431–434. https://doi.org/10.7863/jum.1995.14.6.431.

Dudka, A. A., Sweet, S. M. M. and Heath, J. K. (2010). Stat3 Binding To the Fgf Receptor Is Activated By Receptor Amplification. *Cancer Res 70*, 3391. https://doi.org/10.1158/0008-5472.CAN-09-3033.STAT3.

Dunnett, C. W. and Tamhane, A. C. (1991). Step-down multiple tests for comparing treatments with a control in unbalanced one-way layouts. *Stat Med 10*, 939–947. https://doi.org/10.1002/sim.4780100614.

Ebisawa, T., Tada, K., Kitajima, I. et al. (1999). Characterization of bone morphogenetic protein-6 signaling pathways in osteoblast differentiation. *J Cell Sci 112*, 3519–3527. https://doi.org/10.1242/jcs.112.20.3519.

ECHA (2011). The Use of Alternatives to Testing on Animals for the REACH Regulation 2011. , 69. Available at: https://echa.europa.eu/documents/10162/17231/alternatives_test_animals_2011_en.pdf/9b0f7e93-4d61-401d-ba2c-80b3b9faaf66 [Accessed December 13, 2022].

ECHA (2014). The Use of Alternatives to Testing on Animals for the REACH Regulation 2014. *117*. Available at: https://echa.europa.eu/documents/10162/17231/alternatives_test_animals_2014_en.pdf/587d000c-688e-4cdd-9f59-f7d7aacc677b [Accessed December 13, 2022].

ECHA (2017). The Use of Alternatives to Testing on Animals for the REACH Regulation 2017. *117*, 1–101. Available at: https://echa.europa.eu/documents/10162/17231/alternatives_test_animals_2017_en.pdf/075c690d-054c-693a-c921-f8cd8acbe9c3 [Accessed December 13, 2022].

ECHA (2020). The Use of Alternatives to Testing on Animals for the REACH Regulation 2020. *117*, 85. https://doi.org/10.2823/092305.

ECHA (2022). Understanding REACH. *Eur Chem Agency Helsinki*. Available at: https://echa.europa.eu/regulations/reach/understanding-reach [Accessed December 13, 2022].

Emre, N., Vidal, J. G., Elia, J. et al. (2010). The ROCK inhibitor Y-27632 improves recovery of human embryonic stem cells after fluorescence-activated cell sorting with multiple cell surface markers. *PLoS One 5*. https://doi.org/10.1371/journal.pone.0012148.

Eng, G., Lee, B. W., Protas, L. et al. (2016). Autonomous beating rate adaptation in human stem cell-derived cardiomyocytes. *Nat Commun 7*, 1–10. https://doi.org/10.1038/ncomms10312.

Entcheva, E., Kostov, Y., Tchernev, E. et al. (2004). Fluorescence Imaging of Electrical Activity in Cardiac Cells Using An All-Solid-State System. *IEEE Trans Biomed Eng 51*, 333–341. https://doi.org/10.1109/TBME.2003.820376.

Farrell, R. E. (2017). *RNA Methodologies Laboratory Guide for Isolation and Characterization*. 5th ed. Pennsylvania. United States: Elsevier Inc. https://doi.org/10.1016/b978-0-12-804678-4.00001-4.

FDA (2016). Prescribing information. Fluorouracil injection, for intravenous use. Available at: https://www.accessdata.fda.gov/drugsatfda_docs/label/2016/012209s040lbl.pdf [Accessed December 13, 2022].

Fijnvandraat, A., van Ginneken, A. C. G., de Boer, P. A. J. et al. (2003). Cardiomyocytes derived from embryonic stem cells resemble cardiomyocytes of the embryonic heart tube. *Cardiovasc Res 58*, 399–409. https://doi.org/10.1016/S0008-6363(03)00282-7.

Frank, S., Zhang, M., Schöler, H. R. et al. (2012). Small molecule-assisted, line-independent maintenance of human pluripotent stem cells in defined conditions. *PLoS One 7*. https://doi.org/10.1371/journal.pone.0041958.

Fritz, B., Hallermann, C., Olert, J. et al. (2001). Cytogenetic analyses of culture failures by comparative genomic hybridisation (CGH) - Re-evaluation of chromosome aberration rates in early spontaneous abortions. *Eur J Hum Genet 9*, 539–547. https://doi.org/10.1038/sj.ejhg.5200669.

Galanjuk, S., Zühr, E., Dönmez, A. et al. (2022). The Human Induced Pluripotent Stem Cell Test as an Alternative Method for Embryotoxicity Testing. *Int J Mol Sci 23*, 3295. https://doi.org/10.3390/ijms23063295.

Genschow, E., Spielmann, H., Scholz, G. et al. (2002). The ECVAM international validation study on in vitro embryotoxicity tests: Results of the definitive phase and evaluation of prediction models. *ATLA Altern to Lab Anim 30*, 151–176. https://doi.org/10.1177/026119290203000204.

Genschow, E., Spielmann, H., Scholz, G. et al. (2004). Validation of the Embryonic Stem Cell Test in the International ECVAM Validation Study on Three In Vitro Embryotoxicity Tests. *Altern to Lab Anim 32*, 209–244. https://doi.org/10.1177/026119290403200305.

Genz, A., Bretz, F., Miwa, T. et al. (2021). Package mvtnorm: Multivariate Normal and t Distributions. *J Comput Graph Stat 11*, 950–971. Available at: https://mran.revolutionanalytics.com/snapshot/2020-02-09/web/packages/mvtnorm/mvtnorm.pdf [Accessed December 13, 2022].

Ghanbari, M. (1990). The cross-search algorithm for motion estimation (image coding). *IEEE Trans Commun 38*, 950–953. https://doi.org/10.1109/26.57512.

Gibb, S. (2008). Toxicity testing in the 21st century: A vision and a strategy. *Reprod Toxicol 25*, 136–138. https://doi.org/10.1016/j.reprotox.2007.10.013.

Golob, M., Moss, R. L. and Chesler, N. C. (2014). Cardiac Tissue Structure, Properties, and Performance: A Materials Science Perspective. *Ann Biomed Eng 42*, 2003–2013. https://doi.org/10.1007/s10439-014-1071-z.

Goto, K., Kamiya, Y., Imamura, T. et al. (2007). Selective inhibitory effects of Smad6 on bone morphogenetic protein type I receptors. *J Biol Chem 282*, 20603–20611. https://doi.org/10.1074/jbc.M702100200.

Grem, J. L. (2000). 5-Fluorouracil: Forty-plus and still ticking. A review of its preclinical and clinical development. *Invest New Drugs 18*, 299–313. https://doi.org/10.1023/A:1006416410198.

Gstraunthaler, G., Lindl, T. and van der Valk, J. (2013). A plea to reduce or replace fetal bovine serum in cell culture media. *Cytotechnology 65*, 791–793. https://doi.org/10.1007/s10616-013-9633-8.

Gutberlet, M. (2017). Bildgebende Diagnostik angeborener Herzfehler. In *Bildgebende Diagnostik angeborener Herzfehler* (21–35). Stuttgart; New York: Georg Thieme Verlag.

Hardy, A., Benford, D., Halldorsson, T. et al. (2017). Update: use of the benchmark dose approach in risk assessment. *EFSA J 15*, e04658. https://doi.org/10.2903/j.efsa.2017.4658.

Hayakawa, T., Kunihiro, T., Dowaki, S. et al. (2012). Noninvasive Evaluation of Contractile Behavior of Cardiomyocyte Monolayers Based on Motion Vector Analysis. *Tissue Eng Part C Methods 18*, 21–32. https://doi.org/10.1089/ten.tec.2011.0273.

Hinrichsen, K. V (1990). *Humanembryologie*. Heidelberg: Springer-Verlag Berlin Heidelberg. https://doi.org/10.1007/978-3-662-07815-0.

Holmgren, G., Zeng, X. and Synnergren, J. (2015). Selection of robust reference genes for normalization of quantitative RT-PCR data from differentiating human pluripotent stem cells. *Proc 7th Int Conf Bioinforma Comput Biol BICOB 2015*, 65–70

Hughes, C. S., Postovit, L. M. and Lajoie, G. A. (2010). Matrigel: a complex protein mixture required for optimal growth of cell culture. *Proteomics 10*, 1886–1890. https://doi.org/10.1002/pmic.200900758.

Hyer, J. S., Fong, S. and Kutteh, W. H. (2004). Predictive value of the presence of an embryonic heartbeat for live birth: Comparison of women with and without recurrent pregnancy loss. *Fertil Steril 82*, 1369–1373. https://doi.org/10.1016/j.fertnstert.2004.03.058.

Iyer, P. (2017). *Guidelines for reproductive and developmental toxicity testing and risk assessment of chemicals*. Elsevier Inc. https://doi.org/10.1016/B978-0-12-804239-7.00010-X.

Johnson, P. D. and Besselsen, D. G. (2002). Practical Aspects of Experimental Design in Animal Research. *ILAR J 43*, 202–206. https://doi.org/10.1093/ilar.43.4.202.

Jordan, M. A., Thrower, D. and Wilson, L. (1992). Effects of vinblastine, podophyllotoxin and nocodazole on mitotic spindles. Implications for the role of microtubule dynamics in mitosis. *J Cell Sci 102*, 401–416. https://doi.org/10.1242/jcs.102.3.401.

Kamgoué, A., Ohayon, J., Usson, Y. et al. (2009). Quantification of cardiomyocyte contraction based on image correlation analysis. *Cytom Part A 75A*, 298–308. https://doi.org/10.1002/cyto.a.20700.

Kan, M., Wang, F., Xu, J. et al. (1993). An essential heparin-binding domain in the fibroblast growth factor receptor kinase. *Science (80-) 259*, 1918–1921. https://doi.org/10.1126/science.8456318.

Karnofsky, D. A. and Basch, R. S. (1960). Effects of 5-fluorodeoxyuridine and related halogenated pyrimidines on the sand-dollar embryo. *J Biophys Biochem Cytol 7*, 61–71. https://doi.org/10.1083/jcb.7.1.61.

Kawai, T., Takahashi, T., Esaki, M. et al. (2004). Efficient Cardiomyogenic Differentiation of Embryonic Stem Cell by Fibroblast Growth Factor 2 and Bone Morphogenetic Protein 2. *Circ J 68*, 691–702. https://doi.org/10.1253/circj.68.691.

Keeney, M., Gratama, J. W., Chin-Yee, I. H. et al. (1998). Isotype controls in the analysis of lymphocytes and CD34+ stem and progenitor cells by flow cytometry?time to let go! *Cytometry 34*, 280–283. https://doi.org/10.1002/(SICI)1097-0320(19981215)34:6<280::AID-CYTO6>3.0.CO;2-H.

Kehat, I., Kenyagin-Karsenti, D., Snir, M. et al. (2001). Human embryonic stem cells can differentiate into myocytes with structural and functional properties of cardiomyocytes. *J Clin Invest 108*, 407–414. https://doi.org/10.1172/JCI12131.

Keiser, J., Engels, D., Büscher, G. et al. (2005). Triclabendazole for the treatment of fascioliasis and paragonimiasis. *Expert Opin Investig Drugs 14*, 1513–1526. https://doi.org/10.1517/13543784.14.12.1513.

Kelly, R. G., Brown, N. A. and Buckingham, M. E. (2001). The Arterial Pole of the Mouse Heart Forms from Fgf10-Expressing Cells in Pharyngeal Mesoderm. *Dev Cell 1*, 435–440. https://doi.org/10.1016/S1534-5807(01)00040-5.

Kouhara, H., Hadari, Y. R., Spivak-Kroizman, T. et al. (1997). A lipid-anchored Grb2-binding protein that links FGF-receptor activation to the Ras/MAPK signaling pathway. *Cell 89*, 693–702. https://doi.org/10.1016/S0092-8674(00)80252-4.

Krebs, A., Nyffeler, J., Karreman, C. et al. (2020). Determination of Benchmark Concentrations and Their Statistical Uncertainty for Cytotoxicity Test Data and Functional In Vitro Assays. *ALTEX 37*, 155–163. https://doi.org/10.14573/altex.1912021.

Kuo, C. T., Morrisey, E. E., Anandappa, R. et al. (1997). GATA4 transcription factor is required for ventral morphogenesis and heart tube formation. *Genes Dev 11*, 1048–1060. https://doi.org/10.1101/gad.11.8.1048.

de la Cruz, M. V, Sánchez Gómez, C., Arteaga, M. M. et al. (1977). Experimental study of the development of the truncus and the conus in the chick embryo. *J Anat 123*, 661–86

Laco, F., Woo, T. L., Zhong, Q. et al. (2018). Unraveling the Inconsistencies of Cardiac Differentiation Efficiency Induced by the GSK3β Inhibitor CHIR99021 in Human Pluripotent Stem Cells. *Stem Cell Reports 10*, 1851–1866. https://doi.org/10.1016/j.stemcr.2018.03.023.

Lamothe, B., Yamada, M., Schaeper, U. et al. (2004). The Docking Protein Gab1 Is an Essential Component of an Indirect Mechanism for Fibroblast Growth Factor Stimulation of the Phosphatidylinositol 3-Kinase/Akt Antiapoptotic Pathway. *Mol Cell Biol 24*, 5657–5666. https://doi.org/10.1128/mcb.24.13.5657-5666.2004.

Lau, C., Mole, M. L., Copeland, M. F. et al. (2001). Toward a biologically based dose-response model for developmental toxicity of 5-fluorouracil in the rat: Acquisition of experimental data. *Toxicol Sci 59*, 37–48. https://doi.org/10.1093/toxsci/59.1.37.

Laurent, L. C., Ulitsky, I., Slavin, I. et al. (2011). Dynamic changes in the copy number of pluripotency and cell proliferation genes in human ESCs and iPSCs during reprogramming and time in culture. *Cell Stem Cell 8*, 106–118. https://doi.org/10.1016/j.stem.2010.12.003.

Lauschke, K., Rosenmai, A. K., Meiser, I. et al. (2020). A novel human pluripotent stem cell-based assay to predict developmental toxicity. *Arch Toxicol 94*, 3831–3846. https://doi.org/10.1007/s00204-020-02856-6.

Lecaillon, J. B., Godbillon, J., Campestrini, J. et al. (1998). Effect of food on the bioavailability of triclabendazole in patients with fascioliasis. *Br J Clin Pharmacol 45*, 601–604. https://doi.org/10.1046/j.1365-2125.1998.00725.x.

Lescroart, F., Chabab, S., Lin, X. et al. (2014). Early lineage restriction in temporally distinct populations of Mesp1 progenitors during mammalian heart development. *Nat Cell Biol 16*, 829–840. https://doi.org/10.1038/ncb3024.

Leyder, M., Laubach, M., Breugelmans, M. et al. (2011). Specific Congenital Malformations after Exposure to Cyclophosphamide, Epirubicin and 5-Fluorouracil during the First Trimester of Pregnancy. *Gynecol Obstet Invest 71*, 141–144. https://doi.org/10.1159/000317264.

Li, J., Chen, X., Ding, X. et al. (2013). LATS2 suppresses oncogenic Wnt signaling by disrupting β-Catenin/BCL9 interaction. *Cell Rep 5*, 1650–1663. https://doi.org/10.1016/j.celrep.2013.11.037.

Li, S., Zhou, D., Lu, M. M. et al. (2004). Advanced cardiac morphogenesis does not require heart tube fusion. *Science (80-) 305*, 1619–1622. https://doi.org/10.1126/science.1098674.

Lian, X., Hsiao, C., Wilson, G. et al. (2012). Robust cardiomyocyte differentiation from human pluripotent stem cells via temporal modulation of canonical Wnt signaling. *Proc Natl Acad Sci U S A 109*. https://doi.org/10.1073/pnas.1200250109.

Lian, X., Zhang, J., Azarin, S. M. et al. (2013). Directed cardiomyocyte differentiation from human pluripotent stem cells by modulating Wnt/β-catenin signaling under fully defined conditions. *Nat Protoc 8*, 162–175. https://doi.org/10.1038/nprot.2012.150.

Lindsley, R. C., Gill, J. G., Murphy, T. L. et al. (2008). Mesp1 coordinately regulates cardiovascular fate restriction and epithelial-mesenchymal transition in differentiating ESCs. *Cell Stem Cell 3*, 55–68. https://doi.org/10.1016/j.stem.2008.04.004.

Liston, D. R. and Davis, M. (2017). Clinically relevant concentrations of anticancer drugs: A guide for nonclinical studies. *Clin Cancer Res 23*, 3489–3498. https://doi.org/10.1158/1078-0432.CCR-16-3083.

Lo, B. and Parham, L. (2009). Ethical issues in stem cell research. *Endocr Rev 30*, 204–213. https://doi.org/10.1210/er.2008-0031.

Logan, C. Y. and Nusse, R. (2004). The Wnt signaling pathway in development and disease. *Annu Rev Cell Dev Biol 20*, 781–810. https://doi.org/10.1146/annurev.cellbio.20.010403.113126.

Loh, Y. H., Agarwal, S., Park, I. H. et al. (2009). Generation of induced pluripotent stem cells from human blood. *Blood 113*, 5476–5479. https://doi.org/10.1182/BLOOD-2009-02-204800.

Longley, D. B., Harkin, D. P. and Johnston, P. G. (2003). 5-Fluorouracil: Mechanisms of action and clinical strategies. *Nat Rev Cancer 3*, 330–338. https://doi.org/10.1038/nrc1074.

Macías-Silva, M., Hoodless, P. A., Tang, S. J. et al. (1998). Specific activation of Smad1 signaling pathways by the BMP7 type I receptor, ALK2. *J Biol Chem 273*, 25628–25636. https://doi.org/10.1074/jbc.273.40.25628.

Maitra, A., Arking, D. E., Shivapurkar, N. et al. (2005). Genomic alterations in cultured human embryonic stem cells. *Nat Genet 37*, 1099–1103. https://doi.org/10.1038/ng1631.

Masjosthusmann, S., Blum, J., Bartmann, K. et al. (2020). Establishment of an a priori protocol for the implementation and interpretation of an in-vitro testing battery for the assessment of developmental neurotoxicity. *EFSA Support Publ 17*. https://doi.org/10.2903/sp.efsa.2020.en-1938.

Matlock, B. (2015). Assessment of Nucleic Acid Purity. Technical Note 52646. *Tech Bull NanoDrop Spectrophotometers*, 1–2. Available at: https://assets.fishersci.com/TFS-Assets/CAD/Product-Bulletins/TN52646-E-0215M-NucleicAcid.pdf [Accessed December 13, 2022].

Mayshar, Y., Ben-David, U., Lavon, N. et al. (2010). Identification and classification of chromosomal aberrations in human induced pluripotent stem cells. *Cell Stem Cell 7*, 521–531. https://doi.org/10.1016/j.stem.2010.07.017.

McCulley, D. J., Kang, J.-O., Martin, J. F. et al. (2008). BMP4 is required in the anterior heart field and its derivatives for endocardial cushion remodeling, outflow tract septation, and semilunar valve development. *Dev Dyn 237*, 3200–9. https://doi.org/10.1002/dvdy.21743.

Meilhac, S. M., Esner, M., Kelly, R. G. et al. (2004). The Clonal Origin of Myocardial Cells in Different Regions of the Embryonic Mouse Heart. *Dev Cell 6*, 685–698. https://doi.org/10.1016/S1534-5807(04)00133-9.

Mjaatvedt, C. H., Nakaoka, T., Moreno-Rodriguez, R. et al. (2001). The outflow tract of the heart is recruited from a novel heart-forming field. *Dev Biol 238*, 97–109. https://doi.org/10.1006/dbio.2001.0409.

Molkentin, J. D., Lin, Q., Duncan, S. A. et al. (1997). Requirement of the transcription factor GATA4 for heart tube formation and ventral morphogenesis. *Genes Dev 11*, 1061–1072. https://doi.org/10.1101/gad.11.8.1061.

Mummery, C. L., Zhang, J., Ng, E. S. et al. (2012). Differentiation of human embryonic stem cells and induced pluripotent stem cells to cardiomyocytes: A methods overview. *Circ Res 111*, 344–358. https://doi.org/10.1161/CIRCRESAHA.110.227512.

Murphy, C., Naderlinger, E., Mater, A. et al. (2022). Comparison of human recombinant protein coatings and fibroblast-ECM to Matrigel for induced pluripotent stem cell culture and renal podocyte differentiation_suppl2. *ALTEX*. https://doi.org/10.14573/altex.2112204s2.

Naito, A. T., Shiojima, I., Akazawa, H. et al. (2006). Developmental stage-specific biphasic roles of Wnt/β-catenin signaling in cardiomyogenesis and hematopoiesis. *Proc Natl Acad Sci 103*, 19812–19817. https://doi.org/10.1073/PNAS.0605768103.

Nathan, L., Bawdon, R. E., Sidawi, J. E. et al. (1993). Penicillin levels following the administration of benzathine penicillin G in pregnancy. *Obstet Gynecol 82*, 338–42

National Research Council (2000). Developmental Defects and Their Causes. In *Scientific frontiers in developmental toxicology and risk assessment* (17–25). Washington, DC: National Academy Press. https://doi.org/10.17226/9871.

National Research Council (US) (2007). *National Research Council (US) Committee on Applications of Toxicogenomic Technologies to Predictive Toxicology*. Washington (DC): National Academies Press (US). https://doi.org/https://doi.org/10.17226/12037.

Naujok, O., Lentes, J., Diekmann, U. et al. (2014). Cytotoxicity and activation of the Wnt/beta-catenin pathway in mouse embryonic stem cells treated with four GSK3 inhibitors. *BMC Res Notes 7*, 273. https://doi.org/10.1186/1756-0500-7-273.

Nicoll, R. (2018). Environmental Contaminants and Congenital Heart Defects: A Re-Evaluation of the Evidence. *Int J Environ Res Public Health 15*, 2096. https://doi.org/10.3390/ijerph15102096.

Nolan, T., Hands, R. E. and Bustin, S. A. (2006). Quantification of mRNA using real-time RT-PCR. *Nat Protoc 1*, 1559–1582. https://doi.org/10.1038/nprot.2006.236.

Novartis (2022). Prescribing Information of Egaten. EGATEN® (triclabendazole) tablets, for oral use. Available at: https://www.novartis.com/us-en/sites/novartis_us/files/egaten.pdf [Accessed December 13, 2022].

O'Gorman, M. R. G. and Thomas, J. (1999). Isotype controls - time to let go? *Cytometry 38*, 78–80. https://doi.org/10.1002/(SICI)1097-0320(19990415)38:2<78::AID-CYTO6>3.0.CO;2-E.

OECD (2018a). *Test No. 414: Prenatal Developmental Toxicity Study*. OECD. https://doi.org/10.1787/9789264070820-en.

OECD (1983). *Test No. 415: One-Generation Reproduction Toxicity Study*. OECD. https://doi.org/10.1787/9789264070844-en.

OECD (2001). *Test No. 416: Two-Generation Reproduction Toxicity*. OECD. https://doi.org/10.1787/9789264070868-en.

OECD (2016a). *Test No. 421: Reproduction/Developmental Toxicity Screening Test*. OECD. https://doi.org/10.1787/9789264264380-en.

OECD (2016b). *Test No. 422: Combined Repeated Dose Toxicity Study with the Reproduction/Developmental Toxicity Screening Test*. OECD. https://doi.org/10.1787/9789264264403-en.

OECD (2007). *Test No. 426: Developmental Neurotoxicity Study, OECD Guidelines for the Testing of Chemicals*. OECD. https://doi.org/10.1787/9789264067394-en.

OECD (2018b). *Test No. 443: Extended One-Generation Reproductive Toxicity Study*. OECD. https://doi.org/10.1787/9789264304741-34-en.

Olivetti, G. (1996). Aging, Cardiac Hypertrophy and Ischemic Cardiomyopathy Do Not Affect the Proportion of Mononucleated and Multinucleated Myocytes in the Human Heart. *J Mol Cell Cardiol 28*, 1463–1477. https://doi.org/10.1006/jmcc.1996.0137.

Ornitz, D. M. and Itoh, N. (2015). The Fibroblast Growth Factor signaling pathway. *WIREs Dev Biol 4*, 215–266. https://doi.org/10.1002/wdev.176.

Pamies, D., Bal-Price, A., Simeonov, A. et al. (2017). Good cell culture practice for stem cells & stem-cell-derived models. In *Altex* (95–132). Elsevier GmbH. https://doi.org/10.14573/altex.1607121.

Paulus, W. E. (2016). Geburtseinleitung. In H. Schneider, P. Husslein and K.-T. M. Schneider (eds.), *Praktische Geburtshilfe* (83–113). Berlin, Heidelberg: Springer-Verlag GmbH Berlin Heidelberg. https://doi.org/10.1515/9783112355084-022.

Pellizzer, C., Adler, S., Corvi, R. et al. (2004). Monitoring of teratogenic effects in vitro by analysing a selected gene expression pattern. *Toxicol Vitr 18*, 325–335. https://doi.org/10.1016/j.tiv.2003.09.007.

Peters, A. K., Steemans, M., Mesens, N. et al. (2007). A higher throughput method to the Embryonic Stem cell Test (EST), to detect embryotoxicity in early development. *AATEX 14*, 673–677

Peters, A. K., Wouwer, G. Van de, Weyn, B. et al. (2008). Automated analysis of contractility in the embryonic stem cell test, a novel approach to assess embryotoxicity. *Toxicol Vitr 22*, 1948–1956. https://doi.org/10.1016/j.tiv.2008.09.008.

Peters, K. G., Marie, J., Wilson, E. et al. (1992). Point mutation of an FGF receptor abolishes phosphatidylinositol turnover and Ca2+ flux but not mitogenesis. *Nature 358*, 678–681. https://doi.org/10.1038/358678a0.

Peters, P., Miller, R. K. and Schaefer, C. (2015). *Drugs During Pregnancy and Lactation Treatment Options and Risk Assessment*. Amsterdam: Elsevier. https://doi.org/10.1016/B978-0-12-408078-2.00001-9.

Pistollato, F., Madia, F., Corvi, R. et al. (2021). Current EU regulatory requirements for the assessment of chemicals and cosmetic products: challenges and opportunities for introducing new approach methodologies. *Arch Toxicol 95*, 1867–1897. https://doi.org/10.1007/s00204-021-03034-y.

Prall, O. W. J., Menon, M. K., Solloway, M. J. et al. (2007). An Nkx2-5/Bmp2/Smad1 Negative Feedback Loop Controls Heart Progenitor Specification and Proliferation. *Cell 128*, 947–959. https://doi.org/10.1016/j.cell.2007.01.042.

Qyang, Y., Martin-Puig, S., Chiravuri, M. et al. (2007). The Renewal and Differentiation of Isl1+ Cardiovascular Progenitors Are Controlled by a Wnt/β-Catenin Pathway. *Cell Stem Cell 1*, 165–179. https://doi.org/10.1016/j.stem.2007.05.018.

R Core Team (2022). R: A Language and Environment for Statistical Computing. Available at: https://www.r-project.org/ [Accessed December 13, 2022].

Raab, S., Klingenstein, M., Liebau, S. et al. (2014). A Comparative View on Human Somatic Cell Sources for iPSC Generation. *Stem Cells Int 2014*, 1–12. https://doi.org/10.1155/2014/768391.

Rijsewijk, F., Schuermann, M., Wagenaar, E. et al. (1987). The Drosophila homology of the mouse mammary oncogene int-1 is identical to the segment polarity gene wingless. *Cell 50*, 649–657. https://doi.org/10.1016/0092-8674(87)90038-9.

Riss, T. L., Moravec, R. A., Niles, A. L. et al. (2004). Cell Viability Assays. In S. Markossian, S. G. Sittampalam, A. Grossman, et al. (eds.), *Assay Guidance Manual* (335–359). Bethesda, MA: Eli Lilly & Company and the National Center for Advancing Translational Sciences. Available at: http://www.ncbi.nlm.nih.gov/pubmed/23805433 [Accessed December 13, 2022].

Ritz, C., Baty, F., Streibig, J. C. et al. (2015). Dose-Response Analysis Using R. *PLoS One 10*, e0146021. https://doi.org/10.1371/JOURNAL.PONE.0146021.

Robertson, C., Tran, D. D. and George, S. C. (2013). Concise review: maturation phases of human pluripotent stem cell-derived cardiomyocytes. *Stem Cells 31*, 829–37. https://doi.org/10.1002/stem.1331.

Rosenzweig, B. L., Imamura, T., Okadome, T. et al. (1995). Cloning and characterization of a human type II receptor for bone morphogenetic proteins. *Proc Natl Acad Sci U S A 92*, 7632–7636. https://doi.org/10.1073/pnas.92.17.7632.

Rovida, C. and Hartung, T. (2009). Re-evaluation of animal numbers and costs for in vivo tests to accomplish REACH legislation requirements for chemicals - a report by the transatlantic think tank for toxicology (t(4)). *ALTEX 26*, 187–208

Russell, W. M. S. and Burch, R. L. (1959). *The Principles of Humane Experimental Technique*. London, UK: Methuen. Available at: https://caat.jhsph.edu/principles/the-principles-of-humane-experimental-technique [Accessed December 13, 2022].

Saga, Y. (2000). Mesp1 Expression Is the Earliest Sign of Cardiovascular Development. *Trends Cardiovasc Med 10*, 345–352. https://doi.org/10.1016/S1050-1738(01)00069-X.

Saga, Y., Hata, N., Kobayashi, S. et al. (1996). Mesp1: a novel basic helix-loop-helix protein expressed in the nascent mesodermal cells during mouse gastrulation. *Development 122*, 2769–2778. https://doi.org/10.1242/dev.122.9.2769.

Saga, Y., Miyagawa-Tomita, S., Takagi, A. et al. (1999). MesP1 is expressed in the heart precursor cells and required for the formation of a single heart tube. *Development 126*, 3437–3447. https://doi.org/10.1242/dev.126.15.3437.

Schaefer, C., Spielmann, H., Vetter, K. et al. (2006). Spezielle Arzneimitteltherapie in der Schwangerschaft. In *Arzneiverordnung in Schwangerschaft und Stillzeit* (33–557). Elsevier. https://doi.org/10.1016/B978-343721332-8.50004-1.

Scholz, G., Genschow, E., Pohl, I. et al. (1999). Prevalidation of the Embryonic Stem Cell Test (EST) - A new in vitro embryotoxicity test. *Toxicol Vitr 13*, 675–681. https://doi.org/10.1016/S0887-2333(99)00046-6.

Schünke, M., Schulte, E., Schumacher, U. et al. (2018). *PROMETHEUS Innere Organe*. 5th ed. Stuttgart: Georg Thieme Verlag. https://doi.org/10.1055/b-006-149645.

Seiler, A. E. M. and Spielmann, H. (2011). The validated embryonic stem cell test to predict embryotoxicity in vitro. *Nat Protoc 6*, 961–978. https://doi.org/10.1038/nprot.2011.348.

Seki, T., Yuasa, S., Kusumoto, D. et al. (2014). Generation and Characterization of Functional Cardiomyocytes Derived from Human T Cell-Derived Induced Pluripotent Stem Cells R. Johnson (ed.),. *PLoS One 9*, e85645. https://doi.org/10.1371/journal.pone.0085645.

Sepac, A., Si-Tayeb, K., Sedlic, F. et al. (2012). Comparison of cardiomyogenic potential among human ESC and iPSC lines. *Cell Transplant 21*, 2523–2530. https://doi.org/10.3727/096368912X653165.

Shah, R. M. and MacKay, R. A. (1978). Teratological evaluation of 5-fluorouracil and 5-bromo-2-deoxyuridine on hamster fetuses. *Development 43*, 47–54. https://doi.org/10.1242/dev.43.1.47.

Shuey, D. L., Lau, C., Logsdon, T. R. et al. (1994). Biologically Based Dose-Response Modeling in Developmental Toxicology: Biochemical and Cellular Sequelae of 5-Fluorouracil Exposure in the Developing Rat. *Toxicol Appl Pharmacol 126*, 129–144. https://doi.org/10.1006/taap.1994.1099.

Smith, A. S. T., Macadangdang, J., Leung, W. et al. (2017). Human iPSC-derived cardiomyocytes and tissue engineering strategies for disease modeling and drug screening. *Biotechnol Adv 35*, 77–94. https://doi.org/10.1016/j.biotechadv.2016.12.002.

Smith, K. P., Luong, M. X. and Stein, G. S. (2009). Pluripotency: Toward a gold standard for human ES and iPS cells. *J Cell Physiol 220*, 21–29. https://doi.org/10.1002/jcp.21681.

Snir, M., Kehat, I., Gepstein, A. et al. (2003). Assessment of the ultrastructural and proliferative properties of human embryonic stem cell-derived cardiomyocytes. *Am J Physiol - Hear Circ Physiol 285*, 2355–2363. https://doi.org/10.1152/ajpheart.00020.2003.

Spielmann, H. (2017). Reproduktionstoxikologie. In H. Greim (ed.), *Das Toxikologiebuch* (187–204). Wiley. https://doi.org/10.1002/9783527695447.

Spielmann, H., Seiler, A., Bremer, S. et al. (2006). The practical application of three validated in vitro embryotoxicity tests. *ATLA Altern to Lab Anim 34*, 527–538. https://doi.org/10.1177/026119290603400504.

Stalsberg, H. and DeHaan, R. L. (1969). The precardiac areas and formation of the tubular heart in the chick embryo. *Dev Biol 19*, 128–159. https://doi.org/10.1016/0012-1606(69)90052-9.

Stephens, J. D., Golbus, M. S., Miller, T. R. et al. (1980). Multiple congenital anomalies in a fetus exposed to 5-fluorouracil during the first trimester. *Am J Obstet Gynecol 137*, 747–749. https://doi.org/10.1016/S0002-9378(15)33259-2.

Stover, A. E. and Schwartz, P. H. (2011). Adaptation of Human Pluripotent Stem Cells to Feeder-Free Conditions in Chemically Defined Medium with Enzymatic Single-Cell Passaging. In P. H. Schwartz and R. L. Wesselschmidt (eds.), *Human Pluripotent Stem Cells - Methods and Protocols* (137–146). New York: Humana Press, c/o Springer Science+Business Medi. https://doi.org/10.1007/978-1-61779-201-4_10.

Stucki, A. O., Barton-Maclaren, T. S., Bhuller, Y. et al. (2022). Use of new approach methodologies (NAMs) to meet regulatory requirements for the assessment of industrial chemicals and pesticides for effects on human health. *Front Toxicol 4*, 1–24. https://doi.org/10.3389/ftox.2022.964553.

Sturzu, A. C. and Wu, S. M. (2011). Developmental and regenerative biology of multipotent cardiovascular progenitor cells. *Circ Res 108*, 353–364. https://doi.org/10.1161/CIRCRESAHA.110.227066.

Sullivan, S., Stacey, G. N., Akazawa, C. et al. (2018). Quality control guidelines for clinical-grade human induced pluripotent stem cell lines. *Regen Med 13*. https://doi.org/10.2217/rme-2018-0095.

Suzuki, N., Ando, S., Yamashita, N. et al. (2011). Evaluation of novel high-throughput embryonic stem cell tests with new molecular markers for screening embryotoxic chemicals in vitro. *Toxicol Sci 124*, 460–471. https://doi.org/10.1093/toxsci/kfr250.

Takahashi, K., Tanabe, K., Ohnuki, M. et al. (2007). Induction of Pluripotent Stem Cells from Adult Human Fibroblasts by Defined Factors. *Cell 131*, 861–872. https://doi.org/10.1016/j.cell.2007.11.019.

Takahashi, K. and Yamanaka, S. (2006). Induction of Pluripotent Stem Cells from Mouse Embryonic and Adult Fibroblast Cultures by Defined Factors. *Cell 126*, 663–676. https://doi.org/10.1016/J.CELL.2006.07.024.

Thermo Fisher Scientific (2022). Culturing Pluripotent Stem Cells (PSCs) in Essential 8 ™ Medium. *Thermo Fish Sci 0*, 1–10. Available at: https://www.thermofisher.com/document-connect/document-connect.html?url=https://assets.thermofisher.com/TFS-Assets%2FLSG%2Fmanuals%2Ffeeder_free_PSCs_in_essential8_medium.pdf [Accessed December 13, 2022].

Tian, Y., Cohen, E. D. and Morrisey, E. E. (2010). The importance of Wnt signaling in cardiovascular development. *Pediatr Cardiol 31*, 342–8. https://doi.org/10.1007/s00246-009-9606-z.

Tigges, J., Bielec, K., Brockerhoff, G. et al. (2021). Academic application of Good Cell Culture Practice for induced pluripotent stem cells. *ALTEX*. https://doi.org/10.14573/altex.2101221.

Timpl, R., Rohde, H., Robey, P. G. et al. (1979). Laminin-A Glycoprotein from Basement Membranes. *J Biol Chem 254*. https://doi.org/10.1016/S0021-9258(19)83607-4.

Ueno, S., Weidinger, G., Osugi, T. et al. (2007). Biphasic role for Wnt/β-catenin signaling in cardiac specification in zebrafish and embryonic stem cells. *Proc Natl Acad Sci U S A 104*, 9685–9690. https://doi.org/10.1073/pnas.0702859104.

Ulfig, N. and Brand-Saberi, B. (2017). Kurzlehrbuch Embryologie. In *Kurzlehrbuch Embryologie* (83–90). Stuttgart; New York: Georg Thieme Verlag KG.

Uosaki, H. and Taguchi, Y. (2016). Comparative Gene Expression Analysis of Mouse and Human Cardiac Maturation. *Genomics Proteomics Bioinformatics 14*, 207–215. https://doi.org/10.1016/J.GPB.2016.04.004.

US EPA (1991). Guidelines for Developmental Toxicity Risk Assessment. *Risk Assess Forum 56*, 63798–63826. Available at: https://www.epa.gov/sites/default/files/2014-11/documents/dev_tox.pdf [Accessed December 13, 2022].

US EPA (1996). Guidelines for Reproductive toxicity risk assessment. *Environ Prot Agency 61*, 56274–56322. Available at: https://archive.epa.gov/raf/web/pdf/repro51.pdf [Accessed December 13, 2022].

Virágh, S. and Challice, C. E. (1973). Origin and differentiation of cardiac muscle cells in the mouse. *J Ultrasructure Res 42*, 1–24. https://doi.org/10.1016/S0022-5320(73)80002-4.

VWR (2022). peqGOLD Total RNA Kit instruction manual. , 1–20. Available at: https://si.vwr.com/assetsvc/asset/sl_SI/id/17035099/contents [Accessed December 13, 2022].

Wakui, T. (2017). Method for evaluation of human induced pluripotent stem cell quality using image analysis based on the biological morphology of cells. *J Med Imaging 4*, 1. https://doi.org/10.1117/1.jmi.4.4.044003.

Waldo, K. L., Kumiski, D. H., Wallis, K. T. et al. (2001). Conotruncal myocardium arises from a secondary heart field. *Development 128*, 3179–3188. https://doi.org/10.1242/DEV.128.16.3179.

Walker, L. M., Sparks, N. R. L., Puig-Sanvicens, V. et al. (2021). An evaluation of human induced Pluripotent stem cells to test for cardiac developmental toxicity. *Int J Mol Sci 22*. https://doi.org/10.3390/ijms22158114.

Walter, A., Šarić, T., Hescheler, J. et al. (2015). Calcium Imaging in Pluripotent Stem Cell-Derived Cardiac Myocytes. In *Methods in Molecular Biology* (131–146). https://doi.org/10.1007/7651_2015_267.

Wang, R. N., Green, J., Wang, Z. et al. (2014). Bone Morphogenetic Protein (BMP) signaling in development and human diseases. *Genes Dis 1*, 87–105. https://doi.org/10.1016/J.GENDIS.2014.07.005.

Ward, C., Stadt, H., Hutson, M. et al. (2005). Ablation of the secondary heart field leads to tetralogy of Fallot and pulmonary atresia. *Dev Biol 284*, 72–83. https://doi.org/10.1016/j.ydbio.2005.05.003.

Weeks, J. W., Myers, S. R., Lasher, L. et al. (1997). Persistence of penicillin G benzathine in pregnant group B streptococcus carriers. *Obstet Gynecol 90*, 240–243. https://doi.org/10.1016/S0029-7844(97)00247-0.

Weinhold, B. (2009). Environmental factors in birth defects: What we need to know. *Environ Health Perspect 117*. https://doi.org/10.1289/EHP.117-A440.

Whittaker, S. G. and Faustman, E. M. (1992). Cytotoxicity Assessment in Cultures of Differentiating Rodent Embryonic Cells. *Toxicol Methods 2*, 46–56. https://doi.org/10.3109/15376519209064805.

WHO (2022). Congenital Anomalies. Available at: https://www.who.int/health-topics/congenital-anomalies#tab=tab_1 [Accessed December 13, 2022].

WHO (2006). Report of the WHO Informal Meeting on Use of Triclabendazole in Fascioliasis Control. Available at: https://www.who.int/publications/i/item/WHO-CDS-NTD-PCT-2007.1.

WHO (2013). *WHO Expert Committee on Biological Standardization, Annex 3: Recommendations for the evaluation of animal cell cultures as substrates for the manufacture of biological medicinal products and for the characterization of cell banks Replacement*. Available at: https://cdn.who.int/media/docs/default-source/biologicals/documents/trs_978_annex_3.pdf?sfvrsn=fe61af77_3&download=true [Accessed December 13, 2022].

Wilfinger, W. W., Mackey, K. and Chomczynski, P. (1997). Effect of pH and Ionic Strength on the Spectrophotometric Assessment of Nucleic Acid Purity. *Biotechniques 22*, 474–481. https://doi.org/10.2144/97223st01.

Wilson, J. G. (1977). Handbook of Teratology General Principles and Etiology. In J. G. Wilson and F. C. Fraser (eds.), *Handbook of Teratology General Principles and Etiology* (49–74). New York: Plenum Press. https://doi.org/10.1007/978-1-4684-2850-6.

Winnier, G., Blessing, M., Labosky, P. A. et al. (1995). Bone morphogenetic protein-4 is required for mesoderm formation and patterning in the mouse. *Genes Dev 9*, 2105–2116. https://doi.org/10.1101/gad.9.17.2105.

Witt, G., Keminer, O., Leu, J. et al. (2021). An automated and high-throughput-screening compatible pluripotent stem cell-based test platform for developmental and reproductive toxicity assessment of small molecule compounds. *Cell Biol Toxicol 37*, 229–243. https://doi.org/10.1007/s10565-020-09538-0.

Woodruff, T. J., Zota, A. R. and Schwartz, J. M. (2011). Environmental Chemicals in Pregnant Women in the United States: NHANES 2003–2004. *Environ Health Perspect 119*, 878. https://doi.org/10.1289/EHP.1002727.

Xie, L., Hoffmann, A. D., Burnicka-Turek, O. et al. (2012). Tbx5-Hedgehog Molecular Networks Are Essential in the Second Heart Field for Atrial Septation. *Dev Cell 23*, 280–291. https://doi.org/10.1016/j.devcel.2012.06.006.

Yamada, S., Yamazaki, D. and Kanda, Y. (2018). 5-fluorouracil inhibits neural differentiation via Mfn1/2 reduction in human induced pluripotent stem cells. *J Toxicol Sci 43*, 727–734. https://doi.org/10.2131/jts.43.727.

You, L., Zhang, C., Yarravarapu, N. et al. (2016). Development of a triazole class of highly potent Porcn inhibitors. *Bioorg Med Chem Lett 26*, 5891–5895. https://doi.org/10.1016/J.BMCL.2016.11.012.

Yun Liu, K., May Chow, J. and Sherry, C. (2013). Early Life Obesity and Diabetes: Origins in Pregnancy. *Open J Endocr Metab Dis 03*, 1–12. https://doi.org/10.4236/ojemd.2013.31001.

Zaffran, S. and Kelly, R. G. (2012). New developments in the second heart field. *Differentiation 84*, 17–24. https://doi.org/10.1016/j.diff.2012.03.003.

Zaffran, S., Kelly, R. G., Meilhac, S. M. et al. (2004). Right ventricular myocardium derives from the anterior heart field. *Circ Res 95*, 261–268. https://doi.org/10.1161/01.RES.0000136815.73623.BE.

Zeisberg, E. M., Ma, Q., Juraszek, A. L. et al. (2005). Morphogenesis of the right ventricle requires myocardial expression of Gata4. *J Clin Invest 115*, 1522–1531. https://doi.org/10.1172/JCI23769.

Zhang, J., Wilson, G. F., Soerens, A. G. et al. (2009). Functional cardiomyocytes derived from human induced pluripotent stem cells. *Circ Res 104*. https://doi.org/10.1161/CIRCRESAHA.108.192237.

Zhang, M., Schulte, J. S., Heinick, A. et al. (2015). Universal Cardiac Induction of Human Pluripotent Stem Cells in Two and Three-Dimensional Formats: Implications for In Vitro Maturation. *Stem Cells 33*, 1456–1469. https://doi.org/10.1002/stem.1964.

Zhang, N., Yin, Y., Xu, S.-J. et al. (2008). 5-Fluorouracil: Mechanisms of Resistance and Reversal Strategies. *Molecules 13*, 1551. https://doi.org/10.3390/MOLECULES13081551.

Zhao, Q., Sun, Q., Zhou, L. et al. (2019). Complex Regulation of Mitochondrial Function During Cardiac Development. *J Am Heart Assoc 8*. https://doi.org/10.1161/JAHA.119.012731.

Zhou, T., Benda, C., Dunzinger, S. et al. (2012). Generation of human induced pluripotent stem cells from urine samples. *Nat Protoc 7*, 2080–2089. https://doi.org/10.1038/nprot.2012.115.

Zilles, K. and Tillmann, B. N. (2010). *Anatomie*. Heidelberg: Springer Medizin Verlag Heidelberg.

Zwartsen, A., de Korte, T., Nacken, P. et al. (2019). Cardiotoxicity screening of illicit drugs and new psychoactive substances (NPS) in human iPSC-derived cardiomyocytes using microelectrode array (MEA) recordings. *J Mol Cell Cardiol 136*, 102–112. https://doi.org/10.1016/j.yjmcc.2019.09.007.

9 Appendix

9.1 List of Figures

9.2 List of Tables

9.3 Abbreviations

3R	Replacement, Reduction, Refinement
5-FU	5-Fluorouracil
ACTN2	α-Actinin2
APC	Allophycocyanine
ASAH2	N-Acylsphingosine Amidohydrolase 2
BMP	Bone morphogenetic protein
bp	Base pairs
bpm	Beats per minute
Ca^{2+}	Divalent calcium ions
$CaCl_2$	Calcium chloride
CANX	Calnexin
CAS-Nr.	Chemical Abstracts Service
CD140b	Platelet-derived growth factor receptor beta
CD144	Cadherin 5
cDNA	Complementary DNA
CHIR99021	6-((2-((4-(2,4-Dichlorophenyl)-5-(4-methyl-1H-imidazol-2-yl)pyrimidin-2-yl)amino)ethyl)amino)nicotinonitrile
CK1A	Casein Kinase 1α
C-MYC	MYC proto-oncogene, bHLH transcription factor
CO_2	Carbon dioxide
CTB	CellTiter-Blue®
cTnT	Cardiac muscle Troponin T
dH_2O	Distilled water
DMEM	Dulbecco's Modified Eagle Medium
DMSO	Dimethylsulfoxide
DNA	Desoxyribonucleic acid
dNTP	Desoxyribonukleosidtriphosphate
EBs	Embryoid bodies
ECHA	European Chemicals Agency
ECVAM	European Centre for the Validation of Alternative Methods
EGF	Epidermal growth factor

ESC(s)	Embryonic stem cell(s)
EST	Embryonic stem cell test
EU	European Union
FDA	Food and Drug Administration
FGF	Fibroblast Growth Factor
FHF	First Heart Field
FITC	Fluorescein isothiocyanate
FMO	Fluorescence Minus One
FOXH1	Forkhead box H1
FOXP4	Forkhead box protein P4
Fps	Frames per second
FSC	Forward Scatter
FSC-A	Forward Scatter-Area
FSC-W	Forward Scatter-Width
FTDA	FGF2, TGF-β1, Dorsomorphin, Activin A (Medium for cell culture)
FVS 510	Fixable Viability Stain 510
FW	Forward
GATA4	GATA-binding protein 4
GD	Gestational day
gDNA	Genomic DNA
GS	Goat serum
GSK-3β	Glykogensynthasekinase-3β
dH_2O	Distilled Water
HCS	High Content Screening
hESC(s)	Human embryonic stem cell(s)
hiPSC(s)	Human induced pluripotent stem cell(s)
IC_{50}	Half maximal inhibitory concentration
ID_{50}	Half maximal inhibitory concentration of differentiation
IGF1	Insulin-like growth factor 1
INT1	Wnt family member 1
iPSCs	Induced pluripotent stem cells
ISL1	Insulin gene enhancer protein 1

ITS	Insulin, Transferrin, Selenious Acid
IWP2	Inhibitor of WNT production 2
KLF4	Kruppel like factor 4
KO-DMEM	KnockOut DMEM
LATS2	Large tumor suppressor kinase 2
LDEV	Lactate dehydrogenase elevating virus
LIF	Leukemia inhibitory factor
L-MYC	MYCL proto-oncogene, bHLH transcription factor
LN521	Human recombinant laminin 521
LRP1	Low-density lipoprotein receptor-related protein 1
MCB	Master cell bank
MEA	Microelectrode array
mESC(s)	Mouse embryonic stem cell(s)
MESP1	Mesoderm posterior protein 1
Mg^{2+}	Divalent magnesium ions
$MgCl_2$	Magnesium chloride
MHC	Myosin heavy chain
M-MLV	Moloney murine leukemia virus (Reverse Transcriptase)
mRNA	Messenger ribonucleic acid
MYH6	Myosin heavy chain 6
MYH7	Myosin heavy chain 7
NAM	New approach methodologies
NANOG	Homeobox protein NANOG
NCDZ	Nocodazole
NKX2.5	NK2 homeobox 5
OCT4	Octamer-binding protein 4
OECD	Organisation for Economic Co-operation and Development
PBS	Phosphate-buffered saline
PBS $^{-/-}$	PBS without Ca^{2+} and Mg^{2+}
PBS $^{+/+}$	PBS with Ca^{2+} and Mg^{2+}
PBS-T	PBS with Triton X-100
PCR	Polymerase chain reaction

PE	Phycoerythrin
PenG	Penicillin G
PerCP-Cy5.5	Peridinin chlorophyll protein-Cyanine5.5
PFA	Paraformaldehyde
PORCN	Porcupine
qRT-PCR	Quantitative reverse transcription polymerase chain reaction
REACH	Registration, Evaluation, Authorisation, and Restriction of Chemicals
RNA	Ribonucleic acid
RNase	Ribonuclease
ROI	Region of interest
RT	Reverse transcriptase
RV	Reverse
SEM	Standard error of the mean
SHF	Second heart field
SMAD	Small mothers against decapentaplegic homolog
SOX2	SRY (sex determining region Y)-box transcription factor 2
SSC	Side Scatter
SSC-A	Side Scatter-Area
SSEA4	Stage-specific embryonic antigen-4
TBX5	T-box transcription factor 5
TCBZ	Triclabendazole
TCBZSO	Triclabendazole sulfoxide
TCF/LEF	transcription factor/lymphoid enhancer-binding factor
TGF	Transforming Growth Factor
TNNT2	troponin T2, cardiac type
TS	Transferrin, Selenous acid
US	United States (of America)
WEC	Whole embryo culture
WHO	World Health Organization
Wnt	Name combination of Wingless and INT1
ZFET	Zebrafish embryo test

Eidesstattliche Erklärung/Statutory declaration

Ich versichere an Eides Statt, dass die vorliegende Dissertation mit dem Titel „Der Humane

Induzierte Pluripotente Stammzelltest als Alternative Methode zur Embryotoxizitätstestung" von mir selbständig und ohne unzulässige fremde Hilfe unter Beachtung der „Grundsätze zur Sicherung guter wissenschaftlicher Praxis an der Heinrich-Heine-Universität Düsseldorf" erstellt worden ist. Die Dissertation wurde in der vorgelegten oder einer ähnlichen Form bei keiner anderen Institution eingereicht. Ich habe bisher keine erfolglosen Promotionsversuche unternommen.

I declare that the present dissertation "The Human Induced Pluripotent Stem Cell Test as an Alternative Method for Embryotoxicity Testing" has been prepared and written by me independently and without unauthorized outside assistance in accordance with the "Principles for Ensuring Good Scientific Practice at the Heinrich Heine University of Düsseldorf". The dissertation has not been submitted to any other institution in the form presented or in a similar form. I have not made any unsuccessful attempts at a doctorate to date.

Düsseldorf, den _____

Saskia Galanjuk

Danksagung

An dieser Stelle möchte ich mich bei allen Personen bedanken, die mich auf dem Weg der Promotion unterstützt haben und diese möglich gemacht haben.

Zunächst möchte ich mich vielmals bei Frau Prof. Dr. Ellen Fritsche, für die Aufnahme in ihre Arbeitsgruppe und die Bereitstellung des sehr interessanten Themas bedanken. In den letzten Jahren konnte ich mich durch ihre Unterstützung und Förderung, sowie das entgegengebrachte Vertrauen, beruflich und persönlich sehr weiterentwickeln.

Bei Frau Prof. Dr. Vlada Urlacher bedanke ich mich herzlichst für die fakultätsübergreifende Betreuung und Übernahme der Mentorenschaft, durch die meine Promotion erst möglich wurde.

Ich bedanke mich bei Dr. Leo Kurian und Dr. Deniz Bartsch für die universitätsübergreifende Unterstützung um das Projekt ins Rollen zu bringen.

Julia T. danke ich besonders für die Betreuung während meiner Promotion und für die stetige Hilfestellung, vor allem für die Korrekturen zahlreicher Schriftstücke, Poster und Vorträge.

Ein großer Dank gilt allen ehemaligen und derzeitigen Arbeitskollegen der AG Fritsche, die ich kennen lernen durfte. Danke für eure Hilfe und Unterstützung, vor allem für die zahlreichen Wochenendfütterungen ohne die meine Arbeit nicht möglich gewesen wäre. Danke auch für die tollen Erlebnisse in den letzten Jahren, die vor allem nach den Konferenzen stattfanden oder direkt am IUF zur Weihnachtszeit.

Ein großer Dank gilt Arif, der unermüdlich und egal zu welcher Uhrzeit immer hoch motiviert daran gearbeitet hat die Software CardioVision zu perfektionieren. Es hat wirklich sehr viel Spaß gemacht zusammen an der Software zu arbeiten und vielen Dank für den Exkurs in die Informatik.

Laura G. möchte ich für die kurze aber abwechslungsreiche Zeit und die tatkräftige Unterstützung im Cardiolab danken.

Ein ganz besonderer Dank gilt Etta, die das Cardiolab wesentlich lebendiger gemacht hat und immer für sehr interessanten Gesprächsstoff gesorgt hat, sowohl arbeitsbezogen als auch zu allen anderen Themen. Danke für die Unternehmungen nach der Arbeit, die Gespräche beim Anstehen vor Takumi und alles andere. Danke für ein offenes Ohr und die beste Zeit am IUF.

Ein riesengroßer Dank gilt meinen Eltern Dietmar und Silke und meinem Bruder Alexander. Danke für eure dauerhafte Unterstützung während der gesamten Studienzeit und eure motivierenden Worte, wenn ich sie brauchte.

Der Liebe meines Lebens Johann möchte ich aus tiefstem Herzen für die immerwährende Unterstützung und Motivation während der Studienzeit danken, es war bestimmt nicht immer einfach, vor allem zu den Zeiten der Abschlussarbeiten. Danke für die unermüdliche Geduld und Aufmerksamkeit, wenn ich sie brauchte, um schwierige Phasen durchzustehen.